STUDY OF LASER WELDING OF DISSIMILAR TRANSPARENT THERMOPLASTICS

Thesis submitted by

NITESH KUMAR

Doctor of Philosophy (Engineering)

MECHANICAL ENGINEERING DEPARTMENT
FACULTY COUNCIL OF ENGINEERING &TECHNOLOGY
JADAVPUR UNIVERSITY
KOLKATA, INDIA

2024

JADAVPUR UNIVERSITY
KOLKATA-700032, INDIA

INDEX NO.: 267/18/E

REGISTRATION NUMBER: **1021811026**

Title of Thesis: **Study of Laser Welding of Dissimilar Transparent Thermoplastics**

Name, Designation & Institution of the Supervisors:

Dr. Rajat Subhra Sen
Professor,
Mechanical Engineering Department
Jadavpur University Kolkata-700032 India

Name, Designation & Institution of the Co-Supervisors:

Dr. Nikhil Kumar
Scientist,
University of Warwick
Coventry CV4 7AL, United Kingdom (UK)

List of Publications:

Journal Publications:

1. **N. Kumar**, S. Chakravarty, N. Kumar, R.S. Sen "A Combined RSM – FEM Analysis of Weld Quality in Laser Transmission Welding of Plastics" Materials Express Research,11 (2024) 115310.

2. **N. Kumar**, N. Kumar, A. Mandal, R.S. Sen "Experimentation and LS-DYNA Modelling of Laser Transmission Welding of Plastics" Laser in Engineering, 59 (2024)139-153.

3. **N. Kumar**, N. Kumar, A. Bandyopadhyay. "Optimization of Pulsed Nd: YVO4 Laser Through Transmission Welding of Transparent Acrylic and Polycarbonate" Materials Today: Proceedings, 5 (2018) 5235-5243.

4. R. Bhattacharya, **N. Kumar**, N. Kumar, A. Bandyopadhyay. "A Study on the Effect of Process Parameters on Weld Width and Heat Affected Zone of Pulsed Laser Welding of Dissimilar Transparent Thermoplastics without Filler Materials in Lap Joint Configuration", Materials Today: Proceedings 5 (2018) 3674-3681.

5. **N. Kumar**, N. Kumar, A. Bandyopadhyay "A State-of-the-Art Review of Laser Welding of Polymers — Part I: Welding Parameters" The Welding Journal ,100(2021) 221-228.

6. **N. Kumar**, N. Kumar, A. Bandyopadhyay "A State-of-the-Art Review of Laser Welding of Polymers — Part II: Weld-Quality Studies" The Welding Journal, 100(2021) 249-258.

List of Patents: NIL

Presentation in Conferences:

1. **N. Kumar**, N. Kumar, A. Bandyopadhyay. "The Effect of Process Parameters on Pulsed Nd: YVO4 Laser Welding of Acrylic and Polycarbonate Sheets", COPEN, IIT Madras, Chennai, 2017, pp 13-16.

2. **N. Kumar**, N. Kumar, A. Bandyopadhyay. "The Effect of Process Parameters on Pulsed Through Transmission Laser Welding of Acrylic and polycarbonate sheets", AIMTDR, Anna University, Chennai, 2019, pp521-529(springer book chapter)

3. **N. Kumar**, N. Kumar, A. Bandyopadhyay. "Nd: YVO4 Laser Welding of Two Transparent Polymers in Lap Joint Configuration", ICFTMM, DTU, Delhi, 2019,pp 35-43(Springer book chapter)

4. **N. Kumar**, V. Kumar, S. Chakravarty, N. Kumar, A. Bandyopadhyay. "Study of Effect of Process Parameters on Cutting a Gear Profile on an Acrylic Plate Using Laser Beam Machining", TAME, Kalyani Govt. Engineering College, West Bengal, 2019.

5. **N. Kumar**, N. Kumar, A. Bandyopadhyay. "Optimization of Weld Width in Nd: YVO4 Laser Welding of Dissimilar Transparent Polymers in Lap Joint Pattern". COPEN, IIT Indore,2019.

6. **N. Kumar**, N. Kumar, A. Bandyopadhyay. "Effects of Welding Parameters in Nd: YVO4 Laser Welding of Two Transparent Polymers." COPEN, IIT Indore,2019.

7. **N. Kumar**, N. Kumar, A Mandal, R. S. Sen. "Laser Welding of Two Transparent Plastics without Any Filler Materials"AIMTDR IIT BHU,2024

8. **N. Kumar**, S. Chakravarty, N. Kumar, R.S. Sen "Optimization of Weld Width of Laser Welded Two Transparent Polymers"

Statement of Originality

I, Nitesh Kumar, registered on 14th May 2018 do hereby declare that this thesis entitled **Study of Laser Welding of Dissimilar Transparent Thermoplastics** contains a literature survey and original research work done by the undersigned candidate as part of Doctoral studies.

All information in this thesis have been obtained and presented in accordance with existing academic rules and ethical conduct. I declare that, as required by these rules and conduct, I have fully cited and referred all materials and results that are not original to this work.

I also declare that I have checked this thesis as per the "Policy on Anti Plagiarism, Jadavpur University, 2019", and the level of similarity as checked by iThenticate software is 8%.

Nitesh Kumar
Signature of Candidate:

Date: 09/07/25

Certified by Supervisor(s):
(Signature with date, seal)

1. _____ 09/07/25

Professor
Dept. of Mechanical Engineering
Jadavpur University, Kolkata-32

2. Nikhil Kumar 09/07/25

Scientist
Warwick Manufacturing Group (WMG)
University of Warwick (UK)

Dedicated to My
Loving Parents, Wife
&
Late Dr. Asish
Bandhyopadhyay

CERTIFICATE FROM THE SUPERVISOR/S

This is to certify that the thesis entitled **"Study of Laser Welding of Dissimilar Transparent Thermoplastics"** submitted by **Shri Nitesh Kumar**, who got his name registered on **14th May, 2018** for the award of Ph.D. (Engineering) degree of Jadavpur University is absolutely based upon his own work under the supervision of **Prof. Rajat Subhra Sen** and **Dr Nikhil Kumar** that neither his thesis nor any part of the thesis has been submitted for any degree/diploma or any other academic award anywhere before.

09/07/25

.....

1. Signature of the Supervisor with Date and Office Seal

Professor
Dept. of Mechanical Engineering
Jadavpur University, Kolkata-32

Nikhil Kumar 09/07/25

.....

2. Signature of the Co-Supervisor with Date and Office Seal

Scientist
Warwick Manufacturing Group (WMG)
University of Warwick (UK)

ACKNOWLEDGEMENT

First and foremost, the author wishes to express his **deepest sense of gratitude** to his esteemed supervisors, **Dr. Rajat Subhra Sen**, Professor, Department of Mechanical Engineering, Jadavpur University, and **Dr. Nikhil Kumar**, Scientist, University of Warwick, Coventry, United Kingdom. Their unwavering guidance, invaluable suggestions, insightful discussions, and constant encouragement have been the **cornerstone of this research journey**. Throughout every stage of this thesis, they have provided exceptional mentorship and steadfast support, which not only enhanced the scientific rigor of this work but also inspired the author to strive for academic excellence. The completion of this thesis would not have been possible without their consistent guidance and encouragement.

The author also takes this opportunity to sincerely acknowledge the late **Prof. Asish Bandyopadhyay** of Jadavpur University. His profound guidance, intellectual insights, and motivational support provided the author with the necessary inspiration and direction to conduct and complete this research work. The author remains ever grateful for the invaluable role Prof. Bandyopadhyay played during the **formative stages of his academic and research journey** and cherishes the privilege of having been mentored by such an illustrious scholar.

The author would like to extend his **heartfelt gratitude** to **Prof. Dipten Misra**, Director, School of Laser Science and Engineering, Jadavpur University. His encouragement, visionary leadership, and consistent inspiration played a **vital role in shaping the author's approach** towards scientific inquiry. Prof. Misra's unconditional support during the experimental phases of this work was invaluable and greatly enriched the quality of the research outcomes.

The author is equally grateful to **Prof. Himadri Chattopadhyay**, Department of Mechanical Engineering, Jadavpur University, for his constant encouragement, valuable insights, and unwavering support. His expertise and thoughtful suggestions helped the author navigate the challenges encountered during the research process and maintain a spirit of **perseverance and dedication**.

The author would also like to acknowledge the **significant contributions** of **Ms. Lidiya Priyadarsini Korsapati**, Assistant Professor, Netaji Subhash Engineering College (NSEC), Kolkata; **Dr. K. Ravichandra**, and **Ms. Veparala Niveditha**, CSIR-IICT, Hyderabad. Their collaborative efforts, technical assistance, and continuous encouragement greatly enriched the quality and depth of this research work. The thesis would have been **incomplete without their active involvement** and thoughtful input, and the author is sincerely grateful for their support.

Sincere thanks are extended to **Shri Soumyabrata Chakrabarty**, Assistant Professor of Mechanical Engineering, Brainware University; **Ms. Soumi Dey**, Assistant Professor of Civil Engineering, Brainware University; **Dr. Abhishek Mandal**; **Dr. Nobendu Ghosh**, Assistant Professor, Department of Mechanical Engineering, Jadavpur University; as well as the dedicated staff members of the **Department of Mechanical Engineering** at Jadavpur University. Their **cooperation, technical assistance**, and **moral support** have been invaluable throughout the various stages of this research project, and the author deeply appreciates their contributions.

The author wishes to acknowledge, with immense appreciation, the **camaraderie and support** extended by his friends and colleagues **Dr. Debayan Bhowmick**, **Mr. Anil Kumar Panja**, **Mr. Arnab Das Sarma**, and **Mr. Bidesh Bose** from the **Department of Mechanical Engineering**, Brainware University. Their valuable friendship, encouragement, and constructive discussions provided both professional and personal support during this research journey.

His **heartfelt thanks** also go to all his **friends and seniors** in the **Mechanical Engineering Department** and the **School of Laser Science and Engineering**, Jadavpur University. Their willingness to devote their valuable time, share insights, and provide practical assistance in all possible ways significantly contributed to the **successful completion of this work**. The warm academic environment and the spirit of collaboration in these departments provided the author with both inspiration and motivation.

Finally, and most importantly, the author expresses his **deepest gratitude** to his **beloved parents**, **brother**, and **sisters** for their **unwavering love, blessings, patience**, and **constant moral support** throughout the duration of this research work. Their encouragement has been the **true source of strength** that sustained the author during challenging times and enabled him to remain focused and determined throughout this academic endeavor. Without their unconditional support, this achievement would not have been possible.

Nitesh Kumar

Date: 09/07/25 **Nitesh Kumar**

Place: Kolkata

ABBREVIATIONS

LBW	Laser beam welding
Nd: YAG	Neodymium-doped yttrium aluminium garnet
TTLW	Through Transmission Laser Welding
FEM	Finite Element Model
PEEK	Polyether Ether Ketone
HAZ	Heat-affected zone
UL	Ultimate Load (N)
WW	Weld width (µm)
DOP	Depth of penetration (µm)
HAZ	Heat-affected zone (µm)
ANOVA	Analysis-of-variance
RSM	Response surface methodology
CCD	Central composite design
TEM	Transmission Electron Microscopy
DOPA	Depth of penetration of Acrylic(µm)
DOPP	Depth of penetration of Polycarbonate (µm)
DOF	Degrees of Freedom
SD	Standard Deviation
HAZ	Heat-affected zone
UL	Ultimate Load (N)
WW	Weld width (µm)
FE	Finite Element

Symbols

V	Abbe Number
n	RI-refractive index
E	Young's Modulus (MPa)
ε	Elongation at break (%)
σ_c	Compressive Strength (MPa)
ν	Poisson's ratio
β	Constant coefficients
ϵ	Random experimental error
$\beta_0, \beta_i, \beta_{ij}, \beta_{ii}$	Regression coefficients
d_i	Desirability
P	Laser Power(W)
S	Scanning speed(mm/s)
f	Frequency (KHz)
ρ	Material density (Kg/m^3)
c	specific heat (J/kg.k)
T	Temperature(k)
t	Time (s)
k	Thermal conductivity (W/m.k)
q	Internal heat generation(W/m^3)
h	convective heat transfer (W/m^2k)
T_s	system temperature(k)
σ	Stefan- Boltzmann constant (W/m^2k^4)
ε	Emissivity (W/m^2)
R_a	Reflectivity
Z_a	Depth of the beam (m)
I_a	Laser beam intensity (W/m^2)

CONTENTS

List of Tables

List of Figures

Abstract

Through transmission laser welding (TTLW) method is an innovative plastic joining technology. It is used for its well-known advantages, such as non-contaminant, non-contact processes, ease of control, and automation. Moreover, this is a flexible joining process, has quicker processing times, and can provide quality, consistency and repeatability. The present study is based on transparent-to-transparent polymer (Acrylic and polycarbonate) welding by TTLW without any absorbent. The main objective of the present study is to find the optimum process parameters for obtaining good quality weld between Polycarbonate and Acrylic sheets in lap joint configuration, with Square and Circular contour using a Nd: YVO_4 laser beam. The input process parameters studied are Scanning speed (mm/s), Power(W) and laser frequency (kHz). The output parameters considered to evaluate weld quality are Weld width (WW), Heat Affected Zone (HAZ), Ultimate load (UL) and depth of penetration (DOP). Further, the experimental results are compared with simulation studies. A finite element model (FEM) is developed for the temperature contour for Weld width and depth of penetration analysis focusing on thermal modelling and structural analysis is done by modelling (LS-Dyna). 3D response surfaces and contour plots are generated by Response surface methodology (RSM) and Analysis of variance (ANOVA) is used to measure the combined effects of input parameters on responses. Confirmatory tests were conducted to validate the results of statistical optimisation resulted from desirability function analysis. Experimental results revealed that laser power initially increased weld width, but then it decreased, whereas the HAZ consistently increased. power and scanning speed showed negative effect on ultimate load but positive effected by frequency up to a threshold limit. Scanning speed decreased the weld width up to threshold limit and then increased. Relation between frequency and depth of penetration showed contradictory trend. Lower power with higher frequency and higher power with lower frequency gives higher depth of penetration, thus stronger weld. The results of ANOVA showed that scanning speed exhibited the maximum impact on weld width (89.34%) and HAZ (80.87%). FEM simulations aligned closely with experimental data, showing an average error of 8.09%. For plates of 0.5 mm thickness, maximum ultimate load is achieved is 372.60 N at 7.89 W power, 350 kHz frequency and 2.34 mm/s scanning speed. Whereas, the minimum ultimate load of 121.15 N was obtained using a laser power of 7.42 W, frequency of 300 kHz, and the scanning speed is at 1 mm/s. Structural modelling (LS-Dyna) of laser weld predicts similar load-displacement characteristics compared to that resulting from a physical test. When all of the responses are optimized in one setting, the parameter settings are: the power of 64.2014% of 12 W, frequency of 451.1340 kHz and a scanning speed of 0.6591 mm/s.

Chapter-1

1. INTRODUCTION

Plastics are one of the fastest-growing materials in the current era owing to their light weights, durability, flexibility, weather resistance, strength and comparatively low cost. Plastics do not decay but instead can be recycled. Plastics can be used extensively in various applications, including packaging, aerospace, coating, adhesives, construction, electrical, electronics, medical, household products, and automotive industries [1]. The increasing demands of plastic products have forced the use of plastics in a new technical way so that the process by which plastics can be used should be much more environmentally friendly, faster, and safer. Laser processing of material can be used as an emerging alternative to fulfil these high precision demands of plastic processing.

Standard joining processes for different materials are threads, rivets, staples, welding, etc. Among these, welding is a very popular joining technique in which two or more materials are joined together with or without applying heat, pressure and filler materials. Welding can also be applied to join plastics. Conventional welding techniques such as TIG, MIG, Plasma Arc welding, etc., are not suitable for joining plastics because a large amount of heat is generated during these processes, which damages the parent materials. whereas, in laser welding, heating is localized and the desired power can be controlled for precision heating. Hence, the best solution for joining plastics is laser welding. The present work is carried out by an attempt to join two transparent thin plastic sheets using a transmission laser welding (TTLW) process.

1.1. Through Transmission Laser Welding (TTLW) process

Through transmission, the laser welding method is an innovative plastic joining technology. It is used for its well-known advantages, such as non-contaminant, non-contact processes, ease of control, and automation. Moreover, this is a flexible joining process, has quicker processing times, and can provide quality consistency and repeatability. The laser systems used are generally Nd: YAG laser, fiber laser, and sometimes diode laser is also used. In the case of polymer welding, the upper part should be transparent for the wavelength of the specified laser, and the lower part must absorb the wavelength of the specified laser. One thing that should be kept in mind is that at the joining interface, additives components should be used, or both the parts should be clamped together. The parts to be welded are placed under the laser head. Since both parts are pressed together with predetermined clamping pressure, the heat is transferred from

the upper part to the lower part due to thermal conduction and starts melting. Melting takes place due to localized heating of the interface, which leads to fusing together by creating weld seams.

1.1.1. Types of TTLW

There are four types of TTLW:

a) Contour welding

To generate long and 3D weld seams, contour welding is generally used. Here the laser spot is focused systematically through a predetermined pattern of welding, melting it locally. Depending upon the type of laser used and its corresponding wavelength, the width of the weld can be varied from 0.01 mm to 7.8 mm. Here the melting of the weld takes place sequentially so a small joint gap is permissible.

b) Simultaneous welding

This technique, involves simultaneous use of one or more lasers to heat the entire weld path. High power diode lasers are usually required owing to their compact design. linear welding seams are very easy to achieve. Almost any type of beam geometry can be created by means of special and state-of-the-art beam shaping elements.

c) Quasi-simultaneous welding

In this welding method, the entire joint line can be plasticized at a time. The laser provides continuous energy until the specified welding depth was achieved. To guide the laser, beam long the joint line, a galvanometer- scanner is employed. The laser beam can be guided in the X and Y directions in two-dimensional space. Owing to its quick scanning speeds, the melting of materials occurs throughout the seam of the weld joint line such that the welding components are joined in a quasi-simultaneous fashion along its seam. Measuring the collapse of melt or to monitor the melt travel facilitates the qualitative evaluation of the results of welding process. Any anomalies in the joint line can be identified by a pyrometer.

d) Mask welding

This method is to provide the possibility to generate quasi-static temperature fields. Mask welding is the combination of contour and quasi- simultaneous welding. This process is very much flexible and suitable for small series and mass production.

1.2 LASER (Light Amplification by Stimulated Emission of Radiation)

Laser is indicated by the acronym “Light Amplification by Stimulated Emission of Radiation.” Theodore H. Maiman working in Hughes Laboratories, based on the works

carried out by Arthur Leonard Schawlow and Charles Hard Townes, built the first ever laser in 1960. The main properties of a laser beam are MCC, i.e., monochromatic, coherent, and collinear. A laser differs with sources of light as it generates coherent light. Due to its spatial coherence the laser can be targeted on a specific tight and fixed spot, thus making it used in applications that requires localized precision heating, such as lithography and laser cutting. Spatial coherence also results in the laser beam to stay narrow through longer distances this phenomenon is called collimation, finding applications in laser pointer instruments. A single colour of light can be emitted owing to its properties like high temporal coherence which allows lasers to emit light with a small narrow spectrum of wavelengths. Light pulses with frequencies as short as femtosecond can be produced due to temporal coherence.

Lasers find applications in printers, optical disk drives, fibre and free-space optical communications, barcode scanners, surgical procedures and cosmetology treatments, welding and cutting of metals and plastics/composites, in law enforcement and military devices for tagging/marking targets and measuring speed and range, and for entertainment applications like laser lighting displays.

Spatial coherence can be typically expressed through narrow output beam, which is diffraction-limited. Laser beam can be focused on extremely tiny regions, resulting in very high levels of irradiance, or the shallow divergence of beam results in concentrating their power at a larger distance.

Plane Polarized wave having single frequency whose phase corresponds over a relatively large distance (length of coherence) along the laser beam implies a Temporal or longitudinal coherence. A laser beam generated by a coherent light source or thermal source has a spontaneous amplitude and a phase that varies randomly with respect to position and time, thus having short length of coherence. The components of the laser are shown in Figure 1.1.

A laser beam comprises of an energizing mechanism, a gain medium, and a means to provide the optical feedback. The gain medium is fabricated with a material with suitable properties like permitting it to amplify the light by means of stimulated emission. Light with a specific wavelength that travels through the gain medium gets amplified and its power increases. The process of supplying energy to amplify light through gain medium is called pumping. The energy is typically supplied as an electric current or as a light with a different wavelength. The pump light may be supplied with flash lamp or another laser.

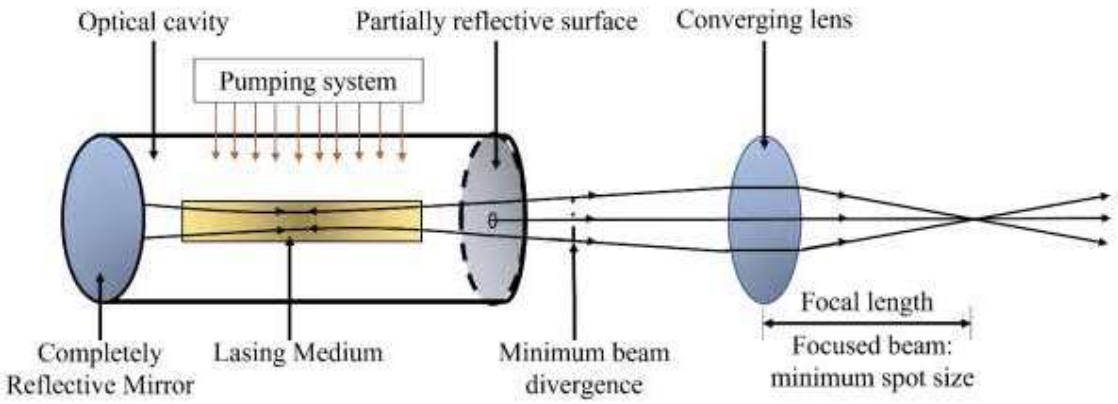

Figure 1.1 Schematic representation of Laser and its components

A laser most commonly uses a pair of mirrors on either end of the gain medium and feedback from the optical cavity. Light travels to and fro between the two mirrors, passing through the gain medium and gets amplified every time. Usually, output coupler which is one of the two mirrors is partially transparent. Depending on the design of the cavity, the light coming out of the laser may from a narrow beam or spread out in space. This device is often called a laser oscillator in analogy to electronic oscillators. Most practical lasers are comprised of additional factors that can affect the properties of the emitted light, such as wavelength, polarization and shape of the beam.

There are numerous methods of plastic welding, and laser welding is a new method. The present word demonstrates the laser welding of two types of plastics viz., polycarbonate and Acrylic in a lap joint configuration. Laser welding is a type of welding included in the fusion welding category. The required heat is produced when a focused, laser beam with high energy density irradiates the surface to be welded. As a result of heating, materials melt, and a portion of the material may vaporize. subsequently, the melted material hardens (solidifies), resulting in the weld seam. During welding, gas is provided onto the surface.

Laser welding of thermoplastics is used to be done by CO_2 lasers or by Nd: YAG laser, which is quite expensive. These techniques were generally used in the early 1990s. Laser transmission welding (LTW) a popular technology used to weld two overlapping thermoplastics of the same or different optical properties uses a laser beam. This technique requires two parts of materials: transparent material that allows the laser beam

to pass through and an absorbent material which absorbs. Two parts are overlapped and pressure is created between the parts. The laser beam travels through the joining seam under pressure. The transparent upper part transmits most of the radiation, and it is absorbed by the lower part, creating localized heating to a certain depth at the joining surface, corresponding to the absorption coefficient and the thickness of the lower part.

1.3. Literature Review

The polymer is known to be an important engineering material due to several reasons. The combination of a wide range of properties like toughness, good strength to weight ratio, non-corrosive, good chemical resistance, moisture resistance, low thermal and electrical conductivity, ease of fabrication into complicated shapes, etc. are unattainable from any other materials. In addition, more desirable properties can be achieved by incorporating various compounding ingredients such as reinforcing agents, colorants, plasticisers, stabilizers, flame retardants, etc.[2].

Laser transmission welding (LTW) uses a high-energy-density joining process. Initially, it was used to join moulded thermoplastic articles or films. Nowadays, it has become an established process for welding polymer products including composites [3–5]. They are widely used in industries like automotive, microelectronics, aerospace, medical, packaging, optoelectronics, microsystems, etc. [6]. Welding of different materials having varying thicknesses and configurations is also possible using this technique [7]. Through an industrial perspective, the key advantage of LTW is the reproducibility of the process without wear and tear of the tool combined with increased productivity and better quality. It is a non-contact, flexible and easily controllable process with almost no contamination [8]. Through laser, narrow and localized heat zones can be created. However, there are various investigations still going on in this field.

Through Transmission Laser Welding abbreviated as TTLW is a process which is a specialized variant of laser welding primarily used for joining thermoplastics. TTLW utilizes a transmission laser beam that passes through one of the transparent components to be welded. The absorbing component (typically the bottom component) absorbs the laser energy, generating heat at the joining surface between the two parts. The heat melts the interface, allowing the parts to fuse together. TTLW is suitable for joining transparent or translucent thermoplastic materials. Common materials include acrylics (PMMA), polycarbonates (PC), polystyrenes (PS), and polyethylene terephthalate glycol (PETG).

Both parts must be transparent or translucent to allow the laser beam to pass through one of them.

TTLW process is widely used with varying types of lasers for joining plastic parts [9]. CO_2 laser produces an infrared (IR) light beam with wavelength bands around 10.6 µm [10]. This type of lasers is limited to welding of films with less thickness (micrometres to 1 mm). Whereas, the Nd: YAG type lasers and diode lasers are suitable to weld thick parts because of the high transmission of the polymers in near Infra-red field [11]. Diode lasers are the most widely used lasers in industries due to their compactness, modular set-up, high energy efficiency and relatively low cost per watt of photon energy [12–14] . The difficulty in joining the plastic parts can be overcome using this innovative type of laser [15–17]. Apart from some research publications, little information is available in the field of LTW of polymers. Although many experiments, process optimization [1,18–20], modelling [21–24] and analysis emphasizing morphology [25–28], performance evaluation, etc. were performed, during the survey of literature, curtains gaps were observed.

1.3.1. Process overview of through transmission laser welding

The most basic configuration of TTLW few welding polymers is an overlap joint arranged by placing a transparent polymer work material on top of absorbing polymer [15,18,19]. The laser beam is transmitted through the transparent upper part and is transformed into heat energy by the lower part (absorbing) [29]. Both parts are to be joined by clamping together during the process. As a result of this clamping force, the two surfaces come close to each other and this intimate contact results in heat conduction from the absorbing lower part to the transmissing part. This allows both parts to melt and create a joint only where the laser beam is directed. Nearly all thermoplastics can be welded using this technique. Special additives/pigments also allow TTLW of two opaque materials as well as two transparent workpieces [30–32]. To determine whether two polymers are wieldable, i.e., weld compatible, weldability charts are presented for six selected materials by Juhl et al.[15]. TTLW has various advantages as compared to conventional welding techniques viz., hot plate welding, ultrasonic welding and adhesion. While these techniques have their own significance, each one has its own limitations related to either the process, or the materials besides dedicated tooling requirements. In terms of

operational costs, electrical power efficiency of diode lasers is 30 per cent greater when compared to typical levels for CO_2 (10%) and Nd:YAG (4%) [17].

It is clearly observed in various studies of TTLW of polymers [33–36] that the main influencing factors are scanning speed, laser power, spot radius, clamping pressure, stand-off-distance, frequency, energy density etc. In this subsection, the major parameters of TTLW have been discussed in brief.

a) Laser power

The laser power is the main source of heat in TTLW [37]. In general, higher power allowed greater travel of speeds for welding and faster welds required higher power. The weld width(WW) increases with increasing laser power [1,20,29,38,39]. During TTL (through transmission laser) diode welding of transparent acrylics to opaque ones (thickness= 4 mm), it was observed that a joint strength increases with an increase in laser power (19-24 W) [23]. A similar result for LTW of white thermoplastics to polycarbonate (PC) (in terms of breaking load) and polyamide (in terms of the maximum load) has been achieved by Mamuschkin et al. [40] and Chen et al. [41] respectively. It is also found TTL (through transmission laser) (Nd: YVO_4) weld of the transparent acrylic (thickness of 0.5 mm) and transparent PC (thickness= 0.5 mm) that weld width increases and breaking load decreases with the laser power (7.6-11.6 W) [24]. The results of the laser welding of ABS (acrylonitrile butadiene styrene) and PC based polymers using CW diode laser with a laser power ranging from 8 to 6 W and scanning speed (SS) of 1.5k, 3k, and 4.5k mm/min concluded that the weld width decreases as the total heat input decreases by increasing the scanning speed or lowering the input power. While no regular trend has been obtained between heat input and average shear strength [20], it was observed during diode laser welding of native and black acrylic plaques containing carbon black (CB) 0.2 wt.% as a colour pigment of dimensions 80 mm * 35 mm * 4 mm each that weld width and shear strength of lap joint increases with the laser power [20]. Tao et al. [42] have obtained a maximum shear strength of 2052N with an optimum power of 700W. They concluded that the optimum power resulted in a large interfacial joining area with no decomposition. It can be inferred from their observations that increase in power results increased joining area up to certain extent and further

An increase in power results in decomposition which in turn reduces the joint firmness. It is also found from the perturbation plot that the joint strength and weld width increases with the laser power in laser transmission joining of PC (thickness= 1 mm) while laser power has a non-significant effect on joint cost [43]. The penetration depth (DOP) against given laser power has been calculated for the poly(propylene) (PP), the low density polyethylene and the high-density one. It has been concluded that the penetration depth increases with laser power for all type of polymers [44]. The results of LTW of polyethylene terephthalate (PET) and PP showed that weld width and depth in absorbing PP increase with laser power [39]. The work of Chen et al. [45] and Coelho et al. [46] shows that the weld strength of LTW of polymers varies with the energy density. They have concluded that there is no regular trend between energy density and weld strength. It has been noticed by Dwivedi and Sharma [47] that the strength of joint of PET and 316 SS (stainless steel) weld increases with the increase of laser power. This is because in the laser transmission joining process, the input heat increases with the increasing laser power resulting in an increased width of the weld seam. Higher the weld width, higher will be the melting joint area [36], and consequently the joint strength. Literature by Ilie et al. [48] reveals that the failure force of diode laser welded ABS first increases then decreases with laser power and hence is the trend for the joint strength concerning the line energy in diode LTW process [49–51]. This is because the heat induced to work materials increases until the line energy reaches a threshold value which would result in improving the joint strength. Above the threshold limit of line energy, the input heat to the material gets excessive resulting in the material burn and partial decomposition, and hence lowering the joint strength. Ghasemi et al. [36] developed a model that simply explains the effects of various process parameters on meltdown characteristics in quasi-simultaneous laser welding (QS). They found that increase in power reduces induction time and overshoot and hence produces higher meltdown when the no. of passes is kept constant. Devrient et al. [52] have found that with increasing the laser power, the cross-section of the heat-affected zone (HAZ) gets bigger and becomes more elliptical or lenticular in shape (losing the symmetry to the joining plane). Tao et al. [42] studied the effects of laser power on the adhesion between the graphene layer and the PC surface. Later, they also studied the effect of bending on the capacitance of the laser irradiated super capacitors.

b) Scanning speed

Scanning speed (SS) is one of the significant factors which can increase the productivity of welding process. In addition, weld width, joint strength, joint cost and depth of penetration are affected by the welding speed [38,43,53]. At a lower scanning speed, an increased irradiation time is required which results in degradation of the polymers due to overheating and consequently a lowered joint strength. Whereas, increasing the welding speed beyond threshold value leads to a lower irradiation duration [51], In turn causing a lowered input heat and a lack of penetration [36], which also decreases the joint firmness [19]. During TTLW of polymers, it has been concluded that the scanning velocity has a negative effect on the joint strength [19,38], while, weld width and joint cost decreases with the welding speed. The velocity has a significant effect on the joint cost. Productivity rate can be increased by enhancing velocity within acceptable joint strength range and joint width [43]. Experiments of Carbon Fiber Reinforced Thermoplastic (CFRTP)/SS (stainless steel) laser direct joining was carried out by Jiao et al. [43], and they have concluded that the scanning speed had a great effect on the size of the thermal defect zone and the joint strength. The laser weld strength of polymers is influenced by various factors like the crystallization (non-isothermal), the growth rate of germs and recrystallization induced dimensions of the Heat affected zone (HAZ) induced. Increase in the welding speed resulted in reduction in the maximum temperature consequently resulting in a faster cooling rate and vice-versa [48]. During the welding, the polymer elements ware heated to the temperature range where crystallization occurs and that range exists within the melting temperature and glass-transition temperature. Crystallinity is a factor strongly dependent on the heating or cooling rates of the polymers [54]. Casalino and Ghorbel [44] have investigated the effects of welding speeds on the keyhole depth of CO_2 laser welding of PP in butt and lap joint configurations of 4 mm thickness. They have observed the keyhole depth decreases with the welding speed due to a decrease in the line energy. The depth-to-width (D/W) ratio of the molten pool has a significant influence on the shear strength (SS) of through transmission welding of the polyethylene terephthalate (PET) and PP. The weld width and depth increase with lower welding speed. However, increase in the shear strength occurred gradually during initial phase and then quickly decreases with the increase in the ratio of D/W [39]. Transmission laser welding of 0.5 mm thick PET plate using incremental Scanning Technique (TWIST) mode and conventional contour welding mode has been investigated by Wang et al. [55]. They have found that

the welding speed has inverse effect on shear strength at TWIST mode, while there was a small change in the shear strength values of the welded lines obtained by traditional contour welding. This is because, in the traditional contour welding, at lower welding speeds the effect of crystallization counteracts the diffusion while the immediate reduction in the melted as well as fused area decreases the shear soundness at the TWIST mode [56]. In the case of QS welding, when compensated with no. of passes, an increase in scanning speed was observed to reduce total weld time and in turn reduce total meltdown [42].

c) Stand-off-distance

Kumar et al. [18] have studied the influence of stand-off-distance (30-34 mm) on diode laser through transmission welding of acrylics. They have found that with an increase in the stand-off-distance, weld width and joint strength decreases. It may indicate that laser spot diameter decreases with increasing strand-off-distance and the weld width becomes narrower. Due to the decrease in weld width, a lesser amount of material is fused. Further, heat conduction between the materials is not sufficient [49]. Thus, joint strength is decreased. In the work of Acharjee et al. [19], diode laser through transmission welding of acrylics has been conducted at varying stand-off-distance (6-15 mm). They have found that joint strength increased with an increment in the focal range up to 9 mm which is followed by a decrease in focal range as the focal distance increases beyond this point. It occurs because of variation in focal distance of the beam controlling the beam spot area. The perturbation plot [29] reveals that the seam width of the weld differs proportionately with the stand-off distance. Enhancing the stand-off distance increases the size of laser beam spot targeted at the weld interface, which results in the dispersion/spreading of the beam energy onto a wider area. Consequently, the native/original material of the weld zone being melted leading to an enhancement in weld seam width. In the work of Wang et al. [38], a statistical technique has been applied to correlate the stand-off-distance and output variables such as weld width (WW), weld depth in the transparent PET (DT), maximum temperature at the weld interface (T_{max}), the temperature maximum of the upper surface of the transparent PET(T_{top}), etc. Also, the model has been validated with the confirmatory tests. Wang et al. [39] have studied the effect of stand-off-distance on the depth of penetration of LTW of polyethylene terephthalate (PET) and Polypropylene (PP). It has been concluded that molten depths increase as stand-off-distance decreases.

This is because stand-off-distance and localized laser energy density and also the molten depths are inversely related.

d) Clamping pressure

Clamping pressure is required to decrease the gap between two polymer plates/sheets. Since heat conduction between the two plates is more important in the TTLW process. With an increase in the clamping pressure, the weld width increases. This may be due to an increase in effectiveness of the intimate contact between the two plates. Kumar et al. [18] have found that clamping pressure has the most influencing effect on the weld width but without significant effect on joint firmness as well as on the joint cost of LTW of PC as mentioned by Wang et al. [42]. The effect of clamping pressure (0-0.8 MPa) on the joint strength of fibre laser welding of CFRTP and SS was studied by Jiao et al. [43]. It has been found that the matrix of PPS melts sufficiently because the pressure at clamping is in the range of 0.1 to 0.2 MPa. The melted PPS was extracted out from the CFRTP/SS interface and the molten PPS for bonding has been lowered when the clamping pressure was raised beyond 0.2 MPa. Consequently, the joint firmness is lowered gradually as the clamping pressure is greater than 0.2 MPa and the highest shear stress has been obtained at 0.15 MPa clamping pressure. A similar trend has been obtained in the study presented by Huang et al. [38] and Liu et al. [50] that the joint strength first increases and then decreases with the increase of clamping pressure in diode LTW process. The response surface plot for the failure force as a function of laser power (10-20 W) and clamping pressure (0.4-0.55 MPa) has been indicated that the optimal zone has to be navigated towards low laser power and high pressure [48]. The meltdown rate has not changed with pressure. However, the total meltdown increased with pressure [36,51] in LTW, using a T-shaped test assembly. There is a possibility to form almost perfect welds using dual clamping devices by employing proper welding parameters and the risk of poor weld seam quality can be avoided or downtime due to imperfect or contaminated clamping devices, or improperly clamped joining components [57]. Clamping pressure was also observed to reduce induction time in QS welding [42].

1.3.2. Weld quality and performance characteristics

Generally, the laser welding performance is measured in terms of increase in the welding speed, joint cost and weld quality. Weld quality can be analysed in terms of the enhancement of mechanical properties viz., failure force, hardness, joint strength, fatigue

strength, and structural/molecular characteristics such as the germs growth rate, non-isothermal crystallization, crystallinity of material and the dimensions of the induced Heat affected zone (HAZ) by recrystallization with reduction or elimination of defects in the weld.

1.3.3. Optimization based studies of TTLW

There are different parameters of welding viz., scanning speed, spot size, laser power, clamping pressure etc., that influence the weld quality (joint strength, weld width, depth of penetration etc.). Optimization techniques applied for the welding process are necessary for continuous improvement of the welding process. Depending on the nature of the TTLW process, researchers have applied different optimization techniques for response/parameter optimization to improve the weld quality. Kumar et al. [18] have applied grey relation analysis to solve the multi-response, i.e. joint strength and weld width simultaneously, to convert multiple optimization problems into a single objective problem. Finally, grey relational analysis is coupled with Taguchi method to analyze and optimize the LTW process. An experimental investigation of LTW of acrylic has been conducted by Acharjee et al. [19]. They have chosen Taguchi orthogonal arrays for the design of experiment and optimization of process parameters (welding speed, power and focal distance). They have determined the best parametric combinations for the maximum weld strength as the laser power at 28 W, welding speed at 5 mm/s and focal distance at 9 mm. From the ANOVA results of laser power, weld strength is the most important factor followed by focal length and welding speed. Kumar et al. [1] have performed a multi-objective optimization of TTLW of different plastics using response surface methodology (RSM). They considered a power of 7.60 to 11.60 W, scanning speed of 0.66 to 2.34 mm/s and frequency (198.86-451.13 kHz) as input factors while ultimate load and weld width have been measured as responses. The optimum parametric combination for maximizing of breaking load and minimizing weld width has been obtained with analysis of desirability function as the laser power at 7.60 W, a welding speed at 1.26 mm/s and a frequency of 372.09 kHz. It has also been found that the power and SS (Scanning Speed) is the most significant factor for breaking load and weld width respectively. Shin and Choi [20] have studied the energy optimization design for laser polymer (ABS and PC) welding processes. The melt zone measurement and HAZ are performed to find the welding energy threshold and the mechanical parameters of welds. The impact of welding process parameters viz., welding speed, laser power, size of the

laser beam and clamp pressure, on weld width and the lap-shear strength for LTW of acrylic (PMMA), with a diode laser system has been studied by Acherjee et al. [29]. They have chosen RSM to develop the mathematical relationships between output variables of the weld joint and the welding process conditions to determine the welding input parameters that lead to the desired weld quality. Similar study has been performed on polymeric laminate structures made of PPMA and aluminum 6061-T6 using laser welding done by Bideskan et al. [58].

Wang et al. [38] built a thermal model based on a combination of finite element method (FEM), genetic algorithm (GA) and RSM techniques to improve the accuracy of the model prediction with a minimal number of trials. In another study, Wang et al. [59] used CCRD (central composite rotatable design) to plan the experiments for laser transmission welding of thermoplastic samples. The input parameters considered were clamp pressure, laser power, joining velocity, scanning number while the responses considered were weld strength, width and cost. Among all the process parameters, velocity along with scanning number has a considerable effect on the joint cost. In addition, they concluded that the RSM models are more suitable to represent the relationship between the process parameters and the responses. Jiao et al. [43], optimized the joint quality of CFRTP/stainless steel joints with laser power, the scan speed and the clamping pressure as process parameters. Their joint quality was assessed based on thermal defect zone width and the joint strength.

Katsiropoulos et al. [53] have applied a generic optimization concept using LTSM-OPT software tool for the optimization of thermal process cycle and laser welding unit parameters for both the quality and cost of the produced part (thermoplastic composite materials). Vidal et al. [60] have developed a customized laser system to obtain high-quality weld seams with weld widths in the range of 0.7 to 1.4 mm. During laser-assisted processing of thermoplastic composites, the individual effects of input parameters on the responses cannot be easily separated without carrying out a large number of experiments. To investigate the impact of process parameters individually from a min number of tests, the Taguchi method has been adopted by Mazumdar and Hoa [61]. They have selected L_9 orthogonal arrays for experimental design, and the ANOVA technique has estimated the percentage contribution of each factor to the quality of bonding. In research of Amanat et al. [62], the effect of the weld process conditions namely laser power (40-80 W) and irradiation time (10-50 s) on the bond quality of Quasi-simultaneous laser beam welded

polyether ether ketone (PEEK) has been studied. They have determined that the laser power is the limiting parameter for bond firmness, while irradiation time has limited effect and the optimal laser power for bonding has 65 to 75 W which results in bond firmness varying from 20 to 45 MPa. Labeas et al. [63] have studied the optimization of the LTW process for thermoplastic composite parts using thermo-mechanical simulation. Dwivedi and Sharma [47] have applied central composite RSM to optimize the LTW of PET and 316L stainless steel. They have determined the optimum values of joining speed, laser power, and stand-off-distance as 18 W, 100 mm/min, and 2 mm respectively, to get the maximum joint strength predicted as 88.48 MPa. The Central Composite Design (CCD) matrix and RSM have been applied in developing the experiments to evaluate the effects due to interaction among the input variables on the destructuring of azo dye solution of AR 274 by wet air oxidation method [64]. In the research of Wang et al. [65] and Acharjee et al. [66], the artificial neural network (ANN) has been employed to establish the relations between laser transmission joining process parameters with joint seam width and joint strength. Wang et al. [65] have applied the desirability function in addition with a genetic algorithm to perform the optimization of the joint width and joint strength. Whereas Acharjee et al. [66] have used multiple regression models for the prediction of responses. Effects of the power intensity of the laser and travel velocity on the joint performance of PETG and stainless steel have been extensively investigated by Tillmann et al.[67]. They have concluded that an increment in laser power and decreasing travel speed led to increase the fracture load to an optimum level. This is due the polymer melting sufficiently and leading to the wetting on the steel side while avoiding the decomposition the polymer sheet, and thus leading to a high joint strength [67]. Innovations in laser welding of thermoplastics and multi-parametric optimization of the mechanical performance of weld joints, generated through transmission technology, requiring basic processing parameters and materials properties have been studied by Kagan [68]. A study on optimization of CO_2 laser welding parameters for PP-clay nanocomposite welds has been conducted using Taguchi method [69] and RSM [70]. Hubeatir [71] has applied Grey relational analysis and Taguchi method to perform multi objective optimization of Laser welding of PMMA using IR semiconductor. He noted that while larger weld widths resulted in stronger welds, deeper penetration results in weaker weld due to the formation of bubbles and porosity. Bhattacharya et al. [72] investigated the effects of power, frequency and scan speed on the geometry of the weld made between Polycarbonate and Acrylic using TTLW. They used an empirical model

through RSM and further performed analysis of variance (ANOVA) to identify the significant parameters with respect to the responses.

The optimization of TTLW process presents numerous challenges due to the intricate interplay among process parameters and inherent system variability. A primary difficulty lies in the nonlinear relationships between welding parameters, which complicate the development of accurate predictive models. Additionally, optimized conditions are often highly specific to particular materials and experimental configurations, limiting their generalizability across different applications. Although statistical techniques such as Response Surface Methodology (RSM) and Taguchi methods are employed to streamline experimentation, these approaches still demand considerable time and resources. Furthermore, often conflicting objectives such as maximizing weld strength while minimizing cycle time frequently necessitates simplifying trade-offs into a single metric, which can obscure critical performance nuances. The reliability of optimization efforts is further compromised by uncontrolled variables, including environmental fluctuations and material inconsistencies.

1.3.4. Simulation-based studies of TTLW

During the TTLW process, finite element simulation of the transient temperature distributions can help in optimizing the processing parameters and material. Accurate estimation of temperatures depends on accurate information of the laser heat source at the weld interface and properties of the work material. In the research of Chen et al. [21], a model was formulated to explain the laser energy distribution characteristics in light scattering polymers. The model comprises of two parameters namely the scattering standard deviation and the beam scattering ratio. After that, the models have been validated using polyamide-6 (PA6), polyamide-6 glass fiber (PA6GF) and PP parts. A three-dimensional, finite element model (FEM) has been constructed by Chen et al. [22], to simulate heat transfer in contour LTW of an amorphous polymer (PC). The modelling results have been found to be in agreement with the experimental observations of weld initiation power and the weld width. Also, the simulation results implied that, in contour welding of Polycarbonates (PC), welding gets initiated once the temperature at the weld interface increases up to the maximum of 200 °C. Aden [23] studied the temperature profile and heat propagation in the joints with respect to Gaussian- and M-shape beams for laser-transmission welding of PC (a non-scattering polymer) and polybutylene terephthalate (PBT) (a strong scattering polymer). He found that for PC, Gaussian beam

generated a non-homogeneous weld seam while an M-shaped beam produced a seam with constant thickness and width. In the case of PBT, he found that both the types of beams generated similar seams. Aden attributed the similarity in seams of PBT to strong scattering nature. In the previous study of Geiger et al. [24], FEM has been used to understand the effect of the optical characteristics of PP on temperature field and geometry of the molten pool during the joining process. They have claimed that their approach can be advantageous in detecting the heat earlier such that the welding portion could be redesigned. Hadriche et al. [54] have established the reliability of a numerical model as per the finite difference method by computing the soundness variables of diode laser welding of PP thermoplastic polymers. Microscopy observation of experimental PP welds has validated the numerical model. They have concluded that the welded parts endured the thermal cycle involving an isotherm cooling that leads to morphological changes due to the phenomenon of non-homogeneous recrystallization. An integrated experiment and simulation study has been carried out to optimize the laser-assisted joining of metals and plastics by Lambiase et al [73]. In the research of Casalino and Ghorbel [44], the model has been developed for PP in keyhole and conduction mode in butt and overlap configurations. They have found that the maximum strain and stress values are very low for the deep penetration welding (0.000889 N/mm^2 and 1.36195 N/mm^2 respectively) as compared to the conduction welding (0.0008056 N/mm^2 and 1.25272 N/mm^2 respectively).

A numerical model has been made by Zoubeir and Elhem [74], considering the following process parameters: a constant laser incident power P (100 W), a constant beam scanning speed SS of 110 mm/s and a clamp pressure of 0.3 to 0.5 MPa to study the temperature field and residual stresses distribution for diode LTW of a PP mini-tank. A model has been made for PET and PP polymer welding to find the relationships of welding parameters, molten pool geometry (width and depth) and shear strength [39]. They have found that the width and depth increment in the whole design space with enhancing laser power, lower stand-off-distance and lower welding speed. Also, the results implied that the molten pool's depth to width (D/W) ratio has a evident influence on the shear strength. Aden et al. [75] have developed a thermal simulation for PA 66 polymer to calculate the temperature distribution and the distributions vertical to the scan direction are compared against their corresponding microtome cuts of the joints. The distribution of temperature in a plane parallel to the welding zone has been used to calculate an area where the

temperature is more than the melting temperature but below the degradation temperature of the polymer. Mayboudi et al. [76] have concluded that when scattering of the laser beam has been accounted for in the thermal model, the agreement between the thermal imager and model has improved significantly. Hence, the beam scattering is an important factor to be considered in thermal modeling of the LTW process. A two-dimensional thermal model has been developed by Becker and Potente [77], to simulate the phase of heating of the Laser thermal welding(LTW) process along the moving laser direction using Finite element modelling (FEM). They have validated the results with experimental data with PP.

Modelling has been developed by Liu et al. [78], for laser heat source by considering light scattering during LTW. They have proposed an algorithm for the energy transformation to transform the line energy intensity to the point energy intensity. The weldability of a polymeric material through simulation has been studied by Ilie et al [79]. Using IR thermography, the results of the simulation has been validated. The welding of fiberglass-doped PP and fiberglass-doped ABS is much difficult because of its low laser transmittance, and Chen et al. [45] have investigated the inter-relationship of welding factors viz., molten pool area and shear strength in welding of PP(fiberglass-doped) and ABS(fiberglass-doped) using simulation and experimentation. Coelho et al. [46] compared weld quality and efficiency for beam spots with circular and elliptical geometry. They found that the joint strength was higher for beam spots with larger diameters, and beam spots of elliptical shape increased weld efficiency, thus resulting in faster processing speeds and/or saving on required laser power. They attributed the higher strength in case of elliptical beam to the longer contact which caused higher heat input to the joint. LTW of polymers causes a high thermal stress at the joint region. Irregular welding parameter combinations can destabilise the joint structure or leads to thermal decomposition of the polymer [80]. A Numerical model has been developed by Flock et al. [80] which allows the prediction of the HAZ and the resulting maximum temperature in LTW that fecilitates an initial optimization of the welding process in advance and helps to reduce the process development time. An efficient tool has been developed by Ilie et al. [48], for determining the weldability of polymeric materials for the reduction of time and costs with the experimental exploration. A thermal simulation model for simultaneous welding of the semicrystalline polymer has been developed which supports determining the size of the HAZ, weld width and shear strength [81]. They have found

that the simulation-based size of the HAZ shows a high similarity to the dimensions of the HAZ found with light microscopy. In the research of Sooriyapiragasam and Hopmann [82], studied the thermo-mechanical simulations for TTLW for the determination of residual stress distribution in the weld seam depending on the welding characteristics. A non-destructive method (IR thermography) has been used for temperature measurement of the joint interface for the live monitoring of the welding process. The temperature profiles derived by IR thermography for a PMMA–ABS/PC couple are compared with those obtained from numerical simulations during the cooling and heating phases. They validated the numerical model with the experimental data [83].

In the work of Mayboudi et al. [84], thermographic observations of the laser-transmission welding (LTW) with a fixed laser beam have been carried out using different surface coatings. The model has been created for the joint between two polyvinyl chloride (PVC) parts from first principle of heat transfer. This model employs contact conduction which is a function of temperature and pressure , Gaussian laser distribution, and many other material properties that differ with varying temperature including the coefficient of absorption [85]. Thermal joint conductance model has been constructed using contact mechanics principles and basic material properties to predict the thermal conductance of metal/polymer joints and are further validated experimentally [46,86]. An empirical equation has been proposed to relate Young's modulus to the thermal expansion of the highly oriented polymers and the experimentally validated over a wide temperature range: from cryogenic to melting temperatures by Bronnikov and his partners [87]. In the research of Kurosaki [12], the simultaneous radiation and conductive heat transfer in Infra-Red welding of thermoplastics devoid of surface damage assisted by a transparent heat sink material(solid) have been studied theoretically and experimentally using a CO_2 laser as an IR source and ZnSe as a transparent heat sink material. crystallization kinetics of isothermal and non-isothermal melt isotactic PP (iPP) have been investigated using a Differential Scanning Calorimetry (DSC) method by Mubarak et al. [25] and Albano et al. [26]. The isothermal melt crystallization kinetics have been analysed using the Avrami equation [26,27]. Kneip et al. [28] have developed a model of energy exchange, based on the FEM to measure the thermal field for partially transparent polymers which were irradiated by a laser and the experiment portion of the study was carried out using a diode as laser source and an IR thermographic camera. A mathematical model utilising Green's function method has been constructed to study the pattern for temperature distribution

and heated areas in a material irradiated by high-energy laser beam [88]. It has been found that there is a considerable impact of weld parameters such as beam power diameter, defocused distance and material properties on the heat shape and size of the heated region or HAZ. A model of the laser diode stack derived from the Zemax ray tracing software that functions in a non-sequential mode has been evolved and verified by comparing the experimental and simulated transverse irradiance profiles at multiple positions along the caustic formed by a lens [89]. Naqwi and Durst [90] have presented a mathematical analytical model of a diode based laser beam, employing Gaussian and Lorentzian distributions. This is appropriate for mono-mode diode lasers, with active layers thinner than the wavelength. A numerical and experimental study of LTW of polyethylene terephthalate (PET) and Ti-6Al-4V has been performed to analyse the weld geometry, molten pool, porosity formation and fluid flow etc., by Ai et al. [91]. They have identified the porosity in the high-temperature region occurring due to the PET decomposition, which has been noted similarly during the experimentation as well. The thermal decomposition of materials heavily influences the joint strength in LTW. Joint strength is decreased at higher temperatures due to thermal deconstruction of material. Hence, Potente et al. [92] have developed a 3-D transient thermal model combining a pyrolysis kinetic model to predict the thermal degradation and melt displacement of polyamide 66 (PA66). In the research of Wilke et al. [93], simulation has been conducted for quasi-simultaneous and simultaneous laser welding processes, including the heating and cooling phase, using temperature-dependent data. Also, the convective cooling and emissivity at the surface of the adherents have been taken into consideration. Chen et al. [22] coupled Rotary-Gauss body heat source with Gauss plane heat source to develop a 3D finite element model to predict the temperature distribution and weld pool geometry in welding of fiberglass-doped polypropylene (PP) and fiberglass-doped acrylonitrile butadiene styrene (ABS). Grififfths and Dowding [94] developed a finite element model for simulating heat input during laser welding of polyethylene film and polypropylene substrate to predict the effect of input parameters on the peel force. Then they used a genetic algorithm to optimize the peel force with respect to the process parameters power, scan speed and spot diameter. In another study done on polycarbonate by quasi-simultaneous laser welding of by Acherjee [95], 3D finite element method on ANSYS platform was used to simulate the heat transfer. The process variables including power, weld speed, no. of passes and line energy were optimized by considering temperature profile, weld pool geometry and time-temperature trend as output parameters.

Modelling limitations in TTLW significantly hinder the accuracy and predictive power of simulation tools. A common issue is the oversimplification of light scattering, where the emission of beam scattering effects in translucent polymers reduces model fidelity. Additionally, many models employ static material properties, disregarding temperature-dependent variations that are critical for accurate thermal predictions. The effects of thermal degradation, including pyrolysis and gas evolution during overheating are frequently ignored, leading to incomplete thermal and structural analysis. Experimental validation is often limited, with many models lacking comprehensive real-world verification. Heat source representations are typically idealized using Gaussian or other simplistic profiles, which may not accurately reflect the actual laser beam distribution. Furthermore, the modelling of interface contact is frequently oversimplified, neglecting the impact of clamping conditions and surface roughness on heat transfer and joint formation. Mechanical effects, such as residual stresses and deformation, are seldom incorporated despite their significance in post-weld performance. The majority of simulations focus solely on single-pass welding, with little attention given to more complex techniques like multi-pass or quasi-simultaneous welding. Real-time integration with adaptive feedback control is notably absent in most models, limiting their applicability for in-process optimization. Joint geometry modelling also remains limited, with an emphasis on simple configurations while neglecting the complexities of industrial geometries. Despite the availability of advanced laser–material interaction models, their high computational cost has led to underutilization. Lastly, critical welding phenomena such as melt flow, melt pool dynamics, and phase changes are often neglected, resulting in models that fail to capture the full physical reality of the welding process.

1.3.5. Morphological characterization-based studies of TTLW

The effects of process parameters viz., the welding speed (3–6 mm/s) and laser power (20–40 W) on the geometry and the microstructure of the diode laser welded PP have been investigated by Ghorbel et al. [13]. They have determined the influence of selected welding parameters on the seam geometry, material crystallinity and defects at different zones of the welded part. They have found that the increasing the laser power and the decreasing the scanning speed simultaneously led to an increase in the volume of the weld zone and depth of penetration. Higher values of laser power and low scanning speed can

lead to degradation of structural, morphological and optical properties of polymers which is undesirable [96]. This was evident in the Microscopic (FTIR) Fourier transforms infrared spectroscopy method that showed that the diode-based laser welding stimulates thermal destructuring of the PP by random incisions in the polymer chains. Also, an increase of the crystallinity index at the cross-section of the welding joint has been noted with a maximum crystallinity recorded at the central region of the weld zone. Heat energy from the laser that got stuck within the polymer layers and may lead to a rise in heat in deeper regions [12]. Certain process parameters resulted in creation of a void due to the thermal destructuring and vaporization of the PP [97,98]. Prabhakaran et al. [51] have found that maximum weld strength is achieved at low laser power and at lower laser speed. It has been found that the partially melted iPP can crystallize very quickly at high temperature (material left out without melting can increases the basic nucleation rate, and the structural order of the polymer melted can fasten up the linear growth rate of spherulite). The Avrami equation describes the initial stage of non-isothermal crystallization [99] given in Equation 1.1.

$$X(t) = 1 - e^{-ktn} \tag{1.1}$$

Where, X(t) is the fraction of material transformed at time t. k is the rate constant related to the nucleation and rate of growth. T is the time. n is the Avrami exponent, which depends on the nucleation mechanism and the dimensionality of growth.

A significant decrease in crystallization rate has been observed which follows the decreased molecular mobility due to an increase in molecular weight, and a decrease in crystallinity associated with the structural defects created along the chains by the branching process. To eliminate the self-nucleation phenomenon, it is essential to bring the polymer to temperatures where decomposition is already existing [34,97]. Various compounding ingredients are added to the polymer matrix which influences the transmission characteristics including the laser wavelength [100,101]. In LTW of thermoplastics, CB is used often for absorption of laser energy and to convert it into heat energy in the absorbing polymer. Acherjee et al. [102] stated that the dosage of CB determines the optical penetration depth. Wang et al. [30] have presented a technique for quantification of morphology of CB in PC and PA6 used in laser welding applications. The microscopic structure of the CB has been revealed by transmission electron

microscopy (TEM). The TEM photos/micrographs of CB have been quantitatively studied using the image processing technique. The microscopic structural details and parameters such as size, shape and distribution of CB particles and aggregates are studied. Transmission electron microscopic images of the weld joint demonstrated that 304 stainless steel(SS) and the PET has been bonded on the atomic, molecular or nanometre level structure through a Chromium oxide film [103]. Abed et al. [104] have studied the LTW of PP using diode laser. They have found that the crystalline morphology observed in different zones in the welded part has related to the specific thermal cycle. Meyer et al. [105] used optical coherence tomography to study the quality of weld in silicon chip bonding. They concluded that by using appropriate wavelengths of light, variable refractive indices of the joining materials can be compensated to accurately assess the quality of the weld. A similar study has been made by Frick and Schkutow [106] in which they observed that scattering decreased with a wavelength increasing from 800 nm towards 2500 nm. Cosson et al. [107] developed an optical method to calculate the extinction coefficient and weld ability of semi-transparent plastics using a laser light as source and a camera to measure the light transmitted through the samples. They related the thickness of the sample to the melting. They suggested that this method could be used to optimize the power along the weld. Optical coherence tomography has also been found to be a promising non-destructive technique to assess the quality of the weld formed by laser transmission welding. In the work of Ma et al. [108], synthesis and characterization of poly (propylene carbonate PC) glycol-based water-borne polyurethane (PU) with a rich solid content have been investigated. The particle size and emulsion distribution patterns were calculated and studied by Zeta-potential analyzer (size range less than a micron) and TEM. Hansch et al. [109] have observed that the pigment has a limited and intensive range of absorption in the visible range. It has been concluded that polymers have different absorption characteristics of laser energy in the near- IR region.

During the study of excimer laser on biodegradable polymer, Hsu et al. [110] found that the polymer crystallinity decreases as a function of laser fluence. Xu et al. [111] have studied the effect of glass fibre (GF) and crystallinity on light transmission during LTW of thermoplastics. They have found that the apparent reflection increased with increase in crystallinity as the backscattering increased. However, the apparent reflection exhibited a complex behaviour by glass-fibre-reinforced polymers. A study on the relationship between the optical characterization of coloured and non-coloured polyamides and laser

welding process parameters has been studied by Grewell et al. [31]. They have concluded that the inclusion of pigments can enhance the scattering of laser radiation, which can minimize energy requirement to make a weld or increase the effective weld time. Wehner et al. [112] have investigated the diode laser in the manufacture of microfluidic devices. A transparent PC plate cover has been welded with the PC base plate with varying CB dosages. They have recommended the higher CB content due to the shallower weld seam. Haberstroh et al. [32] have examined the effect of CB content on formation of the weld line while joining thermoplastics in micro-technology applications. The CB content has varied between 0.5% and 1.5%. It has been observed that, with an increase in the CB content, the penetration depth was reduced from 29 µm to 9 µm. Liu et al. [50] developed a new method to replace CB absorbent with a Fe wire absorbent have found that it resulted in a cleaner and stronger weld. They attributed the higher strength to the higher thermal conductivity of metal than CB. The influence of specific factors like nylon composition, fiberglass, mineral, impact modifier content and the colour version on the near IR transmission have been investigated by Bray et al. [113]. Schmailzl et al. [114] have constructed an experimental setup by integrating a pyrometer with a 3D-scanner to detect gaps in the weld during QS welding by measuring the differences in variation in the measured temperature. They were able to successfully identify weld gaps in the joints made between sheets containing fibre up to 30 percent of the weight. Laser transmission through plastics (PA6 and PC) as a function of thickness and laser incidence angle has been studied by Azhíkannickal et al. [115]. They have concluded that transmission on both materials, for a given thickness, as the laser angle of incidence increases the angle of transmission decreases. Also, for a given laser incidence angle, the transmission decreases with the increase in thickness. The scattering has been amplified by increasing the interaction count between laser light and phase boundaries either by increasing the particle concentration (i.e., GF level and crystallinity) or increasing part thickness [111]. In the research of Liangbin et al. [33], it has been found that high pressure can increase the rate of crystallization and promote the thickening process of PET lamellar crystals. Amanat et al. [62] have studied the influence of power (10 or 20 W), scan speeds (4, 8, 16, 32 or 64 mm/s), and material morphology i.e., amorphous or semi-crystalline on the lap-joint weld firmness of PEEK joined using Through transmission laser welding. They have found that the amorphous PEEK is vulnerable to damage due to increased heat at higher input power, while no apparent evidence of heat decomposition has been found in semi-crystalline PEEK. Also, semi-crystalline PEEK weld firmness is greater than the

that of the amorphous PEEK, at all power ranges and scanning speeds. Air bubbles are observed within the weld line in both semi-crystalline and amorphous PEEK; this may be caused likely due to the instantaneous vaporization of absorbed water molecules within the PEEK [62]. Villar et al. [116] constructed a special setup to monitor the temperature and irradiation time during the laser welding of PEKK in order to keep the maximum temperature from touching degradation of the material. Schmailzl et al. [117] employed a calibrated 3D scanner equipped with an integrated pyrometer to calculate the core temperature of the joint during QS welding of Polyamide 6. Brodhun et al. [118] investigated the effect of various process conditions on temperature distribution during the welding of Thermoplastic fasteners and fiber-reinforced-plastics (FRP) surfaces and in turn on the quality of weld. They have found that the scanning path has the most significant effect on the temperature. Pelsmaeker et al. [34] have proved that Thulium fiber laser welding can be successfully used to join transparent plastics without the application of additives to yield not only shear strengths of up to 5 Mpa but also efficient leak proof against microfluidics. They found that the material properties of ten types of polymers can be conveniently used to justify the high strengths achieved. Pereira et al. [119] studied the effect of no. of passes on the shear strength of lap joint and scarf joint made with Polyamide 6 using Nd:YAG laser. They observed that in the case of single pass, the scarf joint was stronger than lap joint while lap joint was made almost doubly stronger by a double pass. Azimzadegan and Mousavi [120] have investigated the causes and nature of hot cracks in the welds of Hastelloyx formed using Nd: YAG laser welding. They have observed that the solidification cracks originated from liquation cracks in the parent metal.

In the field of medicine, Rodts et al. [121] found that surface welded woven fiber fabrics displayed far greater wear resistance under compression than traditional woven fabrics that used for cartilage replacement in bone joints. Visco and Scolaro [122] studied the effects of absorbed thermal energy and the %wt of filler material on the laser welded joint made in polyethylene containing biomedical grade nanocomposites. They found that the surface roughness reduced while simultaneously increasing the permeability of the joint towards biofluids. They also observed that higher tensile strengths were observed in case of white polyethylene as compared to its darker composites. Further in the case of white polyethylene, they found that the highest tensile strength was obtained at 0.016% wt of filler material. Villar et al. [123] have studied the effect of high performance PEKK as a

packaging material for laser transmission welding of two thermoplastic samples. They have observed that the temperature at the center of the weld zone has reached sufficient level to cause enough melting and mobility of polymer chains. They added that the joint appeared to be strong.

Characterizing the morphology of laser transmission welded joints presents several challenges that limits the depth and reliability of microstructural analysis. High-resolution imaging techniques, such as transmission electron microscopy (TEM) and scanning electron microscopy (SEM), typically offer localized observation, capturing only small zones and thereby overlooking broader weld features essential for comprehensive evaluations. Most morphological characterization methods are ex-situ, lacking real-time feedback capabilities, with in-situ techniques still in early stages of development. The morphology of welded joints is highly sensitive to thermal cycle variations, as localized temperature gradients during welding can significantly influence microstructural evaluation. Interpreting morphological changes is further complicated by the difficulty in distinguishing between nanoscale structural alterations and chemical degradation effects. The presence of fillers or additives add another layer of complexity as their influence on morphology is often entangled with other factors making it challenging for current techniques to isolate their specific contributions. Additionally, thermal degradation can mimic or obscure typical structural changes, making interpretation less reliable. Finally, there is a limited quantitative understanding of the relationship between morphological characteristics and the resulting mechanical performance, leaving a gap in establishing strong structure–property correlations that are critical for process optimization and quality assurance.

1.4. Scope and objective of the present work

The literature survey found that researchers have already shown interest in several areas of laser welding. A comparative summary of the previous works has been presented in Table 1.1. Literature indicate that various academicians have investigated laser welding. However, regarding the "TTLW" on polymer, only a few publications have been found. Researchers have already addressed different aspects (process optimization, characterization, finite element modelling, etc.) of laser welding of plastics. However, investigations on transparent-to-transparent polymer (Acrylic and polycarbonate) welding by TTLW without any absorbent have yet to be addressed and have been studied in this research work. Most researchers focus on the effect of welding parameters such as mode of operation, beam travel direction, beam polarization, frequency, angle of incidence of the laser beam, material morphology, depth of focus, etc. A deep and broad understanding of the laser welding process is required to eventually realize a completely controlled manufacturing process. The requirement is to create the expected weld quality, including reduced wastage rate, welding cycle time, and increased product throughput. This is still challenging for researchers, technologists, and practicing engineers. Quality, in turn, depends on multiple factors like molding machine, product processing parameters etc. Welding parameters influence the quality of the weld. In the domain of "TTLW" of polymer, a solid and rich knowledge database is to be developed. This knowledge database may be created only through extensive and continued research covering different aspects of the "TTLW" of polymers.

Table1.1. Summary of The Past Researcher

Authors	Range of Process Variables	Workpiece Materials	Outcomes
Kumar et al. [18]	Not specified	Not specified	Grey Relational Analysis + Taguchi for optimizing joint strength & weld width
Acharjee et al. [19]	Power: 28 W, Speed: 5 mm/s, Focal Distance: 9 mm	Acrylic (PMMA)	Taguchi DOE; laser power most influential on weld strength
Kumar et al. [1]	Power: 7.6–11.6 W, Speed: 0.66–2.34 mm/s, Frequency: 198.86–451.13 kHz	Various plastics	RSM & desirability; power for breaking load, speed for weld width
Shin and Choi [20]	Not specified	ABS, PC	Energy optimization model; analyzed melt zone & HAZ
Acharjee et al. [29]	Not explicitly detailed	Acrylic (PMMA)	RSM to relate process & output; power, speed, clamp pressure influential
Bideskan et al. [58]	Not specified	PMMA & Aluminum 6061-T6	Similar LTW optimization study with RSM
Wang et al. [38]	FEM + GA + RSM; No range specified	Thermoplastics	Enhanced prediction using FEM-GA-RSM thermal model
Wang et al. [59]	Clamp pressure, power, velocity, scanning number	Thermoplastics	Velocity and scanning number affect joint cost; RSM used
Jiao et al. [43]	Power, speed, clamping pressure	CFRTP / Stainless Steel	Optimized defect zone width & joint strength
Katsiropoulos et al. [53]	Not specified	Thermoplastic composites	Used LTSM-OPT software for quality and cost
Vidal et al. [60]	Not specified	Thermoplastic composites	Custom laser system; weld widths 0.7–1.4 mm
Mazumdar and Hoa [61]	L9 orthogonal array	Not specified	Taguchi & ANOVA to estimate factor contributions
Amanat et al. [62]	Power: 40–80 W, Time: 10–50 s	PEEK	Optimal power 65–75 W; strength 20–45 MPa

Authors	Range of Process Variables	Workpiece Materials	Outcomes
Labeas et al. [63]	Not specified	Thermoplastic composites	Thermo-mechanical simulation for optimization
Dwivedi and Sharma [47]	Power: 18 W, Speed: 100 mm/min, Stand-off: 2 mm	PET / 316L Stainless Steel	RSM; max joint strength: 88.48 MPa
Wang et al. [65]	Not specified	Not specified	ANN + GA + desirability for strength & width
Acharjee et al. [66]	Not specified	Not specified	ANN and regression models for prediction
Tillmann et al. [67]	Power & speed (not detailed)	PETG / Stainless Steel	Increased power + reduced speed = better melting, no decomposition
Kagan [68]	Not specified	Thermoplastics	Reviewed innovations and multi-parametric optimization
Taguchi [69]	Not specified	PP-Clay Nanocomposites	Taguchi method for LTW optimization
RSM [70]	Not specified	PP-Clay Nanocomposites	RSM for LTW parameter optimization
Hubeatir [71]	Not specified	PMMA	Grey & Taguchi: wide weld = strong; deep = weak (porosity)
Bhattacharya et al. [72]	Power, frequency, speed (not detailed)	Polycarbonate / Acrylic	RSM & ANOVA on weld geometry
Chen et al. [21]	Not specified	PA6, PA6GF, PP	Developed a model explaining laser energy distribution using scattering parameters; validated on polymers
Chen et al. [22]	Not specified	PC	3D FEM model for contour LTW; results agree with weld initiation power and width
Aden [23]	Not specified	PC, PBT	Temperature profiling; beam shape impact on weld seam homogeneity studied
Geiger et al. [24]	Not specified	PP	FEM used to study optical characteristics' effects on temperature and molten pool geometry
Hadriche et al. [54]	Not specified	PP	Finite difference model validated by microscopy;

Authors	Range of Process Variables	Workpiece Materials	Outcomes
			morphological changes due to recrystallization
Lambiase et al. [73]	Not specified	Metals and plastics	Integrated experiment and simulation for laser-assisted joining
Casalino and Ghorbel [44]	Not specified	PP	Model for keyhole and conduction mode welding; lower strain/stress in deep penetration
Zoubeir and Elhem [74]	P=100W, SS=110 mm/s, Pressure=0.3–0.5 MPa	PP	Studied temperature field and residual stresses in PP mini-tank
Anonymous [39]	Laser power, SOD, speed (not exact)	PET, PP	Width and depth increase with power; D/W ratio influences shear strength
Aden et al. [75]	Not specified	PA 66	Simulated temperature distribution validated with microtome cut sections
Mayboudi et al. [76]	Not specified	Not specified	Scattering improves thermal model accuracy
Becker and Potente [77]	Not specified	PP	2D thermal FEM model for heating phase; validated with experimental data
Liu et al. [78]	Not specified	Not specified	Developed algorithm for energy transformation in LTW
Ilie et al. [79]	Not specified	PP, ABS	Validated weldability simulation with IR thermography
Chen et al. [45]	Not specified	PP(fg), ABS(fg)	Studied molten pool and shear strength in doped polymers
Coelho et al. [46]	Not specified	Not specified	Elliptical beam spots improved strength and efficiency
Flock et al. [80]	Not specified	Not specified	Numerical model predicts HAZ and peak temp, aids process optimization
Ilie et al. [48]	Not specified	Not specified	Tool for polymer weldability assessment developed
Anonymous [81]	Not specified	Semi-crystalline polymer	Simulation for HAZ and strength; validated with light microscopy

Authors	Range of Process Variables	Workpiece Materials	Outcomes
Sooriyapiragasam & Hopmann [82, 83]	Not specified	PMMA–ABS/PC	Thermo-mechanical model validated with IR thermography
Mayboudi et al. [84]	Not specified	PVC	Heat transfer model using contact conduction and Gaussian distribution
Anonymous [46, 86]	Not specified	Metal/polymer	Thermal conductance predicted using contact mechanics; validated
Bronnikov et al. [87]	Not specified	Oriented polymers	Empirical model relating Young's modulus to thermal expansion
Kurosaki [12]	Not specified	Thermoplastics	IR welding studied theoretically/experimentally using ZnSe heat sink
Mubarak & Albano et al. [25,26]	Not specified	iPP	Crystallization kinetics studied via DSC and Avrami analysis
Kneip et al. [28]	Not specified	Partially transparent polymers	FEM for thermal field; validated with IR thermography
Anonymous [88]	Not specified	Not specified	Used Green's function to study temperature pattern with laser
Anonymous [89]	Not specified	Not specified	Zemax-based ray tracing model for beam profile validation
Naqwi & Durst [90]	Not specified	Mono-mode diode lasers	Analytical model using Gaussian/Lorentzian distribution
Ai et al. [91]	Not specified	PET, Ti-6Al-4V	Simulated molten pool, porosity, flow; validated with experiments
Potente et al. [92]	Not specified	PA66	3D thermal model with pyrolysis kinetics for degradation prediction
Wilke et al. [93]	Not specified	Not specified	Simulation for simultaneous welding including heating/cooling
Griffiths & Dowding [94]	Not specified	PE, PP	FEM to predict peel force; optimized via genetic algorithm
Acherjee [95]	Not specified	PC	3D FEM to optimize power, speed, passes; validated with experiments
Ghorbel et al. [13]	Welding speed: 3–6	PP	Increased power and reduced speed increase

Authors	Range of Process Variables	Workpiece Materials	Outcomes
	mm/s, Laser power: 20–40 W		weld zone volume and depth; high power/speed may degrade properties.
Prabhakaran et al. [51]	Low laser power and speed	iPP	Maximum weld strength achieved; partially melted iPP crystallizes quickly, described by Avrami equation.
Acherjee et al. [102]	Varied CB dosage	Various polymers	CB dosage determines optical penetration depth.
Wang et al. [30]	Not specified	PC, PA6	Used TEM and image processing to analyze CB morphology.
Abed et al. [104]	Not specified	PP	Crystalline morphology depends on thermal cycle.
Meyer et al. [105]	Not specified	Silicon chip	Used optical coherence tomography for weld quality assessment.
Frick & Schkutow [106]	Wavelength: 800–2500 nm	–	Scattering decreases with increasing wavelength.
Cosson et al. [107]	Laser light source and camera	Semi-transparent plastics	Optical method to estimate extinction coefficient and optimize weld power.
Ma et al. [108]	Not specified	Poly(propylene carbonate)-based PU	Characterized particle size using Zeta potential analyzer and TEM.
Hansch et al. [109]	Not specified	Various polymers	Pigments show absorption in visible range; near-IR absorption varies.
Hsu et al. [110]	Laser fluence variation	Biodegradable polymer	Crystallinity decreases with laser fluence.
Xu et al. [111]	Not specified	Glass-fiber reinforced thermoplastics	Reflection increases with crystallinity; complex with GF.
Grewell et al. [31]	Not specified	Colored and non-colored polyamides	Pigments enhance scattering, improving energy efficiency.
Wehner et al. [112]	CB content varied	PC	Higher CB → shallower weld seam.
Haberstroh et al. [32]	CB content: 0.5%–1.5%	Thermoplastics	Higher CB → reduced penetration depth (29 µm → 9 µm).
Liu et al. [50]	Not specified	Fe wire vs CB	Fe wire gives cleaner, stronger weld due to higher conductivity.
Bray et al. [113]	Not specified	Nylon with additives	Composition and color affect IR transmission.

Authors	Range of Process Variables	Workpiece Materials	Outcomes
Schmailzl et al. [114]	QS welding with 3D scanner	Fiber composites	Identified weld gaps based on temp variation; effective up to 30% fiber.
Azhíkannickal et al. [115]	Incidence angle and thickness	PA6, PC	Transmission decreases with thickness and angle.
Liangbin et al. [33]	High pressure	PET	High pressure → faster crystallization and thicker crystals.
Amanat et al. [62]	Power: 10–20 W, Scan speed: 4–64 mm/s	Amorphous and semi-crystalline PEEK	Amorphous PEEK damaged at high power; semi-crystalline has better weld strength.
Villar et al. [116]	Controlled temperature and time	PEKK	Setup ensures no material degradation during welding.
Schmailzl et al. [117]	QS welding	Polyamide 6	Used pyrometer and scanner to measure joint core temperature.
Brodhun et al. [118]	Various paths and conditions	FRPs	Scanning path most significantly affects temperature and weld quality.
Pelsmaeker et al. [34]	Not specified	Transparent plastics	Thulium fiber laser yields strong, leak-proof joints without additives.
Pereira et al. [119]	Single/double pass	Polyamide 6	Double pass lap joints are stronger; scarf joints stronger in single pass.
Azimzadegan & Mousavi [120]	Not specified	Hastelloyx	Hot cracks originate from liquation cracks.
Rodts et al. [121]	Not specified	Woven fiber fabrics	Laser welded fabrics show greater wear resistance for implants.
Visco & Scolaro [122]	% filler and energy	Polyethylene nanocomposites	White PE shows higher tensile strength and lower roughness.
Villar et al. [123]	Not specified	PEKK	Sufficient melt and chain mobility observed; strong joint formed.

Therefore, the following objectives for this research work have been emerged:

➢To compare the joint quality of laser welding of Polycarbonate and Acrylic sheets.

➢The aim is to find the optimum process parameters for obtaining good joint quality. Also, the laser optic lens will be protected from the reflecting laser beam of the Nd: YVO_4 laser beam welding of lap joint configuration of Acrylic and polycarbonate sheets.

➢To derive mathematical models based on experimentation results.

➢To measure the weld width, HAZ, and tensile strength for the welded samples and the base metal.

➢To determine the optimum welding condition for good-quality joints.

➢To evolve a finite element model (FEM) for the temperature contour and depth of penetration analysis.

➢To create 3D response surfaces and contour plots to measure the combined effect of input parameters on responses.

➢To study the influence of welding parameters using the analysis-of-variance (ANOVA) technique.

➢To develop FE modelling for the welding process focusing on thermal and structural analysis.

Chapter 2

2. Materials and Methodology

TTLW of the polymer has inherent complexity as the melting point of the polymer is too low which leads to burnout. The hindrance to proper joining strength has been increased for welding two optically transparent polymers. This work deals with this specific level of complexity without using any absorbent. The aim of introspection and optimization of laser welding of optically transparent dissimilar polymers requires appropriate material selection, parameter selections, identification of quality indicators, experimental design and setup. Subsequent paragraphs present a detailed description of the materials and methodology adopted in this work.

2.1. Materials

The polymers acrylic and polycarbonate sheets have been used as workpiece material in this work. These specific polymers are selected due to their wide range of lightweight applications in aerospace, automobile, defence, etc., that require an easy high-quality joining process. Both the sheets were optically transparent to visible light; however, the acrylic absorbs the energy released by the laser photons while applied. The scheme of using these two polymers has been presented in Table 2.1. It has been depicted in Table 2.1 that two types of laser contour have been used for experimentation circular and square and two types of thickness have been used to understand the behaviour of the laser concerning the plate thickness. Moreover, the effect of positioning of the plates such as top and bottom part has been analysed. The analysis in different weld geometries is necessary as the square profile leads to corner burn which reduces the weld quality while the circular profile eliminates the possibility of corner burn. The schematic diagram of the two-contour used in this work has been presented in Figure 2.1 (a, b). Temperature-dependent properties such as thermal conductivity (k), density (ρ), and specific heat (Cp) of acrylic and polycarbonate are necessary for the modelling of the physical welding process. The thermo-physical properties along with the compositions of acrylic and polycarbonate of plastic sheets have been presented in the subsequent paragraphs.

Table 2.1. Material used in this work

Dimensions (mm)	Top sheet	Bottom sheet	Weld geometry
80 x 35 x 1.5	Acrylic	Polycarbonate	Circular
100 x 35 x 0.5	Polycarbonate	Acrylic	Square

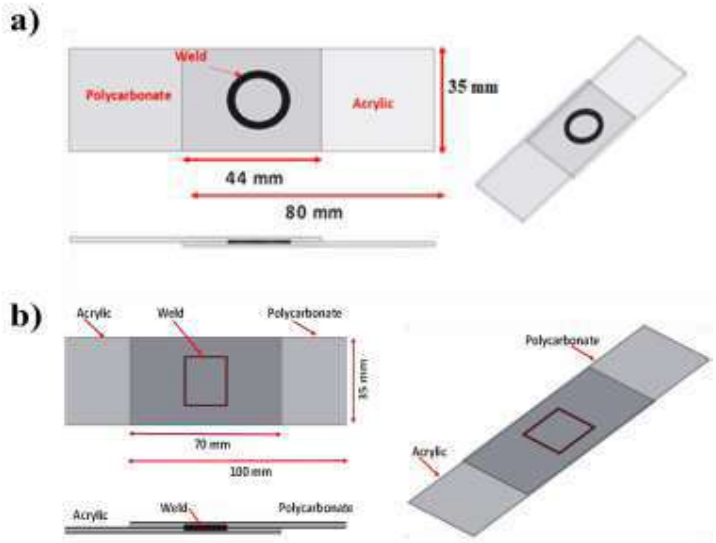

Figure 2.1. Schematic diagram of (a) circular and (b) square weld geometry used in laser welding

2.1.1. Acrylic

The acrylic sheet used in this work are optically transparent. Table 2.2 presents the detailed properties of the acrylic used, and Figure 2.2 shows its chemical structure.

Table 2.2. Properties of Acrylic

Physical Parameters	
Properties	**Values**
Abbe Number (V)	40.5
RI-refractive index (n)	1.54
Flammability	94 HB
Limiting Oxygen Index	(17-20)%
Water Absorption-Equilibrium (ASTM)	2%
Radiation resistance	Low
UV resistance	Poor
Mechanical Parameters	
Young's Modulus (E)	3.2 GPa
Tensile strength (σ_t)	70 MPa
Elongation at break (ε)	4%
Compressive Strength (σ_c)	97.22-124.10 MPa
Poisson's ratio(ν)	0.35-.04
Rockwell hardness	D-785 M-94
Notch test	2.16 J/m
Thermal Properties	
Glass transition temperature	114°C
Upper limit of working temperature	70°C
Lower limit of working temperature	-40°C
Linear Thermal Expansion Coefficient	$65x10^{-6} K^{-1}$
Electrical properties	
Surface resistivity	15 Ω/m^2
Volume resistivity	$>10^{14} \Omega.m$

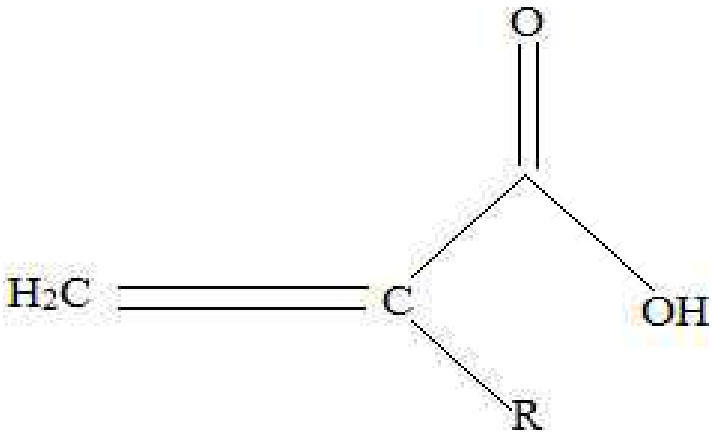

Figure 2.2 Chemical structure of acrylic

2.1.2. Polycarbonate

The polycarbonate sheet used in this work are optically transparent. Table 2.3 presents the detailed properties of the polycarbonate used. Figure 2.3 shows the chemical structure of polycarbonate.

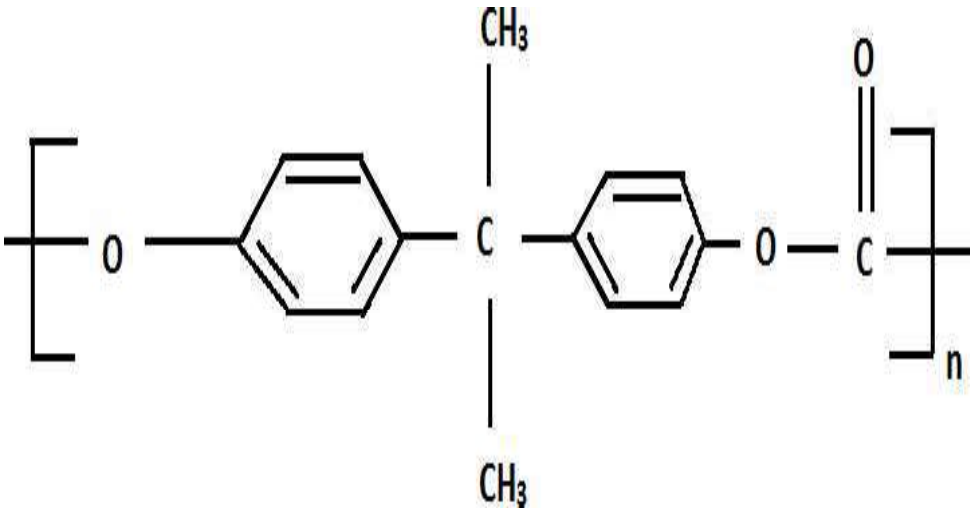

Figure 2.3 Chemical structure of polycarbonate

Table 2.3. Properties of Polycarbonate

Physical Properties	
Properties	**Values**
Abbe Number (V)	34.0
Refractive Index (n)	1.584-1.586
Flammability	98 HB
Limiting Oxygen Index	(25-27)%
Water Absorption-Equilibrium (ASTM)	0.16%
Radiation resistance	Fair
UV resistance	Fair
Mechanical properties	
Young's Modulus (E)	2.4 GPa
Tensile Strength (σ_t)	75 MPa
Elongation at break (ε)	80 %
Compressive Strength (σ_c)	>80 MPa
Poisson's ratio(ν)	0.37
Rockwell hardness	M-70
Notch test	20-35 J/m
Thermal properties	
Glass transition temperature	147°C
Upper limit of working temperature	130°C
Lower limit of working temperature	-40°C
Linear Thermal Expansion Coefficient	$65x10^{-6}K^{-1}$
Electrical properties	
Surface resistivity	$10^{15}\Omega/m^2$
Volume resistivity	$>10^{14}\Omega.m$

2.2. Experimentations

The design of the experiments (DOE) has been carefully made as per response surface methodology-central composite design (RSM-CCD) with the help of the Design-Expert package of version 10 to understand the effects of welding process parameters on responses such as weld width, ultimate load, depth of penetration and heat-affected zone (HAZ). The physical experimentation has been modelled with finite element formulations to predict the depth of penetration and weld width conducted by COMSOL software. The behaviour of welded joint ultimate tensile strength and displacement have been conducted by LS-DYNA. Furthermore, optimization has been conducted to obtain the optimum parametric condition for good weld quality, and also analysis-of-variance (ANOVA) has been conducted to determine the significant input parameter/s in the process. Mathematical models were developed to correlate the responses with input parameters.

2.2.1. Statistical Optimization by Response Surface Methodology (RSM)

RSM is one of the beneficial DOE methods that is recently becoming popular. This methodology comprises a set of reviews of basic experimental designs used to fit linear response surface models and method descriptions for calculating optimum conditions of operation. The steps of the RSM are given as follows:

- Development of relevant experimental plan for choosing non-dependent variables.
- Statistical modelling to establish an approximate relation among the process variables and responses.
- Optimization of the method for selecting process variable values which produce the desirable responses.

If all of the non-dependent variables are controllable, measurable, and are continuous during the experiments, then the y (response surface) can be presented with very minimal error by (Eq. 2.1):

$$y = f'(x)\epsilon \qquad (2.1)$$

where in,

$x = (x1, x2, \ldots, x_k)$,

$f'(x)$ = vector function of p elements.

β = vector of p unknown constant coefficients,

ϵ = random experimental error assumed zero mean.

In RSM, an apt model is essential to develop the actual response surface. The approximated model is built with observed results data from the process. Multiple regression analysis is generally used for this. Generally, a second order polynomial equation is employed in RSM, and it is given as follows (Eq. 2.2):

$$y = \beta_0 + \sum_{i=1}^{k} \beta_i x_i + \sum\sum \beta_{ij} x_i x_j + \sum_{i=1}^{k} \beta_{ii} x_i^2 + \varepsilon \qquad (2.2)$$

where, parameters $\beta_0, \beta_i, \beta_{ij}, \beta_{ii}$ are termed as regression coefficients for *i= 0, 1..., k and j= 0, 1…..k.*

Analysis of Desirability Function

In this approach, the individual responses are subjected to transformation to their corresponding desirability values. The values of desirability depend on the target of the response and the allowed tolerance range as well. As the response reaches its target value, Unity is assigned, which is the most desired situation. Beyond a particular acceptable limit, the desirability value is assumed as zero. In this present study, individual desirability function contains one of the characteristics as follows:

For the goal of maximum, desirability (d_i) is defined as (Eq. 2.3):

$$di = \begin{cases} 0 & ; if\ response\ (y_i) \le low\ value\ (L_i) \\ \left(\frac{y_i - L_i}{H_i - L_i}\right)^{w_i} & ; as\ response\ (y_i) varies\ from\ low\ (L_i)\ to\ high\ (H_i) \\ 1 & ; if\ response\ (y_i) \ge high\ value\ (H_i) \end{cases} \qquad (2.3)$$

For the goal of minimum, the desirability will be defined by (Eq. 2.4):

$$di = \begin{cases} 1 & ; if\ response\ (y_i) \le low\ value\ (L_i) \\ \left(\frac{H_i - y_i}{H_i - L_i}\right)^{w_i} & ; as\ response\ (y_i) varies\ from\ low\ (L_i)\ to\ high\ (H_i) \\ 0 & ; if\ response\ (y_i) \ge high\ value\ (H_i) \end{cases} \qquad (2.4)$$

Weight (w) can be given to a goal to underline a particular desirability function. Weights can be assigned values from 0.1 to 10.0. weights greater than 1.0 give more emphasis to the goals, while weights less than 1.0 give lesser emphasis.

D, the simultaneous objective function is the geometric mean of transformed responses (Eq. 2.5):

$$D = \left(d_1^{r_1} \times d_1^{r_2} \times \ldots\ldots\ldots\ldots \times d_1^{r_n}\right)^{\frac{1}{\Sigma r_i}} = \left(\prod_{i=1}^{n} d_i^{r_i}\right)^{\frac{1}{\Sigma r_i}} \quad (2.5)$$

here, n is the no. of responses in the measure. Each response is given an importance relative to the other responses. These importance (r_i) values vary between 1, which is the least important, and 5, the most important [5].

2.2.2. Process Control Parameters

In the literature, it has been found that several process parameters namely laser power, scanning speed, stand-off distance, pulse width, frequency, incident angle, spot diameter and plate thickness may influence the quality of weld. In the current work, after careful study, the following parameters have been selected as the control parameters of weld process, such as laser power, scanning speed and pulse frequency. These process control parameters along with their levels have been presented in Table 2.4 and Table 2.5.

Table 2.4. Process control parameters for 0.5 mm acrylic and polycarbonate sheet

Parameter	Notation	Unit	Level				
			(-2)	(-1)	(0)	(1)	(2)
Laser Power	P	W	7.12	7.42	7.88	8.35	8.67
Scanning speed	S	mm/s	0.65	1.00	1.50	2.00	2.34
Frequency	f	kHz	265.91	300.00	350.00	400.00	434.09

Table 2.5. Design matrix of 0.5mm acrylic and polycarbonate sheet

Experiment No.	P(W)		S(mm/s)		f(kHz)	
	Coded value	Actual value	Coded value	Actual value	Coded value	Actual value
1	0	8.35	+2	2	0	300
2	0	8.35	0	1	+2	400
3	-1	7.89	-1	2.34	-1	350
4	0	7.42	-2	2	0	300
5	0	8.35	0	2	0	400
6	-2	7.89	0	1.5	0	350
7	0	7.11	0	1.5	0	350
8	+1	7.89	-1	1.5	-1	350
9	+1	7.89	+1	1.5	+1	350
10	+1	7.89	+1	1.5	-1	265.91
11	-1	7.42	+1	1	-1	400
12	+1	7.42	-1	2	+1	400
13	-1	7.89	-1	1.5	+1	350
14	0	7.42	0	1	-2	300
15	0	8.35	0	1	0	300
16	0	7.89	0	1.5	0	350
17	0	7.89	0	1.5	0	350
18	0	7.89	0	0.66	0	350
19	+2	8.67	0	1.5	0	350
20	-1	7.89	+1	1.5	+1	434.09

Table 2.6. Process control parameters of 1.5 mm acrylic and polycarbonate sheet

Parameter	Notation	Unit	Level				
			(-2)	(-1)	(0)	(1)	(2)
Laser Power	P	W	7.60	8.40	9.60	10.80	11.60
Scanning speed	S	mm/s	0.66	1.00	1.50	2.00	2.34
Frequency	f	kHz	198.86	250.00	325.00	400.00	451.13

Table 2.7. Design matrix of 1.5 mm acrylic and polycarbonate sheet

Experiment No.	P(W)		S(mm/s)		f(kHz)	
	Coded value	Actual value	Coded value	Actual value	Coded value	Actual value
1	0	7.600	+2	2.340	0	325.000
2	0	9.600	0	1.500	+2	451.134
3	-1	8.400	-1	1.000	-1	250.000
4	0	9.600	-2	0.659	0	325.000
5	0	9.600	0	1.500	0	325.000
6	-2	7.600	0	1.500	0	325.000
7	0	9.600	0	1.500	0	325.000
8	+1	10.800	-1	1.000	-1	250.000
9	+1	10.800	+1	2.000	+1	400.000
10	+1	10.800	+1	2.000	-1	250.000
11	-1	8.400	+1	2.000	-1	250.000
12	+1	10.800	-1	1.000	+1	400.000
13	-1	8.400	-1	1.000	+1	400.000
14	0	9.600	0	1.500	-2	198.866
15	0	9.600	0	1.500	0	325.000
16	0	9.600	0	1.500	0	325.000
17	0	9.600	0	1.500	0	325.000
18	0	9.600	0	1.500	0	325.000
19	+2	11.600	0	1.500	0	325.000
20	-1	8.400	+1	2.000	+1	400.000

2.2.3. Response Parameters

The weld quality has been characterized by the weld width (WW), ultimate tensile strength (UTS), Heat-Affected Zone (HAZ) and depth of penetration (DP), of the welded samples. Therefore, for the present work, the above parameters are selected as the response parameters of the laser welding process. The response parameters have been measured using experimentation and further verified using thermal and structural modelling.

2.2.4. Laser Welding Setup

Pulsed Nd: YVO_4 (Neodymium-doped yttrium orthovanadate) laser (Make: Electrox; Model: EMS 100) control was used to conduct all the experiments. The pictorial view of the laser welding setup is shown in Figure 2.4. A suitable clamping pressure is required for the experiment that was performed using a clamping device, as shown in Figure 2.5. The overlapped zone is then clamped in the clamping device. 20 runs of experiments have been conducted following the design matrix made with variable input parameters like power, frequency and scanning speed.

Figure 2.4. Laser welding setup

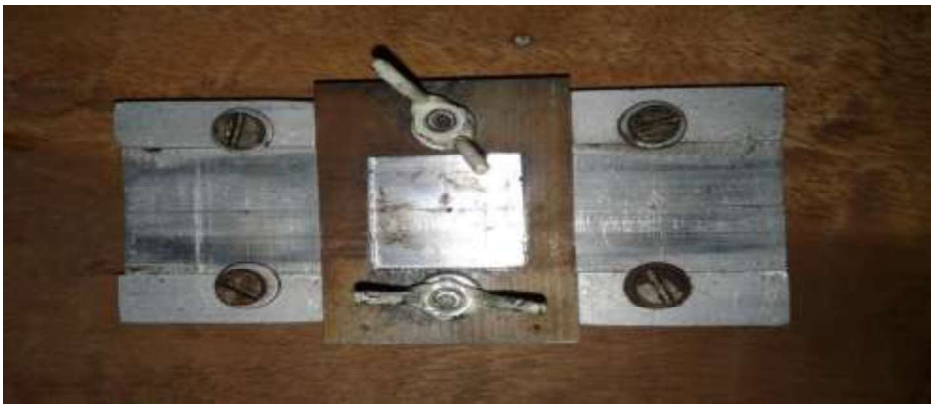

Figure 2.5. Clamping device

2.2.5. Response Measurements

a) Weld width and HAZ

The weld width and HAZ are basic quality parameters for weld quality. The weld width and HAZ has been measured from the micrographs taken from the welded samples. The micrographs of the samples have been taken with the help of an optical transmissive microscope (Make: Dewinter; Model: Pro 5.0) at four different points and measurement has been done using suitable image processing software. The photograph of the optical microscope used in this work is presented in Figure 2.6.

Figure 2.6. Optical microscope used for WW and HAZ measurements

b) Ultimate load

The ultimate load of the welded joint was measured in a 100 kN, electro-mechanical controlled universal testing machine (Make: INSTON; Model: 8801) with a cross-head speed 0.5 mm/min. Figure 2.7 shows the pictorial view of the test setup. The schematic diagram for tensile testing of welded joints has been presented in Figure 2.8.

Figure 2.7. Tensile test setup

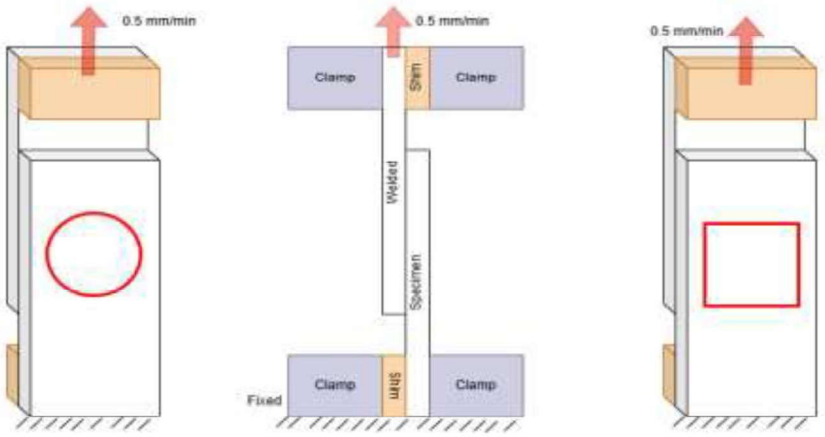

Figure 2.8. Schematics of tensile test specimens

2.2.6. Simulation studies

a) Thermal modelling

Thermal modelling has been done after the experiment to have a deep insight into the heat transfer effect on the physical welding process. The process parameters are set as per the physical experiment. Some assumptions have been taken reasonably to reach time-saving and easy computation. The process of computing the FE (Finite Element) model using COMSOL 5.3a has been used.

Assumptions

the following assumptions were made in order to develop an FE model for the simulation of the process

I. Materials i.e., acrylic and polycarbonate are homogeneous and isotropic throughout the domain of study
II. The half portion of the physical welding is studied as there is symmetry in the model.
III. A small part of the square welding profile has been selected to reduce the number of nodal points.
IV. Perfect contact is there between melting parts of plates.
V. The phase change phenomenon due to heating is neglected.
VI. The Gaussian mode of laser intensity is followed.

Governing Equations

The following 3D heat transfer equations are used to model heat transfer in the LTW of acrylic and polycarbonate that defines the distribution of temperature within the body as per the law of conservation of energy given in Eq. 2.6, [124].

$$\rho c \frac{\partial T}{\partial t} = \nabla(k\Delta T) + q \tag{2.6}$$

Where material density is denoted by ρ, c is the specific heat, T is the temperature and t denotes time, Thermal conductivity was denoted by k while q represents internal heat generation.

Heat transfer between the workpiece and surrounding medium by convection icons is given by Eq. 2.7, [145].

$$q_{conv} = h(T_s - T_0) \tag{2.7}$$

Radiation heat transfer is given by Eq. 2.8, [124].

$$q_{rad} = \sigma\varepsilon({T_s}^4 - {T_0}^4) \tag{2.8}$$

where h is the convective heat transfer coefficient, T_s system temperature, T_0 ambient temperature, σ is Stefan- Boltzmann constant (5.64 x 10^4 W/m^2K^4) and ε is the emissivity of the material.

The materials used are transparent but in acrylic, there is some absorptivity of light so acrylic has been selected as the absorbent part and polycarbonate is the transparent part. The heat flux equation is modified from Beer-Lambert law [124]. It is given by Eq. 2.9.

$$q(x,y,z) = \begin{cases} 0 & transparent\ part \\ (1 - R_a)\alpha I_a\ exp\ exp\ (-KZ_a) & absorbent\ part \end{cases} \tag{2.9}$$

where R_a is the reflectivity of the absorbent part for acrylic it is 0.97. α is the absorbent coefficient its value for transparent acrylic is 15454 m^4, Z_a is the depth of the beam inside the lower part and I_a is the laser beam intensity after passing through the transparent polycarbonate which can be defined as Eq. 2.10, [124].

$$I_a = \frac{(1-R_t)P}{A} \tag{2.10}$$

where P is the power and R_t is the reflectivity of the transparent part; here for polycarbonate it is 0.05. Depending upon these governing equations the finite element (FE) model of the laser transmission welding (LTW) has been developed.

b) Structural Analysis

Three Dimensional models were built for the moving and static grips based on the rigid bodies, where the static grip was allowed 6 degrees of freedom (i.e., U_x= U_y=U_z=R_x=R_y=R_z=0). The moving grip was displaced in the direction of loading with a constant velocity profile. An explicit analysis technique was employed to solve all the LS-DYNA models. Thus, an iterative solver is not required for convergence. Each time step's solution was calculated directly without any iteration

Chapter 3

3. Results and Discussion

3.1 Study of TTLW using square contour on Acrylic and Polycarbonate

This section presents the results of square contour laser welding on acrylic and polycarbonate sheets of 0.5 mm thickness. Different input parameter levels are used to prepare the welded joints (Table 2.2). To assess the joint's weld quality, the three responses such as weld width (WW), ultimate load (UL) and heat affected zone (HAZ) have been measured. The measured responses have been optimized. The optimal setting should maximize UL, minimize WW and HAZ. The observed results according to the experimental plan have been presented in Table 3.1.

Table 3.1. Design of experiment and measured value of responses

SI No	P (W)	f (kHz)	S (mm/s)	WW (µm)	HAZ (µm)	UL (N)
1	8.35	300	2	127.16	34.92	318.24
2	8.35	400	1	224.3	85.87	161.08
3	7.89	350	2.34	112.65	24.27	372.6
4	7.42	300	2	114.09	20.85	340.1
5	8.35	400	2	121.5	40.22	242
6	7.89	350	1.5	166.1	42.35	150.46
7	7.11	350	1.5	140.61	35.98	270.23
8	7.89	350	1.5	177.55	43.45	155.2
9	7.89	350	1.5	177.84	43.02	192.29
10	7.89	265.91	1.5	162.23	56.84	155.46
11	7.42	400	1	233.04	66.2	170.1
12	7.42	400	2	131.79	31.25	362.38
13	7.89	350	1.5	177.17	45.87	176.2
14	7.42	300	1	224.45	79.49	121.15
15	8.35	300	1	234.83	95.35	132.9
16	7.89	350	1.5	177.55	44.83	155.2
17	7.89	350	1.5	177.84	41.81	178
18	7.89	350	0.66	304.64	105.8	221.17
19	8.67	350	1.5	150.38	61.28	208.48
20	7.89	434.09	1.5	189.11	52.61	196.58

Samples after lap joints using laser transmission welding have been shown in Figure 3.1. The measurement of WW and HAZ has been done using transmitting microscope with an objective lens of 50x magnifications. To measure WW and HAZ microscopic image at four different locations have been taken and analyzed by appropriate image processing technique discussed earlier. The microscopic image of minimum WW on different location has been shown in Figure 3.2 and maximum WW have been shown in Figure 3.3. The microscopic images for HAZ minimum and maximum are shown in Figure 3.4 and Figure 3.5 respectively.

Figure 3.1. Lap welded samples

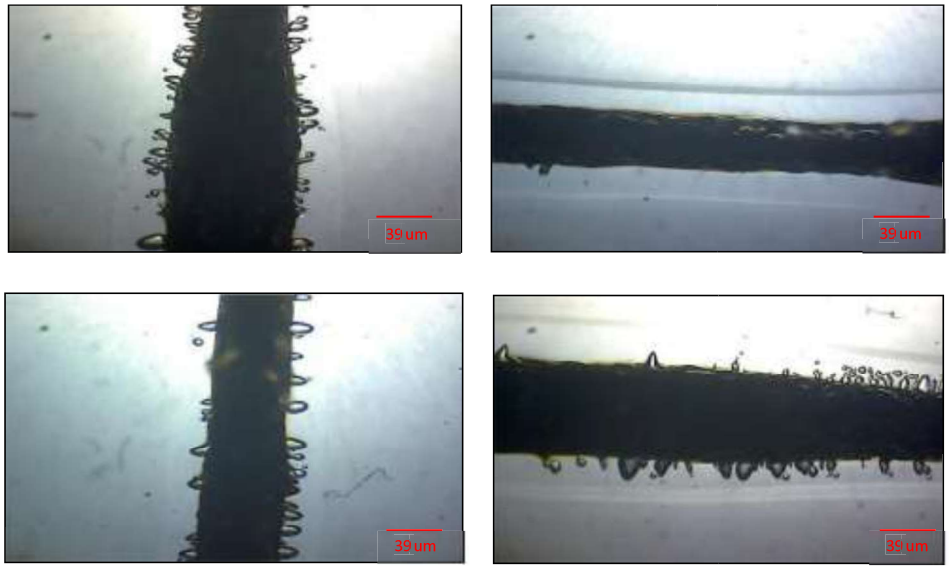

Figure 3.2 Microscopic view of sample having minimum WW (112.65 µm)

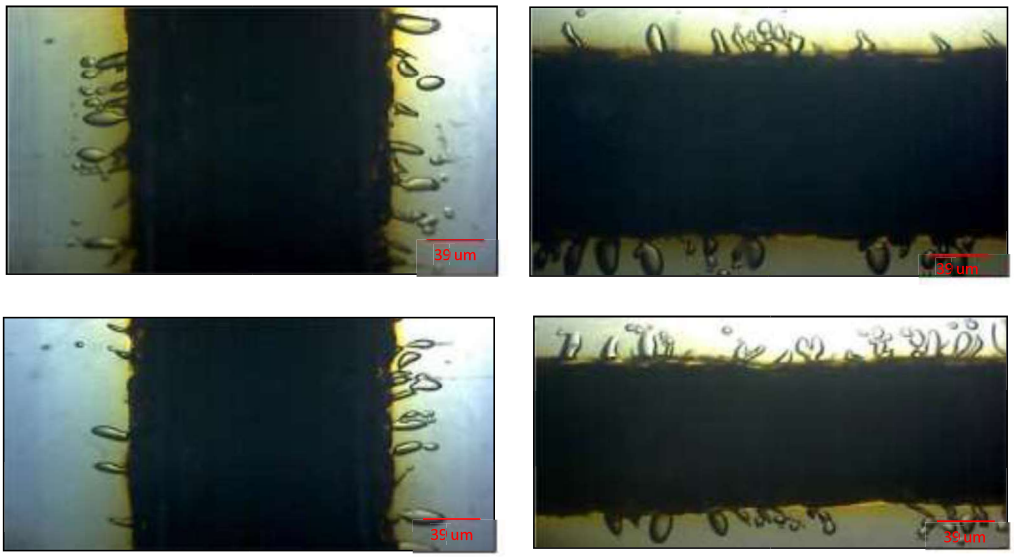

Figure 3.3 Microscopic view of sample having maximum WW (304.64 µm)

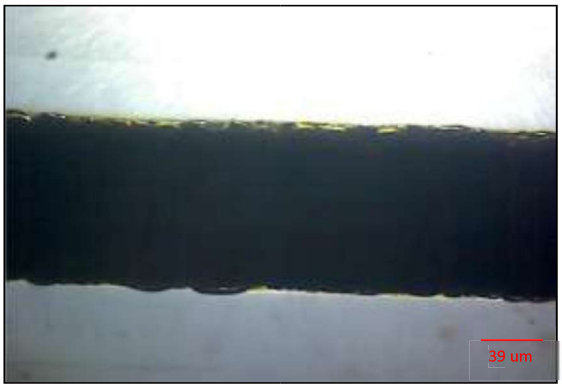

Figure 3.4. Microscopic image of sample having minimum HAZ (20.85 µm)

Figure 3.5. Microscopic image of sample maximum value of HAZ (105.8µm)

The experimental result presented in Table 3.1 shows that the WW from 112.65 µm to 304.64 µm, HAZ varies from 20.85 µm to 105.8 µm and UL varies from 121.15 N to 372.60 N. Pictorial view of lowest and highest UL after pull test has been shown in Figure 3.6. During pull test it has been observed that the breaking occurred near the weld zone in most of the cases. The maximum loads that can withstand by the welded samples are less than the original strengths of both of the transparent substances. During laser scanning, decomposition occurs which may lead to degradation in material properties in fused region at the interface, but the rest of the part remains intact. All the samples have failed through the fused material or across the upper sheet. But none of the materials have failed across the lower sheet i.e. acrylic sheet.

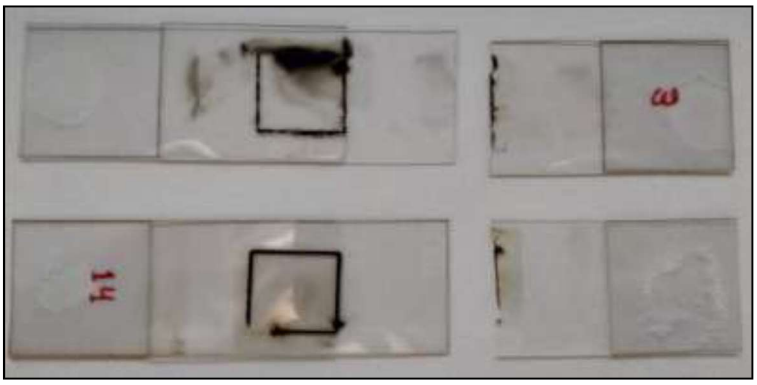

Figure 3.6. Photograph of the samples having the lowest ultimate load (121.15 N) (Top) and highest ultimate load (372.60 N)

3.1.1. Analysis of Variance (ANOVA)

The process parameter/s that have a substantial impact on the quality characteristic is the aim of the ANOVA. Design-Expert software was used to conduct the regression model's significance test, the test of significance on individual coefficients for each model, and the lack-of-fit test. The responses' analysis-of-variance displays the significant models ($p<0.05$) at a 95% confidence level in Tables 3.2 to 3.4.

3.1.1.1. ANOVA for Weld Width

The ANOVA table of the quadratic model for weld width (WW) is given in Table 3.2. The model terms to be considered statistically significant, it is required for the associated p-values to be less than 0.05. The main effect of the scanning speed (S), power (P), frequency (f), the quadratic effects of the power (P^2), the scanning speed (S^2), and two-way interactions of SSf and Pf are the significant model terms associated with weld width. R^2 (99.23%), predicted R^2 (95.62%) and adjusted R^2 (98.53%) which are adequacy measures were in significantly reasonable agreement which shows that the model is adequate. As desired, the lack of fit is not found to be significant to the pure error. Regression equation for the WW is shown in Equation (3.1)

$$WW = -3292 + 867P + 1.780f - 277.4S - 49.76P^2 - 0.000019f^2 + 46.55S^2 - 0.2271Pf + 0.53PS + 0.0699f\ \text{S} \quad (3.1)$$

Table 3.2. ANOVA table (WW)

Sources	SS (adjusted)	MS (adjusted)	P-Value	Remarks (Significant-S, Not significant -NS)
Model	45128.4	5014.3	0.000	S
Linear	40878.3	13626.1	0.000	S
P	26.4	26.4	0.406	S
f	220.3	220.3	0.031	S
S	40631.6	40631.6	0.000	S
Square	3989.5	1329.8	0.000	S
P^2	1655.0	1655.0	0.000	S
f^2	0.0	0.0	0.977	NS
S^2	1945.3	1945.3	0.000	S
2-Way Interaction	247.6	82.5	0.134	NS
Pf	223.0	223.0	0.030	S
PS	0.1	0.1	0.954	NS
fS	24.4	24.4	0.424	S
Error	351.0	35.1		
Lack-of-Fit	240.7	48.1	0.206	NS
Pure Error	110.3	22.1		
Total	45479.4			

3.1.1.2. ANOVA for HAZ

Table 3.3 shows the ANOVA values in the table for the quadratic model for HAZ. The main effects of the power (P), scanning speed (SS) and frequency (f) are the significant model terms associated with the HAZ. Most of the quadratic and two-way interaction terms are also significant except the $P \times f$ term. R^2 (99.77%), predicted R^2 (98.78%) and adjusted R^2 (99.56%) which are adequacy measures were in significantly reasonable

agreement which shows that the model is adequate. As desired, the lack of fit is not found to be significant to the pure error. Regression equation for HAZ is shown in Equation (3.2).

$$HAZ = 777 - 102.1P - 1.356f - 155.0S + 8.28\,P^2 + 0.001574f^2 + 30.38SS^2 - 0.0070Pf - 6.70\,PS + 0.1923\,fS \quad (3.2)$$

Table 3.3 ANOVA table (HAZ)

Sources	SS (adjusted)	MS (adjusted)	P-Value	Remarks (Significant-S, Not significant -NS)
Model	10253.3	1139.25	0.000	S
Linear	9079.5	3026.49	0.000	S
P	753.2	753.16	0.000	S
f	14.8	14.76	0.032	S
S	8311.5	8311.54	0.000	S
Square	985.1	328.35	0.000	S
P^2	45.8	45.79	0.001	S
f^2	223.2	223.16	0.000	S
S^2	828.9	828.87	0.000	S
2-Way Interaction	204.6	68.21	0.000	S
$P\ f$	0.2	0.21	0.772	NS
$P\ S$	19.4	19.42	0.017	S
$f\ S$	185.0	184.99	0.000	S
Error	24.0	2.40		
Lack-of-Fit	12.2	2.44	0.486	NS
Pure Error	11.8	2.36		
Total	10277.2			

3.1.1.3 ANOVA for ultimate load

Table 3.4 shows the ANOVA values of the quadratic model for the UL. For the model terms to be considered statistically significant, it is required for the associated p-values to be less than 0.05. The main effect of the scanning speed (SS), power (P) and frequency(f) are the significant factors associated with the ultimate load. Most of the quadratic and tow way interaction terms are also significant except the f^2 term. R^2 (98.01%), predicted R^2

(91.25%) and adjusted R^2 (96.23%) which are adequacy measures were in significantly reasonable agreement which shows that the model is adequate. As desired, the lack of fit is not found to be significant to the pure error. The regression equation for the UL is shown in equation (3.3):

$$UL = 4889 - 1599P + 6f + 710S + 123P^2 + 0.00164f^2 + 117.2S^2 - 0.742\,Pf - 80.8PS - 0.750fS \quad (3.3)$$

Table 3.4 ANOVA table (ultimate load)

Sources	**SS (adjusted)**	**MS (adjusted)**	**P-Value**	**Remarks (Significant-S, Not significant -NS)**
Model	122977	13664.2	0.000	S
Linear	93950	31316.7	0.000	S
P	4007	4007.2	0.002	S
f	884	883.5	0.089	S
S	89059	89059.5	0.000	S
Square	20495	6831.5	0.000	S
P^2	10133	10132.7	0.000	S
f^2	242	241.7	0.348	NS
S^2	12340	12340.5	0.000	S
2-Way Interaction	8024	2674.6	0.002	S
P f	2382	2382.3	0.011	S
P S	2825	2825.5	0.007	S
fS	2816	2816.1	0.007	S
Error	2491	249.1		
Lack-of-Fit	1089	217.8	0.606	NS
Pure Error	1402	280.5		
Total	125469			

3.1.2. Model Validation

The relationship between the actual and predicted values of responses is given in Figures. 3.7(a-c), As per the images, the models built are sufficiently approximate and the results predicted are in firm agreement with the data measured by experiments.

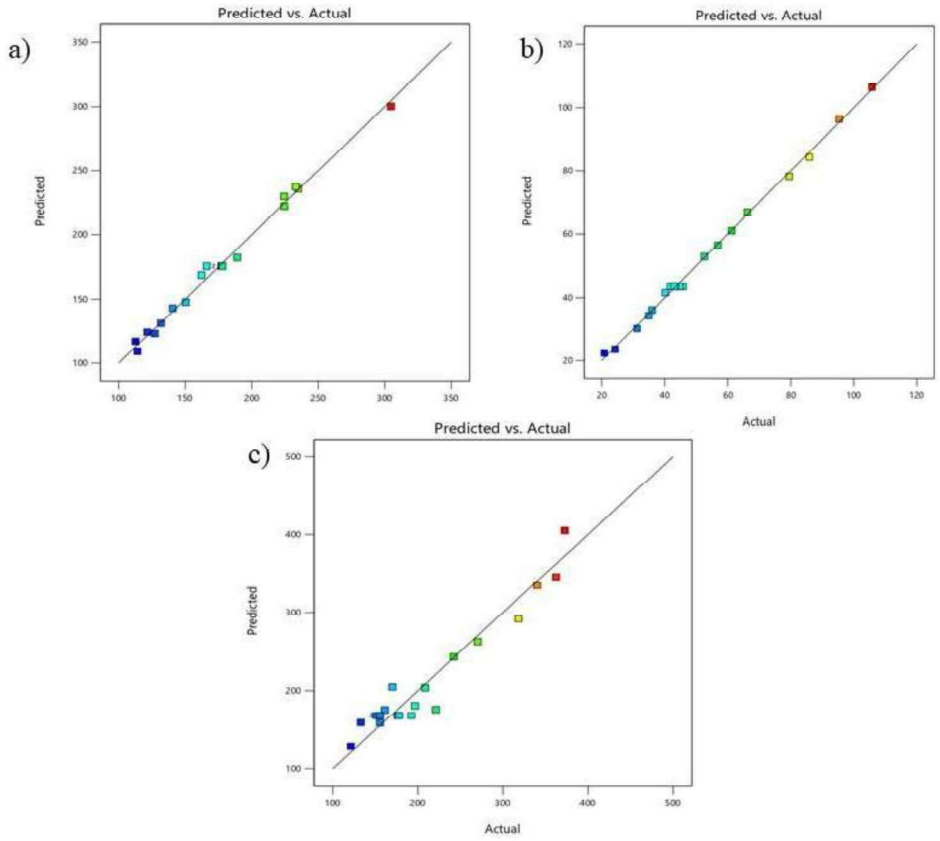

Figure 3.7. Results of experiments and predicted plots for (a) Weld Width (WW) (b) Heat Affected Zone (HAZ) and (c) Ultimate Load (UL)

3.1.3. Effects of the weld parameters on UL, WW, and HAZ (Responses)

Figure 3.8. (a-c) shows the response surface plots for weld width. Figure 3.8. (a) shows the combining effect of power and scanning speed, indicating higher scanning speed results narrow weld width and higher power results wider weld width. Figure 3.8. (b) shows the combining effect of power and frequency which indicates that first WW increases following an increase in power and then slightly decreases. The WW also increases with an increase in frequency, this is due to the increase in the density of laser input power per time cycle with the increase of the frequency. Figure 3.8. (c) shows that for any range of

power, WW decreases rapidly for increasing scanning speed and slightly for higher frequency. The surface plots inferred that WW varies significantly depending upon power and scanning speed. It can depict that increasing the power input results wider weld width yielding more base material decomposition while low laser power results in less molten weld area and narrow WW.

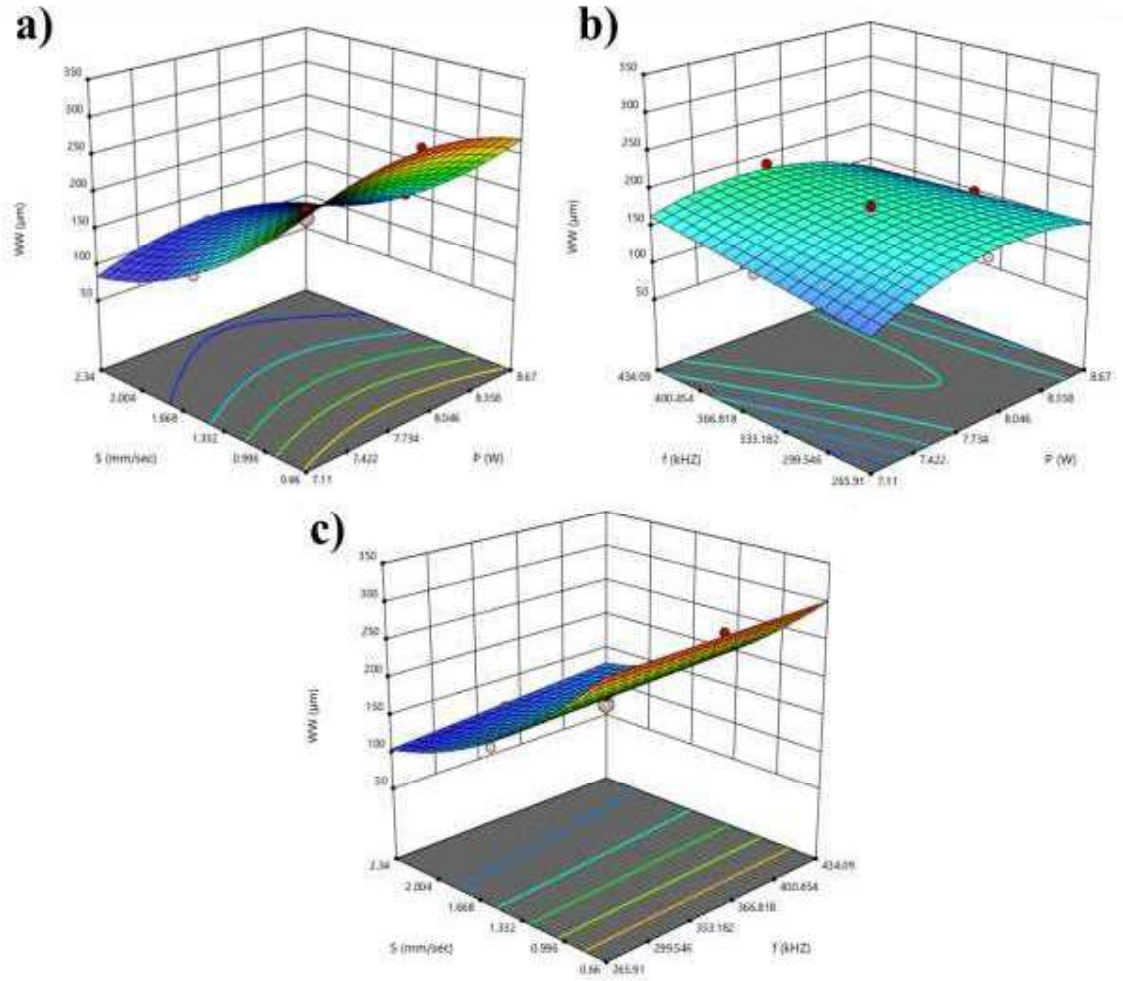

Figure 3.8. Surface plots for weld width vs (a) scanning speed and power when frequency is 350 kHz; (b) frequency and power when scanning speed is 1.5 mm/s; (c) frequency and scanning speed when power is 7.89 W

Figure 3.9. (a-c) show the surface plots for HAZ. Figure 3.9. (a) shows the combined effect of power and scanning speed. Higher scanning speed results in narrow HAZ and higher power results wider HAZ. If both the value of power and scanning speed is high, it results high value of HAZ. Figure 3.9. (b) indicates the combining effect of power and frequency. A higher value of power and frequency yields a higher value of HAZ. HAZ increases with

increasing power and frequency as with increasing frequency, the density of laser input power also increases. Figure 3.9. (c) shows the combined effect of frequency and scanning speed. HAZ decreases rapidly for increasing scanning speed and slightly for higher frequency. It can be seen that HAZ varies significantly depending on power and scanning speed. Frequency shows very little effect on it. Hence, it can be observed that greater power input results in greater HAZ and a higher value of scanning speed results lower value of HAZ.

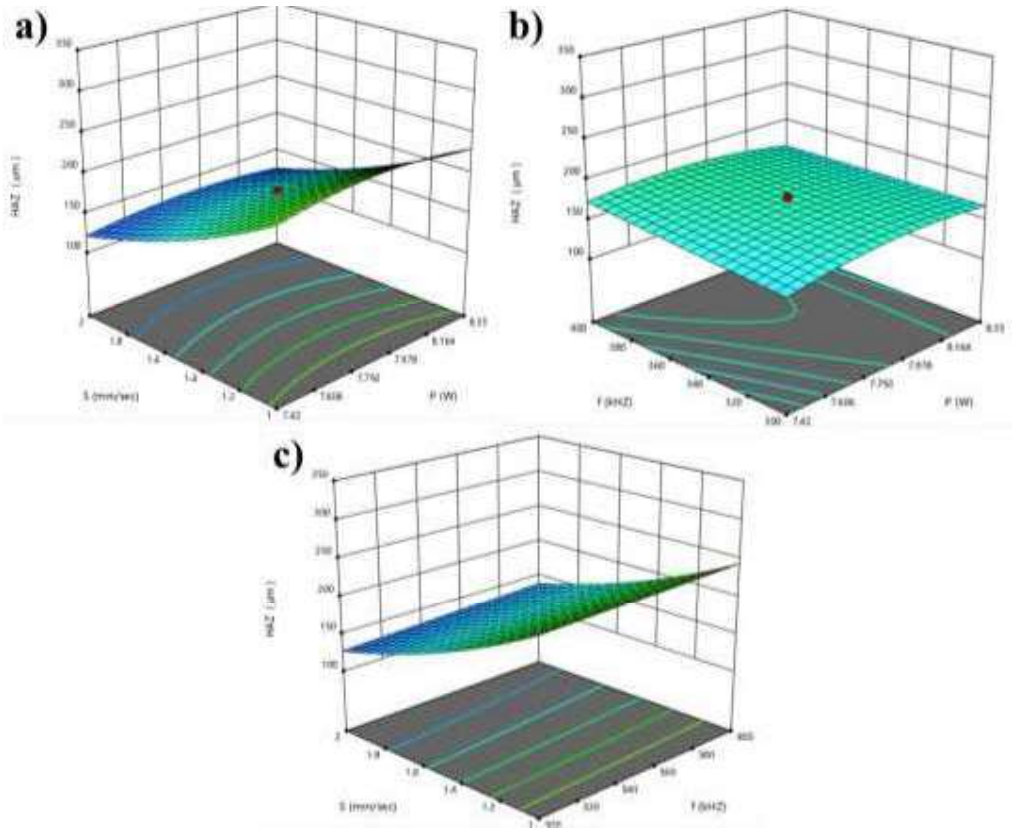

Figure 3.9. Surface plots for HAZ vs (a) scanning speed and power when frequency is 350 kHz; (b) frequency and power when scanning speed is 1.5 mm/s; (c) frequency and scanning speed when power is 7.89 W

Figure 3.10 (a – c) shows the surface plots for the UL. Figure 3.10 (a) shows the combined effect of power and scanning speed. Higher scanning speed results in narrow WW and HAZ and higher power results in wider WW and HAZ. If both the value of power and scanning speed are high, it results high value of UL. Figure 3.10 (b) indicates the combining effect of power and frequency. A higher value of power and frequency yields a higher value

of UL. With increasing power and frequency, the UL also increases, as the density of laser input power also increases. Figure 3.10 (c) shows the combined effect of frequency and scanning speed. HAZ decreases rapidly for increasing scanning speed and slightly for higher frequency. It can be seen that the UL varies significantly depending on power and scanning speed. Frequency shows very little effect on it. Hence, it can be observed that greater power input results in a greater UL and a higher value of scanning speed results lower value of UL.

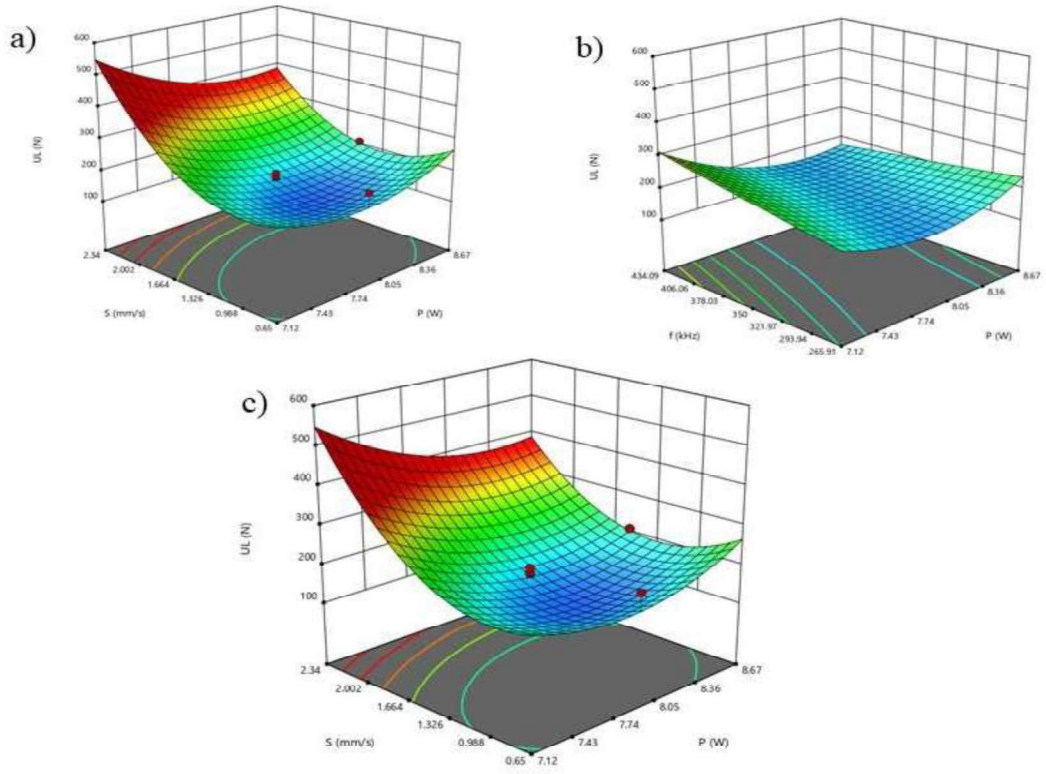

Figure 3.10. Surface plots for Ultimate Load vs (a) scanning speed and power when frequency is 350 kHz; (b) frequency and power when scanning speed is 1.5 mm/s; (c) frequency and scanning speed when power is 7.89 W

3.1.4. Optimization

The statistical software Design-Expert has an optimization feature which identifies a set of factor levels that meet specified criteria for every response and factor. This method explores space of the design, leveraging the mathematical model created for the determination of the factor settings that can best optimize different combinations of one or many objectives. Different goals can be included into an overall desirability function (D).

A specific point that optimizes this desirability function can be identified using this optimization. In this work the common optimization criteria (SS, P and f) have been selected as the criterion, the goals are set to minimize the WW, maximize the UL, and simultaneously minimize the HAZ; whereas, the weld process parameters have been selected within the value range of studied design space. The following criteria indicating the goals, and their upper and lower limits, Additionally, the importance of each goal for each response and factor are illustrated in Table 3.5 The results for the best five sets of Pareto optimal parameter combinations of selected criterion for acrylic and polycarbonate are shown in Table 3.6. Minimum WW and HAZ as well as maximum UL can be obtained within the 7.139 W -7.703 W laser power range. scanning speed varies from 2.183 mm/s - 2.316 mm/s and frequency varies from 347.362 kHz - 267.059 kHz.

Table 3.5. criteria for numerical optimization of acrylic and polycarbonate

Parameters / responses	**Limits**		**Goals**	**Importance**
	Lower	Upper	Criterion	
Power(W)	7.12	8.67	Within range	3
Scanning speed (mm/s)	265.91	434.09	Within range	3
f (kHz)	0.65	2.34	Within range	3
WW (µm)	112.65	304.64	Minimize	3
HAZ (µm)	20.85	105.8	Minimize	3
UL (N)	121.15	372.6	Maximize	3

Table 3.6. Optimum conditions for welding as per the criteria selected criteria acrylic and polycarbonate

Sl. No.	**P (W)**	**SS (mm/s)**	**f (kHz)**	**WW (µm)**	**HAZ (µm)**	**UL (N)**	**D**
1	**7.533**	**2.183**	**290.079**	**102.686**	**19.870**	**394.464**	**1 Selected**
2	7.139	2.112	308.513	83.511	18.935	432.879	1
3	7.553	2.316	267.059	92.936	20.239	458.387	1
4	7.124	2.175	347.362	90.659	19.865	470.767	1
5	7.703	2.243	282.417	106.025	20.734	403.797	1

3.1.5. Validating test/Confirmatory Test

The confirmatory tests were conducted to validate the results of statistical optimisation resulted from desirability function analysis. The welding conditions were selected randomly from Table 3.6. Table.3.7 shows the test results of the experiments performed with optimum process conditions. The predicted results are obtained from Table.3.6. and 3.7 indicates that the error percentage between optimum and experimental values is very small thus validating the technique applied for optimization.

Table 3.7. Results of Optimization validation tests

Optimal Condition			Response	WW (µm)	HAZ (µm)	UL (N)
Power (W)	**Scanning speed (mm/s)**	**frequency (kHz)**				
			Actual	103.23	18.65	389.546
7.533	2.183	290.079	Predicted	102.686	19.870	394.464
			|Error %|	0.523	6.14	1.25

3.1.6. Thermal modelling of WW and Depth of Penetration (DOP) Predictions

This section discusses the thermal modelling of TTLW of polycarbonate and acrylic. Validation of the capability of the developed Finite Element Model (FEM) was validated and the results of temperature distributions have been found, from that WW have been measured a. The WW has been then compared with the experimental result shows in Table 3.1. The temperature distribution for different positions at different times has been observed. The parameters used are same as the experimental design i.e., a scanning speed of 2 mm/s and a power of 8.35 W. However, for simplicity, the simulation frequency of the heat source has been considered to be constant. In the following paragraphs the results of temperature and WW analysis via simulation have been presented.

3.1.6.1. Temperature Analysis

The temperature distributions have been shown in different location and time in Figure 3.11. It is evident from Figure 3.11 that more heat is absorbed in the lower plate, which is acrylic. The upper polycarbonate plate gets relatively lower heat by mode of conduction and gets fused to create the welding joints. More temperature has been observed at the beginning and at the end as compared to the centre point which is due to the fact that at the beginning and ending heat could not decapitate to material bulk [125]. This observation has given validation for performing the experiment considering a square welding contour rather than straight line lap welding. The simulation inferred that the temperature is high in a precise localized region which creates a micro level weld width, but as the power density is high, the fusion of materials has occurred successfully resulting in good welding strength [126].

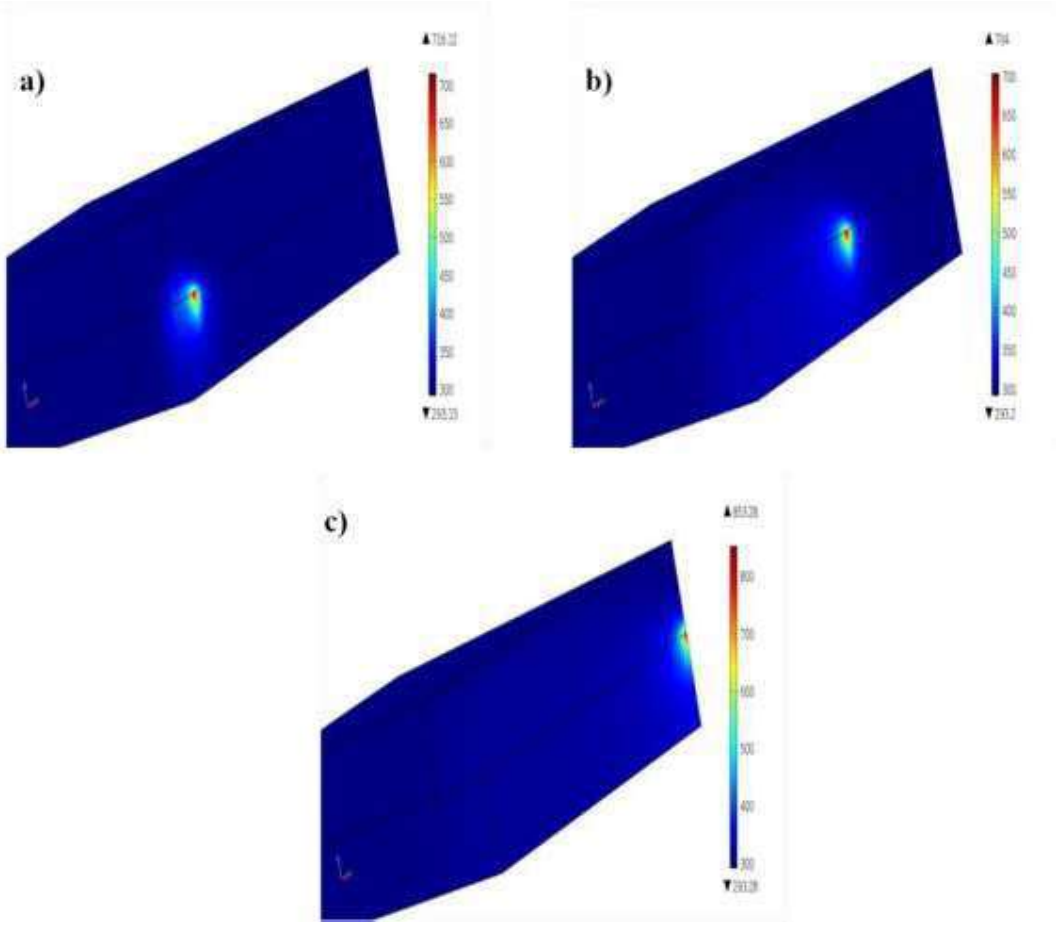

Figure 3.11. Temperature distribution of weld at different locations of weld zone at (a) beginning of the welding (i.e.t =0.1s) (b) centre of weld path (i.e.t = 0.625s) and (c) end of weld path (t = 1.25s)

The temperature distribution of centre points i.e., at t = 0.625 s for total welding time has been shown in Figure 3.12. It is observed that temperature at a particular point reaches maximum for a short period of time, then it gets reduced during which only melting of material occurs without evaporation which in terms result in good weld quality [127]. It is also observed from the graph (Figure.3.12) that the beam temperature distribution follows a Gaussian profile, which validates the assumption.

From the simulation results, it is evident that the heat interaction mainly happens on the acrylic plate which is the lower part, so only the lower absorbent part has been considered now for thermal study to observe the temperature distribution at the interface. Figure 3.13 (a) reveals the surface plot for temperature distribution at the beginning of the welding (t =0.1s), and Figure 3.13 (b) shows the surface plot for temperature distribution at the centre of the welding profile (t = 0.625 s). Figure 3.13 (c) shows the surface plot of temperature distribution at the end (t =1.25 s). The figure shows the temperature distribution along with the interface of two material where fusion has occurred. It is evident from Figure 3.13 that maximum heat is in the centre of the laser beam. Preheating has been observed to be in the small domain, which in result decreases the HAZ and weld quality gets enhanced [128].

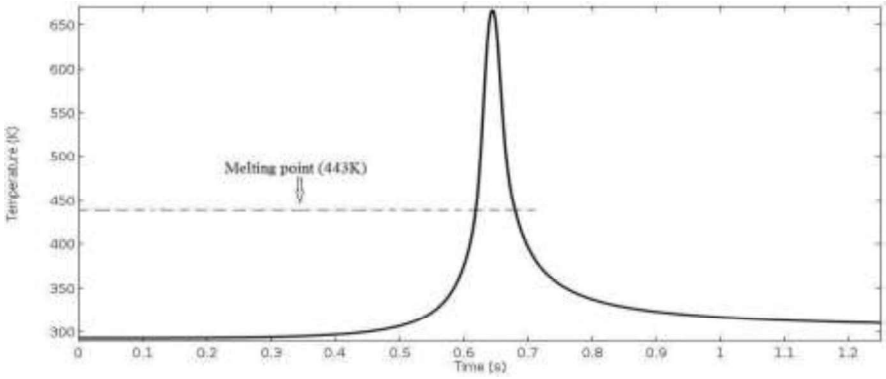

Figure 3.12. Temperature distribution of centre point for all time steps

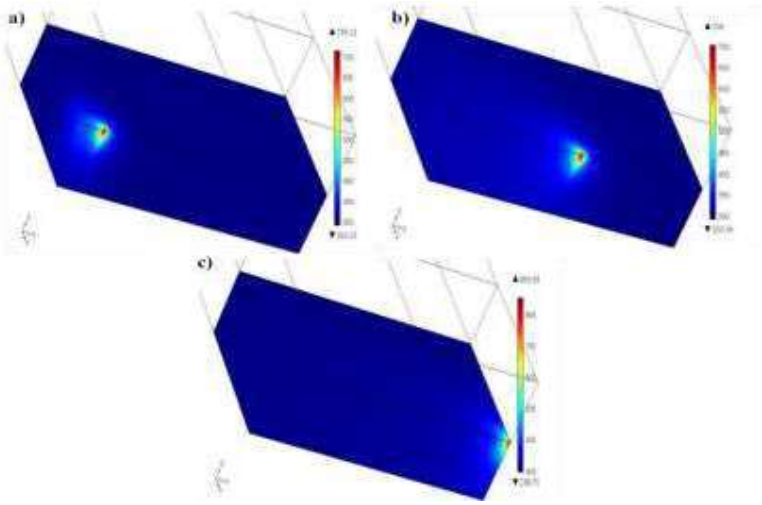

Figure 3.13. Temperature distribution surface plot (a) in the beginning of the welding (t =0.1s), (b) at centre of the welding profile (t = 0.625 s) and (c) at extreme end (t =1.25 s).

3.1.6.2. WW Analysis

A close view of temperature distribution along with the interface has been shown in Figure 3.14. Clear temperature contours are observed from the figure. From that, the regions having temperatures more than the melting point of the materials (443K) are considered to be WW. Now by taking a line along with the interface at the centre point, the temperature distribution of every point on that line has been observed. The temperature distribution along the line has been plotted in the Figure 3.15.

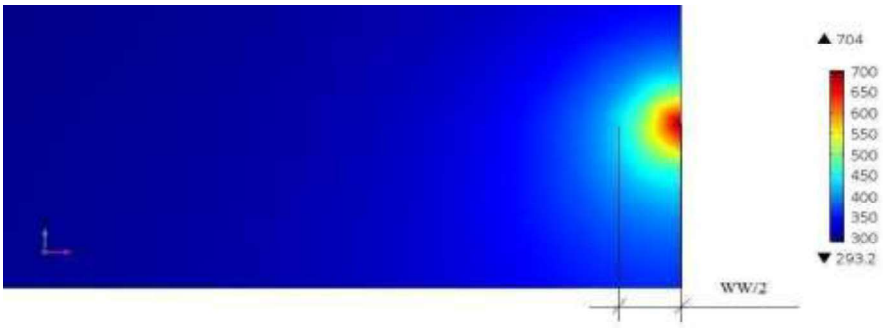

Figure 3.14. Temperature contour of the interface for weld width measurement

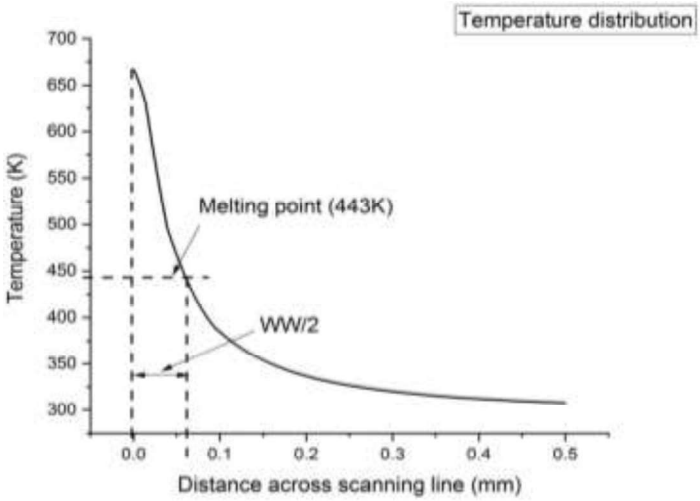

Figure 3.15. Temperature distribution along the scanning line for WW

In Figure 3.15, a horizontal line is drawn parallel to x axis intersecting the temperature distribution curve of acrylic has been drawn (dashed in Figure 3.15.) and then from the intersection vertical lines were drawn. The intersection between the x-axis and the vertical line (dashed in Figure 3.15) gives the distance value which is half of the WW, as the model has been considered for half portion. The process parameters were power of 8.35 W and a scanning speed of 2 mm/s. the WW from the simulation was 123 µm and the experimental weld width for the same set of process parameters was 124.55 µm. Hence, it has been observed that violation of response is negligible. The WW for other sets of process parameters have been measured in the same manner and given in Table 3.8.

Table 3.8. Weld width from simulation

Sl No.	P (W)	SS (mm/s)	WW (µm)
1	8.35	2.00	123.00
2	8.35	1.00	199.00
3	7.89	2.34	109.20
4	7.42	2.00	107.20
5	7.89	1.50	162.80
6	7.11	1.50	129.20
7	7.42	1.00	266.00
8	7.89	0.66	318.00
9	8.67	1.50	133.00

3.1.6.3. Comparison of Experimental and Simulation results of weld width

The same process parameters have been used in the experiment and simulation for comparing them. In the simulation, frequency was assumed to be constant so the design table for simulation has only 9 sets of process parameters. Taking each of these 9 sets of process parameters simulation has been done. The solution of the numerical simulation yields temperature distribution from which the weld width for all the process parameters can be measured using the aforesaid method. The experiment has the same set of parameters so the WW from the experiment and simulation have been compared and percentage error has been calculated. The comparisons along with percentage error are given in Table 3.9**.** It has been observed from Table 3.9. that the error percentage is in low range with a maximum error of 16.85% and the minimum error is as low as 1.24%. This indicates that the model which have been made using numerical simulation is validated. Some error is observed due to the considered assumptions for modelling the problem but the error is seen to be in acceptable range.

Table 3.9. Comparison between experiment and simulation results of WW

Sl No.	P (W)	SS (mm/s)	Experimental WW (µm)	Simulation WW (µm)	Percentage Error (%)
1	8.35	2.00	124.55	123.00	1.24
2	8.35	1.00	229.56	199.00	13.31
3	7.89	2.34	112.65	109.20	3.06
4	7.42	2.00	114.09	107.20	6.03
5	7.89	1.50	177.02	162.80	8.03
6	7.11	1.50	140.61	129.20	8.11
7	7.42	1.00	227.63	266.00	16.85
8	7.89	0.66	304.64	318.00	4.38
9	8.67	1.50	150.83	133.00	11.82

3.1.6.4. Measurement of Depth of Penetration using Simulation

The simulation model has been proved to be an adequate model of the experiment. Thus, depth of penetration measurement which is a complex process experimentally can be predicted using simulation. For process parameters of power 3.5 W and scanning speed 2 mm/s, the depth of penetration has been predicted. Figure 3.16 shows the temperature distribution in depth direction. From that, the regions having temperature more than the melting point of the acrylic (443K) are considered to be depths of penetration of acrylic (DOPA) shown in Figure 3.17 (a) and on the upper part, the regions having temperature more than melting point of polycarbonate (420K) are considered to be depth of penetration of polycarbonate (DOPP) in Figure 3.17 (b). A line has been drawn at centre towards down and up and temperature distributions are plotted along these lines in Figure 3.18 (a) and Figure 3.18 (b) respectively. In the graphs a horizontal line on melting points of the materials has been drawn (dashed) and then from the intersection another horizontal line has been drawn. The intersection between the x-axis and the vertical line (dashed) gives the distance value which is the depth of penetration. For process parameters as 8.35 W power and 2 mm/s scanning speed the DOPA is 121.37 µm and 41.67 µm. The depth of cut for other process parameters have been predicted in the same manner and tabulated in Table 3.10. From the table it has been observed that maximum depth has been reached 228.07 µm, and 106.21 µm has been the minimum depth of penetration.

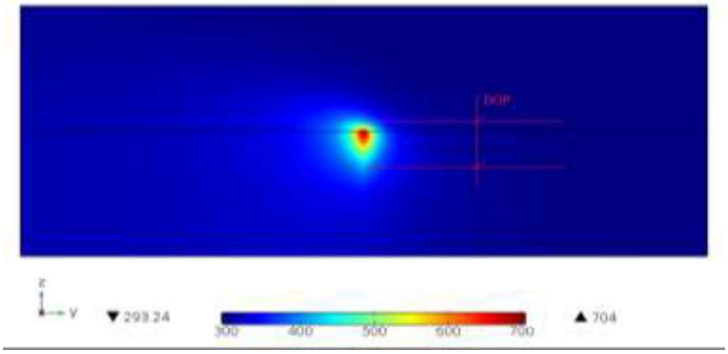

Figure 3.16. Temperature distributions in depth direction

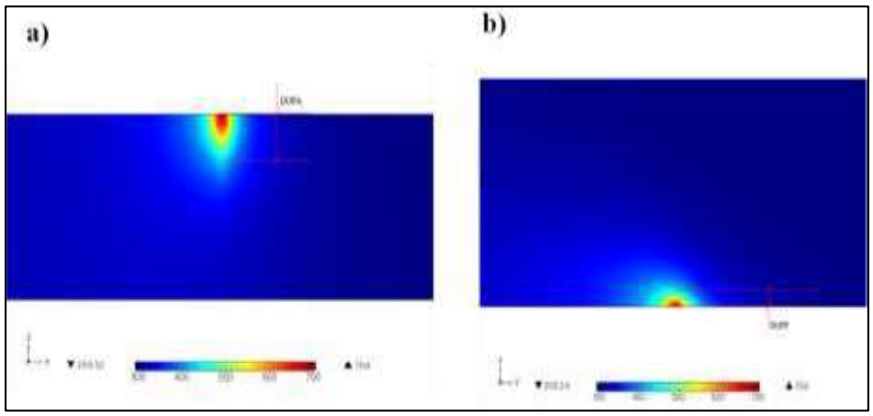

Figure 3.17. (a) DOPA, (b) DOPP

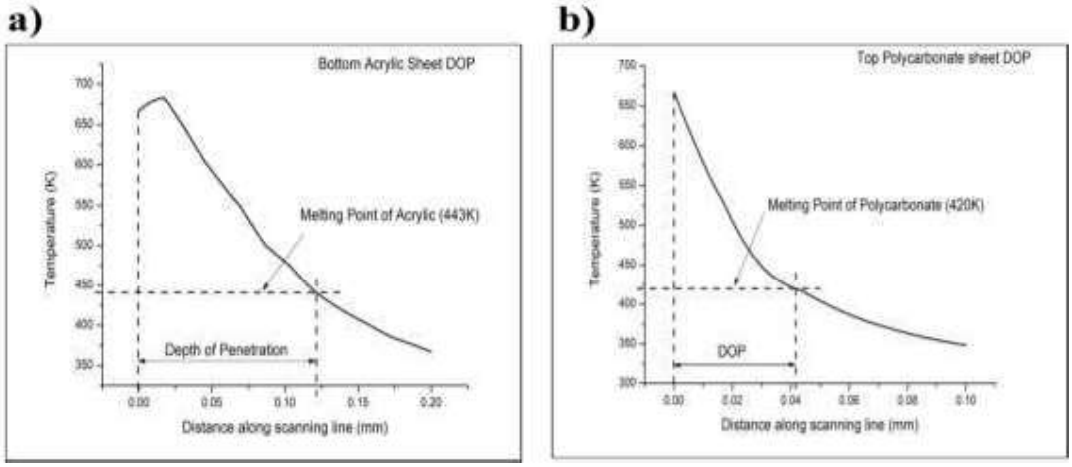

Figure 3.18. Temperature Distribution along the scanning line for (a) DOPA, (b) DOPP

Table 3.10. Table of the depth of penetration

Sl No.	P (W)	SS (mm/s)	DOPA (µm)	DOPP (µm)	DOP (µm)
1	8.35	2.00	121.37	41.67	163.04
2	8.35	1.00	156.72	57.88	214.6
3	7.89	2.34	112.99	27.79	140.78
4	7.42	2.00	109.29	26.89	136.18
5	7.89	1.50	149.09	50.72	199.81
6	7.11	1.50	105.58	42.05	147.63
7	7.42	1.00	138.76	11.92	150.68
8	7.89	0.66	165.23	62.84	228.07
9	8.67	1.50	68.37	37.84	106.21

3.1.7. Structural analysis of TTLW of Acrylic and Polycarbonate using LS-DYNA Modelling

To understand the joint firmness of these laser welds at an early design stage, laser welds were modelled using the software LS-Dyna. The simulations have been done for the 20 mm square laser weld which is developed based on the experiment results data of shear tests of lap joints. The test data and the predicted load-displacement curves are in close agreement.

The stress-strain behaviours of the parent source materials were measured using a gauge length of 56.4 mm [129] samples were tested with a cross-head speed of 0.5 mm/min. Figures 3.19 (a) and 3.19 (b) give the geometry of the test pieces and stress-strain curves of polycarbonate and acrylic source materials respectively. The welding is followed by characterization of the weld quality and results have been tabulated and analysed after that. Three key process parameters such as laser power (W), frequency (kHz) and scanning speed (mm/s) have been selected. As for the design of the experiment, the Randomization of process parameters was performed using a 3-factor 5-level Response surface methodology (RSM) and their effects on joint strength in terms of ultimate load [7]. The threshold/ limiting values for the weld process parameters were chosen corresponding to the joint strengths resulted from the initial pilot study (trial & error method). to evaluate the physical strength of the weld, load vs. displacement curves from lap shear tests were recorded and used for model validation.

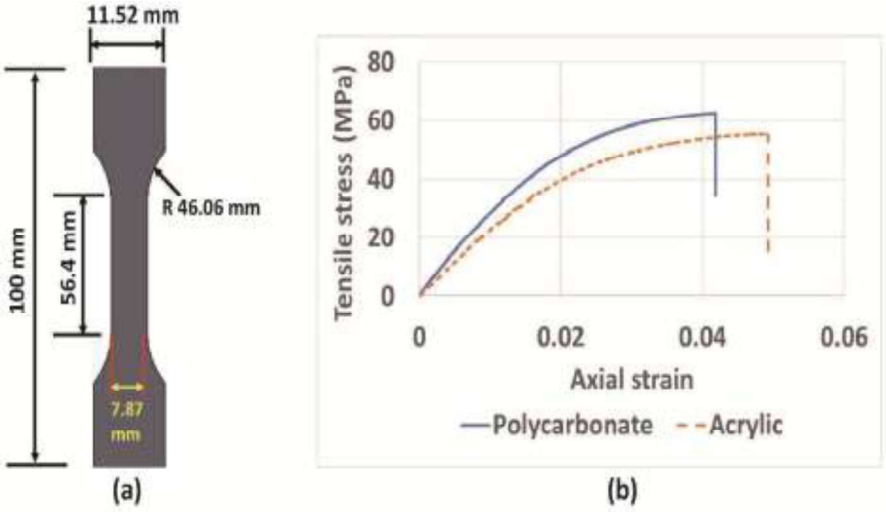

Figure 3.19. (a) Schematic representation of the tensile specimen and (b) stress-strain curve of the base materials (polycarbonate and acrylic)

3.1.7.1. Finite Element modelling approach

In the laser weld modelling process, shell elements were used to simulate the plastic sheet components representing parent materials, however, solid brick elements were found to provide greater precision in the determination of stress in three directions. Consequently, a hexagonal mesh structure was used to indicate the zone of welding. Das et al [129], Kumagai et al. [130] and Patil et al. [131] also considered the same type of elements for their parent materials and welds when constructing a laser weld model, to reduce the running/computational time associated with the model without sacrificing the precision of the outcomes, it was important to consider the shell elements of the sheet metal components and the solid elements of the welds in order. In addition, a Finite element (FE) model was created utilising the LS-Dyna platform to accurately measure the mechanical properties and mechanism of failure of the joints by laser welding [22]. The lap shear of test samples was given as model representations in Figure 3.20, which demonstrates the location of the square seam. The model consists of a square weld, a static grip, a lower part, an upper part and a moving part. In addition, to reproduce the load cell behaviour each welded specimen's static grip is connected with an elastic spring in the experimental tests. As per the experimental measurements, the sheets (including the static grip and the upper part) were designed with the properties of polycarbonate (Refer 2.1.2), while the moving part and the lower part were designed with the properties of acrylic material (Refer 2.1.1). It was determined that the sheet materials of four components viz., moving grip component, static grip component, lower component and upper components respectively should be modelled using a standardized membrane formulation. Initially, the analysis of mesh sensitivity was conducted to find the optimum size of mesh and mesh shape for the lap shear joint configuration and was found to be a square mesh with a side of 0.5 mm. Additionally, the weld is modelled to be a solid hexagonal mesh, with an element size ranging between 0.56 mm and 0.63 mm, which was adequate to replicate the characteristics of welded metal. (i.e., increment in number of layers and load-displacement showed no effects on the mechanical properties). Figure 3.21. provides an enhanced representation of the section views as well as the joint mesh side and from the lap share model, which was composed of 28,000 shells, 44,505 nodes, and 384 solids element count. Two contact-based restrictions were established for the weld zone, namely (i) the upper region between the top surface and the lower part, and (ii) the bottom region between the lower and upper parts. These contacts were introduced through the use of an LS-

DYNA*TIED_SURFACE_TO_SURFACE contact card. This approach of modelling is beneficial for the incorporation of the weld zone into other device models, as the placement of the weld zone is allowed without altering the mesh geometry. Models were created for both moving and static grips, which were based on rigid bodies. The moving grip was moved in the loading direction with a velocity profile while the static grip was limited to 6 degrees of freedom (DOF). The materials of the three cards used were those of the weld zone and base material, which included rigid bodies for the static grip and the moving grip respectively. The lower and upper parts were made of deformable bodies, while fusion zone cards were used in the zone of welding. LS-Dyna material card *MAT-020: RIGID was employed for the rigid body modelling, while *MAT- 024: Piecewise linear plasticity was employed for the simulation of the material characters of the deformable base material and the zone of weld fusion. A tabulated approach was employed in the material model according to LS-Dyna to incorporate the behaviours of stress-strain of the base materials into the model. All materials were assumed to have an isotropic hardness effect. The properties of the base material were obtained by mechanical testing, whereas the characterisation of the fusion zone was much difficult owing to the difficulties in obtaining the properties of the fusion zone. The hardness curve of the fusion zone was derived based on the results of the test of the base material. As the fusion zone or welding joints are composed of polycarbonate and acrylic only, the fusion zone hardness curve has been calculated as the average of the polycarbonate and acrylic base material properties. Additionally, to obtain the fracture within the desired grip displacement a fracture strain was necessary. This fracture strain was used as the initiator of fracture in the simulations when the experimental measurements were reached.

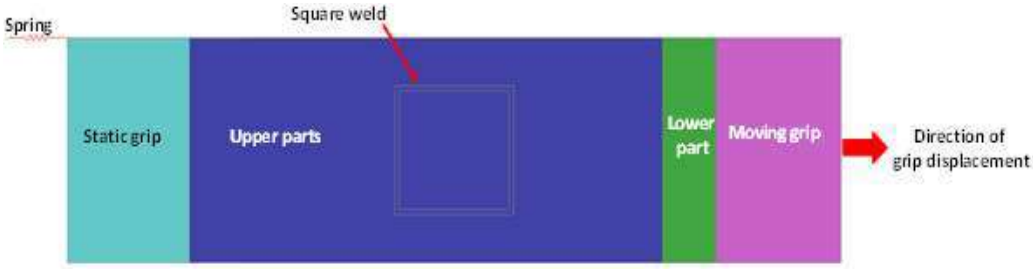

Figure 3.20. Schematic representation of lap shear test sample simulation model

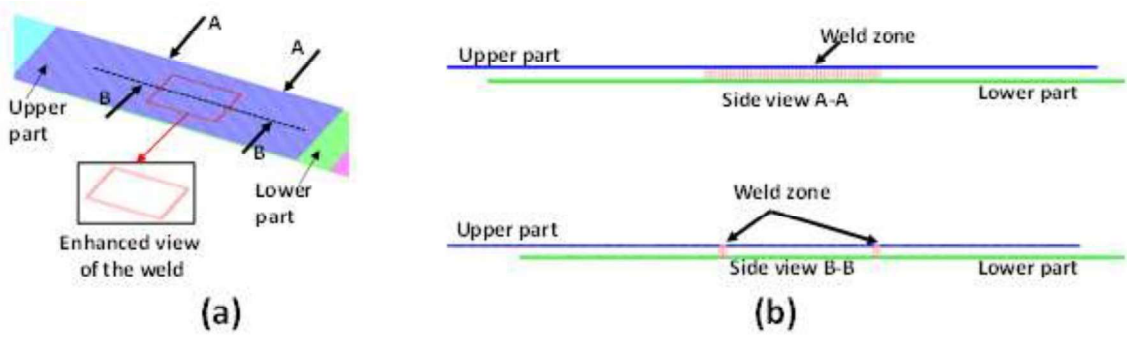

Figure 3.21. Detailed representation of mesh model (a) The joint (enlarged view) and (b) side view of the weld zone A-A and the sectional view at the middle of the weld zone B-B

3.1.7.2. Characterisation of Laser welded joints

As explained in Chapter 2 and Table 2.2, the welded joints of acrylic and PC were prepared by varying levels of different welding parameters in triplicates. The strength of the joint is one of the most important factors in determining whether or not a weld is good or bad. The welded joint strength was determined using lap shear tests. Based on the lap shear tests conducted on standard width specimens, the strength of the was determined as the ultimate load (UL) of the weld. Accordingly, Table 3.1 provides the experimentally measured values of the average ultimate load (UL) together with the corresponding standard deviation (SD). It can be observed that the highest ultimate load was obtained for experiment no. 3 (372.60 N) when the laser power was 7.89 W, scanning speed was 2.34 mm/s and frequency was 350 kHz. However, the lowest ultimate load was obtained for experiment no. 14 (121.15 N) when the laser power was 7.42 W, the frequency was 300 kHz and the scanning speed was 1 mm/s. This variation in strength may be due to the geometry of the weld bead (i.e., depth of penetration and weld width) [132]. To analyze the effects of weld process parameters viz., P, SS and f, on the ultimate load, the main effect plots of the ultimate load were given in Figure 3.22 showing the variation of ultimate load concerning power, frequency and scanning speed. Figure 3.22 indicates that with increase in power ultimate load has a decreasing trend though there is some abnormality in the result. Due to more power, there is more power density which interacts in the welding zone so more heat is generated. As more heat is generated more material gets evaporated which leads to a larger weld zone and low strength. ultimate load increases with increasing scanning speed as heat interaction time is low, so evaporation and weld width are low

which results in more strength. The frequency has a nominal/non-significant effect on controlling the ultimate load.

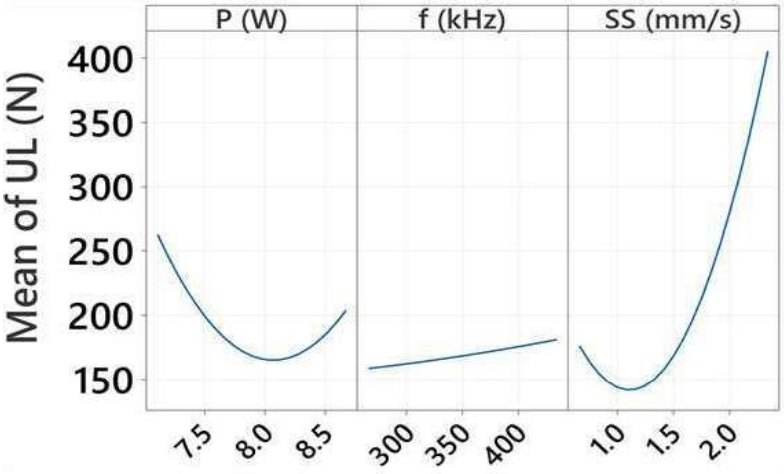

Figure. 3.22 The main effects plot for the ultimate load

3.1.7.3. Laser weld modelling of joint strength and failure prediction

The properties of the base material were procured from the information given by the manufacturer as well as through performing tensile tests as per the standards shown in Figure 3.23. The hardening curve of the weld joint/fusion zone was generated based on the hardness curve of the base materials by averaging them, as the fusion zone (FZ) consisted of both the top and bottom base materials made of acrylic and polycarbonate. Figure 3.23 shows the hardening curves for the acrylic and polycarbonate base materials and fusion zone. The fracture strain was chosen as per the experimental lap shear test, to trigger the fracture in the simulation at the grip displacement. Additional model-specific details and material data were listed in Table 3.11. For the development of the lap shear finite element model Sample no. 3 (Table 3.1) was selected since the maximum ultimate load (UL) average and the base metal failure were obtained from the same sample. To validate the developed model, one load-displacement curve was selected from the results of three tests performed on sample no 3. Figure 3.24 shows the results of computing the lap shear model by the mechanical characters obtained from the sub-areas viz., fusion zone, acrylic and polycarbonate base metal zones in the LS-Dyna software. Figure 3.24 (a) shows that the results of the experimental lap shear test and the curve of load displacement obtained using simulation are very similar. The maximum ultimate load (UL) resulting from the simulation test and lap shear tensile strength test was 360.78 N and 362.38 N respectively. Figure 3.24. (b) shows the images of the deformation sequences corresponding to specific grip

displacements of 0.2, 0.4 and 0.61 mm respectively. It can be seen that the failure was initiated at a grip displacement of 0.61 mm from the circumference of the weld and then broke from the upper sheet (polycarbonate) base material. According to Figure 3.24. (c), for the given load conditions at a grip displacement of 0.61 mm, the failure mode resulting from the simulation matches the experimental data. From Figure 3.24 (b) and (c), the failure that occurred in the heat-affected zone (HAZ) must have been due to the reason that this zone is comparatively smoother than the weld zone and base metal [133]. To derive the maximum ultimate load (UL) from a lap shear model, one of the most significant factors to be considered is fracture strain. A suitable fracture strain was selected after performing a fracture strain-based sensitivity analysis of lap shear strength to initiate the fracture at the selected load for the upper HAZs of the material.

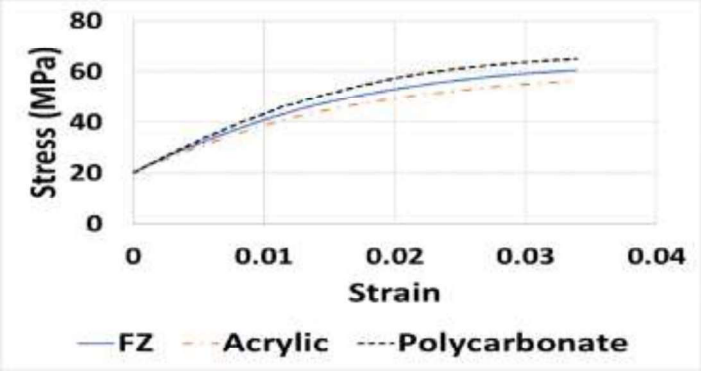

Figure 3.23. Plastic flow curves (base materials Acrylic and PC, and fusion zone FZ)

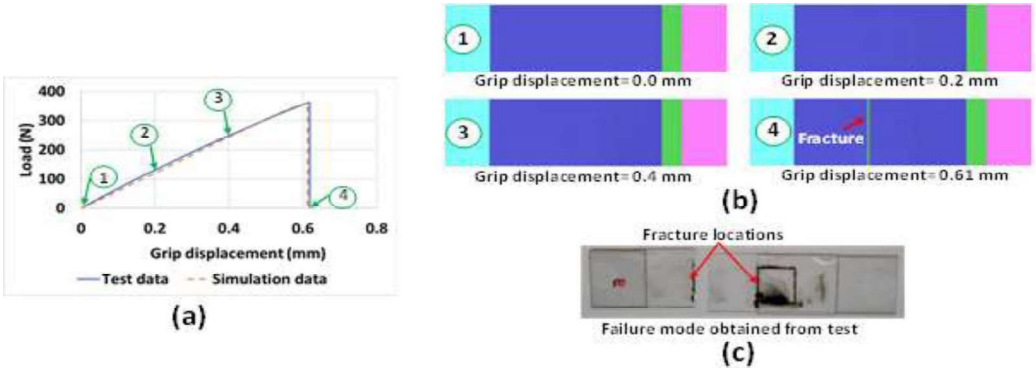

Figure 3.24. Lap shear sample test simulation (a) comparison between grip displacement curve and load obtained from simulation and physical tensile tests (b) sequence of images from the simulation at specific grip displacement and (c) fracture sample from the physical tensile test

Table 3.11. Additional data of materials and model-specific information used in developing the Finite element (FE) model

Property	Description
Type of Element	Shell: lower & upper sheets, moving grip & static grip Solid: Fusion zone (FZ) Discrete: spring-based load cell
Elastic Spring Stiffness (N/m)	100000.00
Rigid body constraints	Constraints in Y and Z displacements & in X, Y and Z rotations
Fusion Zone (FZ) plastic curve	Average to both the base materials flow curve
Fracture Strain	Selected accordingly with the fracture initiation in the experimental load-displacement curve of the lap shear test
Base metal and weld contact	TIED_SURFACE_TO_SURFACE

3.2. Study of TTLW using circular contour on Acrylic and Polycarbonate

In the present work two transparent plastic materials namely, Polycarbonate and Acrylic were subjected to Through Transmission Laser Welding (TTLW) using varied levels of laser power, scanning speed and frequency have been carried out to form lap joints without the application of filler material. The effect of welding parameters on the weld quality has been studied through inspection and tests. The design of experiments and analysis was carried out using the Statistical software Design Expert. Ultimate load (UL), Depth of penetration (DOP) and weld width (WW) have been considered as the responses. Response surface methodology (RSM) has been applied for multi-objective optimization to minimize WW and to maximize UL and DOP simultaneously. Validation of the selected optimizations were conducted by confirmatory tests.

3.2.1. Weld quality analysis

Figure 3.25 (a) shows the pictorial view of welded samples with maximum UL (experiment no. 13), before the test and after the test respectively. Whereas, Figure 3.25 (b) shows for sample with minimum ultimate load (experiment no. 11). The load vs extension plots for maximum and minimum UL have been shown in Figure 3.26 (a) and Figure 3.26 (b) respectively. The photographic view of the weld seam of the same at five different positions is shown in Figure 3.27. The WW at five different positions for each sample have been

measured and the average of those values has been taken as the weld width of the welded sample. The photographic view of the DOP is shown in Figure 3.28. The measured value of WW, UL and DOP of polycarbonate (DPP) and acrylic (DPA) is given in Table 3.12.

Figure 3.25. Experiment no.13 (power 8.40 W, Scanning Speed (SS) 1 mm/s and frequency 400 kHz) at the state of (a) before the pull test and (b) after the pull test. Experiment no. 11 (power 8.40 W, scanning speed (SS) 2 mm/s and frequency 250 kHz) at the state of (a) before the pull test and (b) after the pull test.

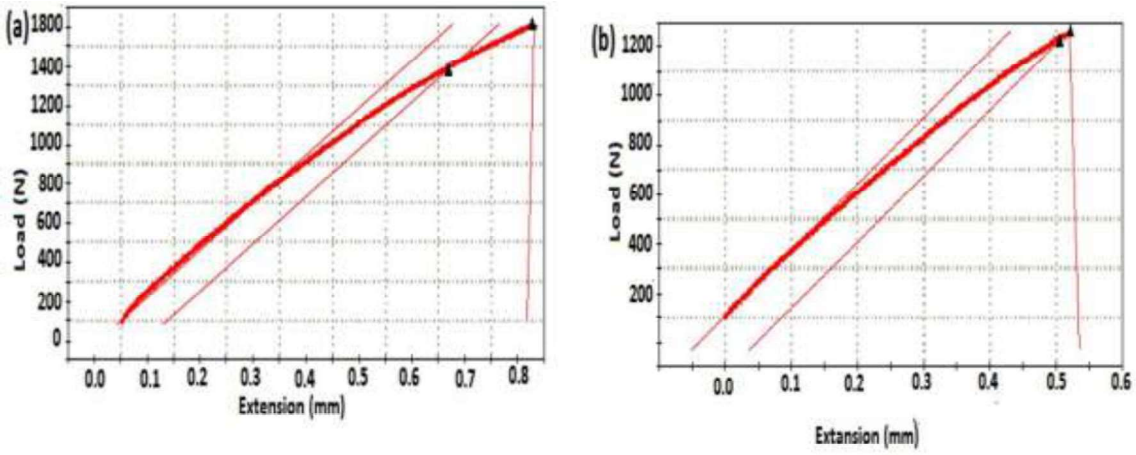

Figure 3.26 (a): Load vs. extension plot for the maximum UL (experiment no. 13) (b): Load vs. extension plot for the minimum UL (experiment no. 11)

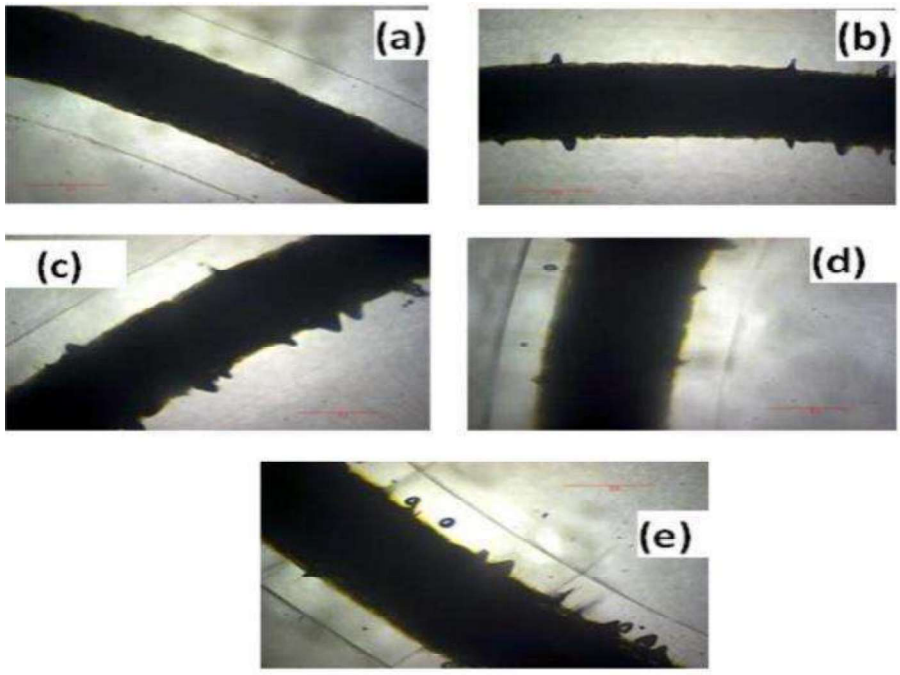

Figure 3.27 Photographic view of WW at five different locations of the welded sample of experiment no. 1 (9.60 W power, scanning speed (SS) 2.34 mm/s, frequency 325kHz)

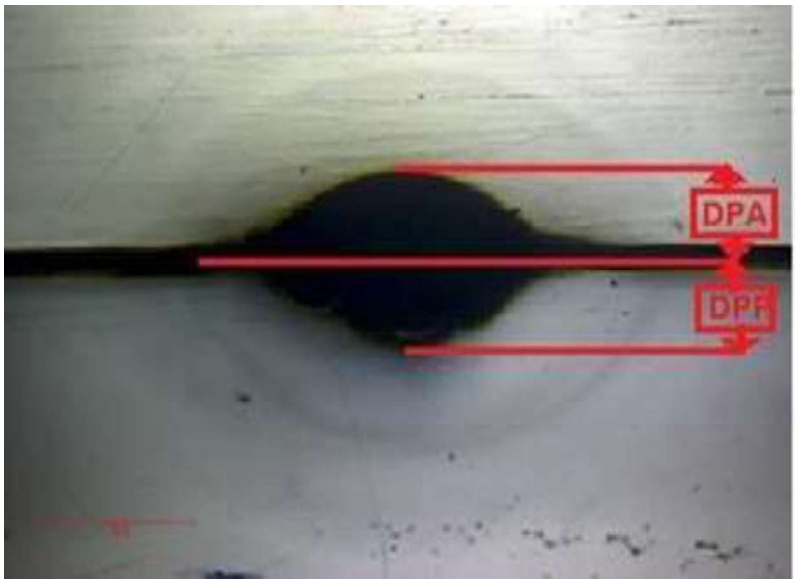

Figure 3.28 Transverse cross-section of the sample (power of 9.60 W, scanning speed (SS)of 2.34 mm/s, frequency 325 kHz) with the location of responses (DPA and DPP)

Table 3.12 Measured values of the ultimate load, weld width and Depth of penetration of welded samples

SI No	P (W)	SS (mm/s)	f (kHz)	UL (N)	WW (µm)	DPA (µm)	DPP (µm)
1	9.6	2.34	325.0	1179.020	827.794	344.440	501.070
2	9.6	1.50	451.1	1074.980	965.030	488.506	533.333
3	8.4	1.00	250.0	1290.540	1143.930	491.136	528.375
4	8.4	0.65	325.0	1223.040	1528.220	779.302	919.050
5	9.6	1.50	325.0	1478.400	1013.490	437.500	507.955
6	7.6	1.50	325.0	1426.860	714.617	278.409	348.837
7	9.6	1.50	325.0	1361.320	1038.850	447.814	502.326
8	10.8	1.00	250.0	1087.200	1344.140	854.651	911.110
9	10.8	2.00	400.0	1160.420	805.549	441.860	500.060
10	10.8	2.00	250.0	1282.300	1012.470	560.050	546.230
11	8.4	2.00	250.0	1065.520	671.378	370.588	367.816
12	10.8	1.00	400.0	1168.950	1230.960	841.860	846.080
13	8.4	1.00	400.0	1515.320	1065.840	562.500	570.176
14	9.6	1.50	198.8	1141.060	984.289	517.647	541.176
15	9.6	1.50	325.0	1372.010	1026.380	468.966	505.747
16	9.6	1.50	325.0	1380.790	1048.290	486.047	512.558
17	9.6	1.50	325.0	1359.300	1095.090	479.310	503.721
18	9.6	1.50	325.0	1377.750	1053.040	451.136	514.186
19	11.6	1.50	325.0	1094.370	1091.290	694.118	690.110
20	8.4	2.00	400.0	1149.070	693.765	408.046	448.276

3.2.2. Empirical modelling using RSM

To develop the relationship of UL, WW and DOP in terms of laser power (P), scanning speed (SS) and frequency(f) empirical model has been developed by RSM. Equations 4.1, 4.2, 4.3, and 4.4 are the developed mathematical relations for UL, WW, DPA and DPP respectively.

$$UL = -2264 + 41.4P - 521S + 16.87f - 0.373P^2 - 233.5S^2 - 0.01622f^2 + 19.45PS - 0.0581Pf - 1.150Sf \quad (4.1)$$

$$WW = -3626 + 109.6P - 1097S + 6.51f - 0.549P^2 + 169.3S^2 - 0.00526f^2 + 2.19PS - 0.0441Pf + 0.022Sf \quad (4.2)$$

$$DPA = -549 + 10.8P + 200S + 1.02f + 0.1834P^2 + 180.3S^2 + 0.00432f^2 - 10.49PS - 0.0400Pf - 0.464\ S \quad (4.3)$$

$$DPP = -1153 + 34.17P - 301.8S + 1.717f + 0.328P^2 + 282.665S^2 + 0.001701f^2 - 10.711PS - 0.03891Pf + 0.1917Sf \quad (4.4)$$

3.2.3 ANOVA

Table 3.13 shows the ANOVA table of the quadratic model for UL. The associated p-value less than 0.05 indicates that the terms are statistically significant for the given model. The main effect of the power (P), quadratic effects of the power (P^2), scanning speed (S^2), frequency (f^2), in addition to the combined interaction effects of the power (P) and scanning speed i.e., (P×S), power and frequency (P×f), scanning speed and frequency (S×f) are the significant terms in the model associated with the UL. The associated values of R^2 (93.87) adjusted R^2 (88.36) and predicted R^2(68.63) which indicate sufficiency of the model are in reasonable agreement and are close to 100%. Adequate precision compares the signal-to-noise ratio and it is desirable to get a ratio greater than 4 which indicates adequacy of the selected model. The adequacy in precision compared the signal to noise ratio where a ratio higher than 4 is desirable. The value 48.5802 which is the adequate precision indicates adequate model discrimination. The lack-of-fit is insignificant to the pure error, as this is desirable.

Table 3.13. ANOVA for ultimate load (Ultimate load)

Sources	Adj SS	Adj MS	P value	Remarks (S-significant, NS-not significant)
Model	361610	40179	0.000	S
Power (P)	86616	86616	0.000	S
Speed (S)	5412	5412	0.161	NS
Frequency (f)	182	182	0.787	NS
P^2	20060	20060	0.015	S
$_S2$	49110	49110	0.001	S
$_f2$	120022	120022	0.000	S
PS	75629	75629	0.000	S
Pf	15178	15178	0.030	S
Sf	14866	14866	0.031	S
Error	23600	2360		
Lack of Fit	13480	2696	0.380	NS
Pure Error	14866	2024		
Total	385210			

Table 3.14 shows the ANOVA table of the quadratic model for WW. The associated p-value of less than 0.05 for the model indicates that the model terms are statistically significant. The main effect of the power (P), scanning speed (S), frequency (f), the quadratic effect of the power (P^2), scanning speed (S^2), frequency (f^2), along with the interaction effect of the power and scanning speed (PS), interaction effect of power and frequency (Pf) are the significant model terms associated with the weld width. The adequacy measures R^2(98.08), adjusted R^2 (96.36) and predicted R^2 (87.45) are in reasonable agreement and are close to 100%, which indicate adequate model. The value of adequate precision of 40.2852 indicates adequate model discrimination. The lack-of-fit is not significant to the pure error, as this is desirable.

Table 3.14. Analysis of variance for weld width

Source	**Adj SS**	**Adj MS**	**P value**	**Remarks (S-significant, NS-not significant)**
Model	830548	92283	0.000	S
Linear	732280	244093	0.000	S
Power (P)	15412	15412	0.000	S
Speed (S)	565767	565767	0.000	S
Frequency (f)	12201	12201	0.021	S
Square	88566	29522	0.000	S
P^2	43483	43483	0.000	S
$_S2$	25806	25806	0.003	S
$_f2$	12608	12608	0.019	S
Two-way interaction	9702	3234	0.179	NS
PS	958	958	0.460	NS
Pf	8738	8738	0.043	S
Sf	6	6	0.954	NS
Error	16229	1623		
Lack of Fit	12271	2454	0.120	NS
Pure Error	3957	791		
Total	846777			

Table 3.15 shows the ANOVA table of the quadratic model for DPA. The associated p-value of less than 0.05 for the model indicates that the model terms are statistically significant. The main effect of the power (P), scanning speed (S), frequency (f), the quadratic effect of scanning speed (S^2), frequency (f^2), along with the interaction effect of the power and scanning speed (PS), power and frequency (Pf), scanning speed are the significant model terms associated with the breaking load. The associated values of R^2(97.81), adjusted R^2(85.61) and predicted R^2(95.86) are in reasonable agreement and are close to 100%, which indicate adequacy of the model. The adequate precision compares the signal to noise ratio and a ratio greater than 4 is desirable. The value of adequate precision of 32.1351 indicates adequate model discrimination. The lack-of-fit is not significant to the pure error, as this is desirable.

Table 3.15 Analysis of variance for depth of penetration in Acrylic (DPA)

Source	**Adj SS**	**Adj MS**	**P value**	**Remarks (S-significant, NS-not significant)**
Model	460376	51153	0.000	S
Linear	391628	130543	0.000	S
Power (P)	179406	179406	0.000	S
Speed (S)	211851	211851	0.000	S
Frequency (f)	371	371	0.000	S
Square	37125	12375	0.001	S
P^2	4847	4847	0.055	NS
S^2	29275	29275	0.000	S
f^2	8498	8498	0.017	S
Two-way interaction	31622	10541	0.002	S
PS	22008	22008	0.001	S
Pf	7188	7188	0.025	S
Sf	2426	2426	0.156	NS
Error	10327	1033		
Lack of Fit	8481	1696	0.060	NS
Pure Error	1846	369		
Total	470703			

Table 3.16 shows the ANOVA table of the quadratic model for DPP. The associated p-value of less than 0.05 for the model indicates that the model terms are statistically significant. The main effect of the power (P), scanning speed (S), the quadratic effect of the scanning speed (S^2), frequency (f^2), along with the interaction effect of the power and scanning speed (PS), power and frequency (Pf), scanning speed and frequency (Sf) are the significant model terms associated with the breaking load. The associated values of R^2(99.88), adjusted R^2(99.77) and predicted R^2 (99.21) are in reasonable agreement and are close to 100%, which indicate adequacy of the model. The adequate precision compares the signal to noise ratio and a ratio greater than 4 is desirable. The value of adequate precision of 7.55337 indicates adequate model discrimination. The lack-of-fit is not significant to the pure error, as this is desirable.

Table 3.16. Analysis of variance for depth of penetration in polycarbonate (DPP)

Source	**Adj SS**	**Adj MS**	**P value**	**Remarks (S-significant, NS-not significant)**
Model	469839	52204	0.000	S
Linear	367377	122459	0.000	S
Power (P)	156679	156679	0.000	S
Speed (S)	210698	210698	0.000	S
Frequency (f)	0	0	0.941	NS
Square	72289	24096	0.000	S
P2	155	155	0.130	NS
S2	71964	71964	0.000	S
0f2	1320	1320	0.001	S
Two-way interaction	30172	10057	0.000	S
PS	22945	22945	0.000	S
Pf	6813	6813	0.000	S
Sf	414	414	0.023	S
Error	571	57		
Lack of Fit	456	91	0.077	NS
Pure Error	114	23		
Total	470410			

3.2.4. Model Validation

The predicted vs actual plot for UL, WW, and DOP in acrylic and polycarbonate has been shown in Figure 3.29 (a-d). These plots reveal that the models developed were adequate and are in good agreement with the measured data.

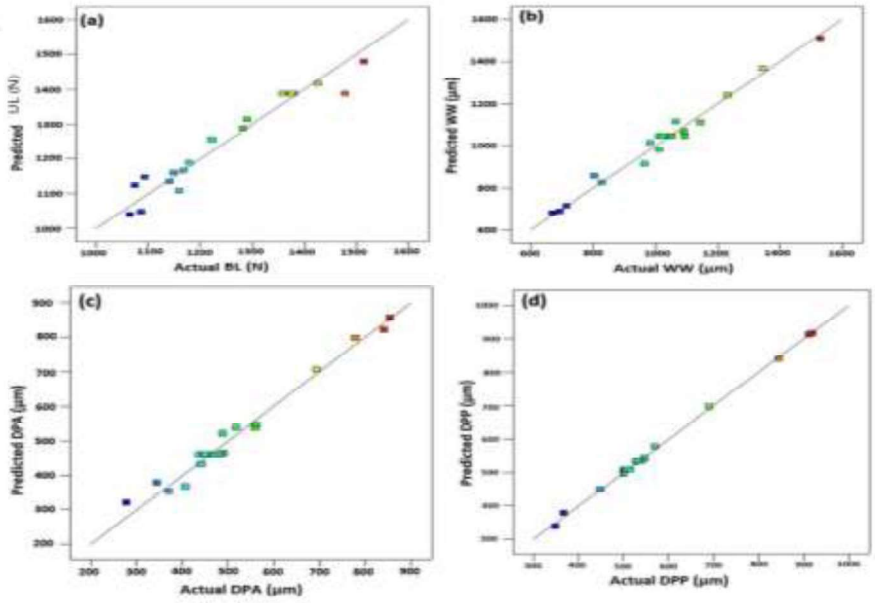

Figure 3.29. Predicted vs. actual values plots (a) UL (b) WW(c) DPA and (d)DPP)

3.2.5. Effects of the weld Parameters on UL, WW, and DPA and DPP (Responses)

Response surface plots and contour plots for UL are shown in Figure 3.30 (a - c). In case of Figure 3.30 (a), UL decreases as the frequency increases for higher scanning speed. With the increase of frequency, peak power decreases and average power increases. Lower scanning speed provides higher interaction time to absorb sufficient heat energy. It is essential to melt both welding interfaces and generate strong weld. Increase in scanning speed results in poor weld. On the other side by increasing frequency, higher laser power leads to decomposition of material at weld interface, consequently leads to poor weld and results lower ultimate load. Figure 3.30 (b) shows UL depends on power and frequency. It shows that as the scanning speed increases, higher power leads to lower breaking load. Lower the scanning speed, greater is the interaction time during welding. When power is low, lower scanning

speed provides enough heat energy to melt the substrates and produce lesser HAZ, which produces good welding. Figure 3.30 (c) shows that by increasing power, UL first increases and then decreases from lower to higher range of frequency. Lesser power with lower scanning speed and higher power with higher scanning speed result better welds. Variations in frequency do not show any remarkable change in UL throughout.

Therefore, it can be stated that low range of power with low range of scanning speed or higher range of power with higher range of scanning speed and mid-range of frequency results in desired welding.

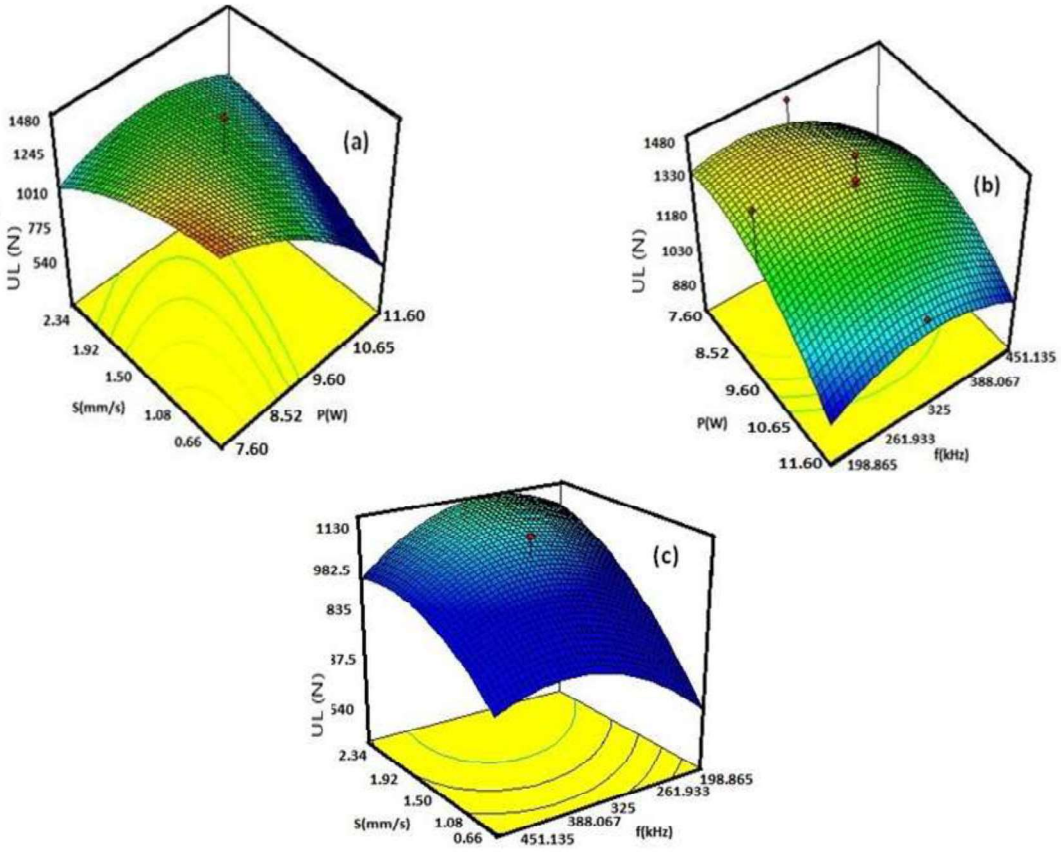

Figure 3.30 interaction between different variables on UL, (a) S and P (b) P and f, and (c) S and f shown by Response surface plots while the third parameter is held constant at its central value

Response Surface plots and contour plots for WW are shown in Figure 3.31(a) to Figure 3.31 (c). Figure 3.31 (a) shows that with an increase in frequency, higher scanning speeds result in narrow WW and higher power results in wider weld widths. Figure 3.31 (b) indicates that with higher scanning speed, first WW increases with an

increase in power and then decreases slightly. With increased frequency weld width decreases but not significantly. Figure 3.31 (c) shows that for any range of power, WW decreases rapidly for increasing scanning speed and slightly for higher frequency. It can be seen that WW varies significantly depending on power and scanning speed. Frequency shows very little effect on it. So, it can be inferred that greater power input results in wider weld width, greater HAZ, more base material decomposition and lesser power results in less molten weld area and narrow weld WW.

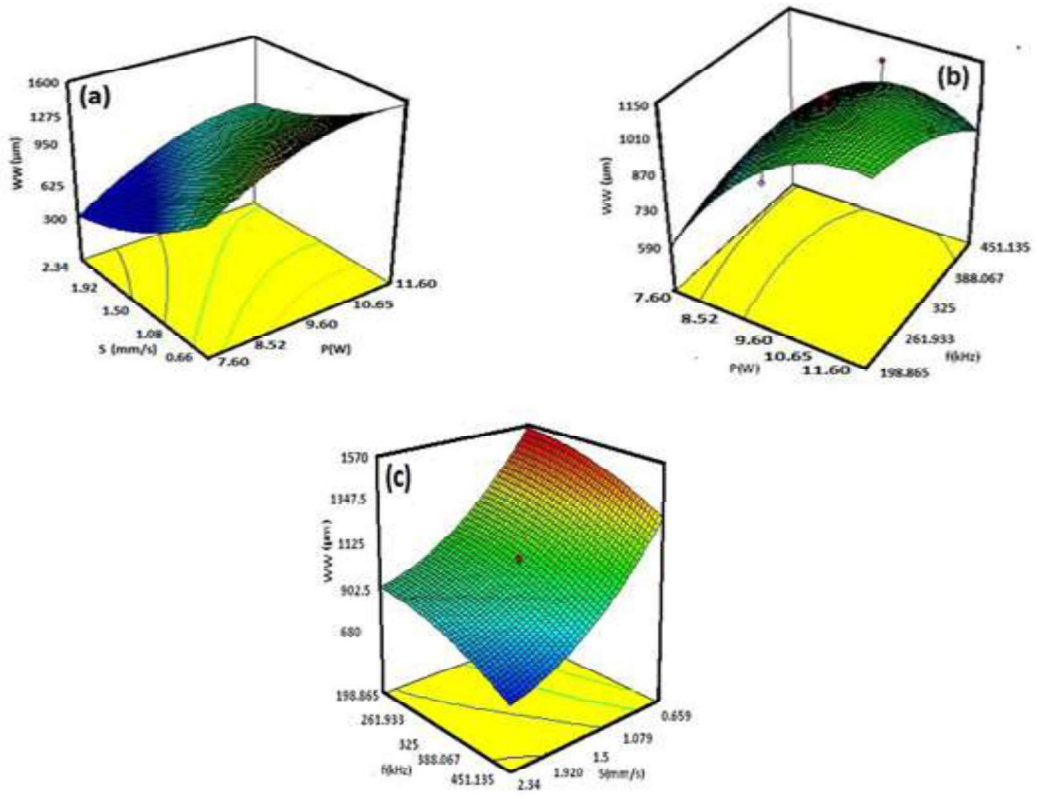

Figure 3.31 Response surface plots showing the interactions between different variables on WW (a) S× P (b) P × f, and (c) S × f while the third parameter is held constant at its central value

To determine the influence of welding input parameters on the responses, a 3-dimensional response surface is generated and plotted in line with the fitted quadratic model. The plots with one variable held constant at their corresponding centre values and the other two were shown within the working range shown in Figure 3.32 (a to c) and Figure 3.33 (a to c). From Figure 3.32 (a), it can be shown that DPA continually rises as laser power rises. Scan Speed affects DPA negatively since quicker welds don't allow enough time for heat transmission, which leads to partial fusion. Figure 3.32 (b) demonstrates that power and frequency have opposing impacts on DPA at constant speed. Furthermore, a change in power has a bigger impact on DPA than a change in frequency does. It is evident from Figure 3.32 (c) that frequency and speed have opposing impacts on DPA. The impact of a change in scanning speed is marginally greater than that of a change in frequency, though. It is important to note from Figure 3.32 (b) that DPA initially dips and then rises when power is set to the maximum value, scanning speed is kept constant, and frequency decreases from the maximum value to the minimum. Together, Figure 3.32 (c) suggests that frequency has a separate impact on DPA. Similarly, Figure 3.32 (c) demonstrates that DPA again slightly declines at first and then rises when power is constant, Scan speed is set to the highest value, and frequency decreases from its greatest value to its lowest value. This combined observation of Figure 3.32 (a) to Figure 3.32 (c) suggests that frequency affects DPA independently. The effects on DPP of altering two factors while holding a third constant are shown in Figs. Figure 3.33 (a) to Figure 3.33 (c). DPP displays an increase with an increase in power and a decrease with an increase in scan speed, much like DPA. However, Figure 3.33 (b) and Figure 3.33 (c) demonstrate that a change in frequency only has a very small impact on DPP when power and Scan speed are set to stable values. This indicates that frequency cannot significantly alter DPP on its own.

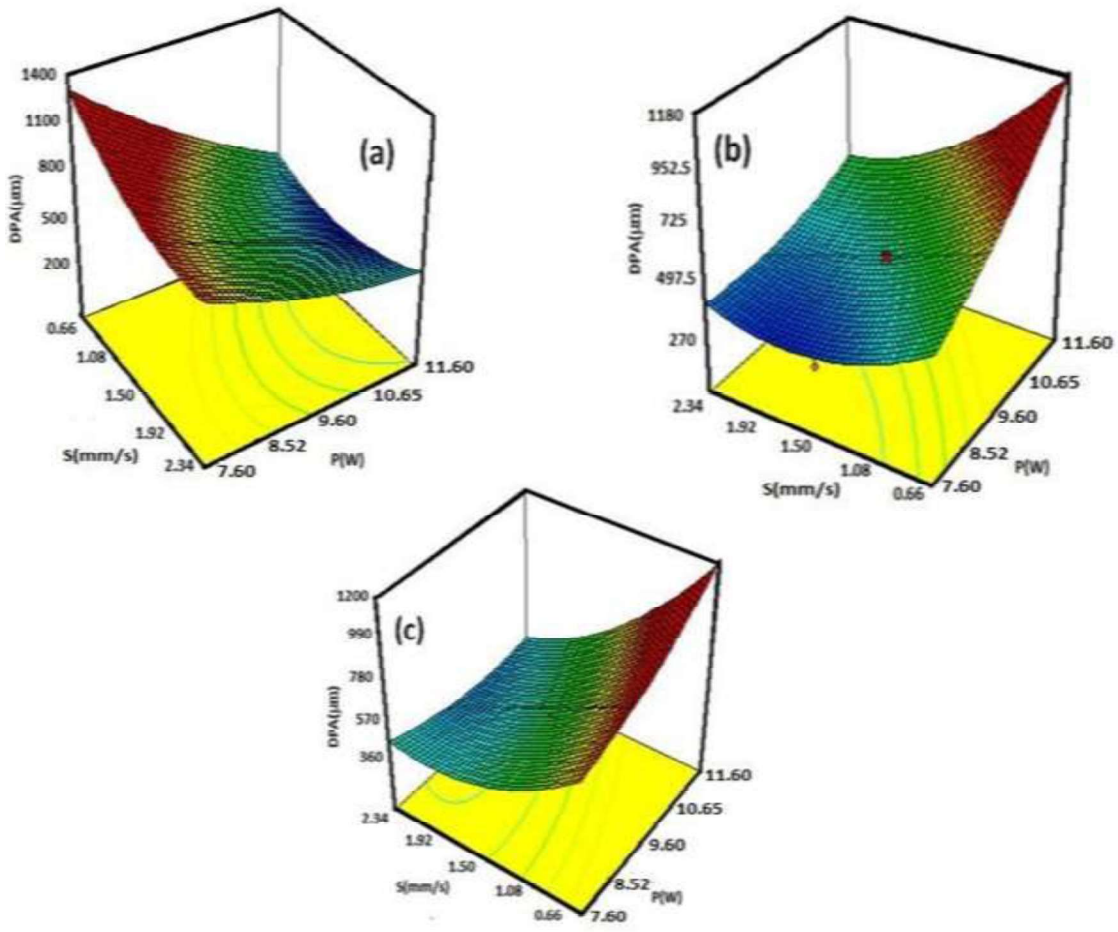

Figure 3.32. The interaction effects of a) S and P, b) P and f and C) f and S; on the DPA, appeared accordingly surface plots situating the third parameter at its centre value.

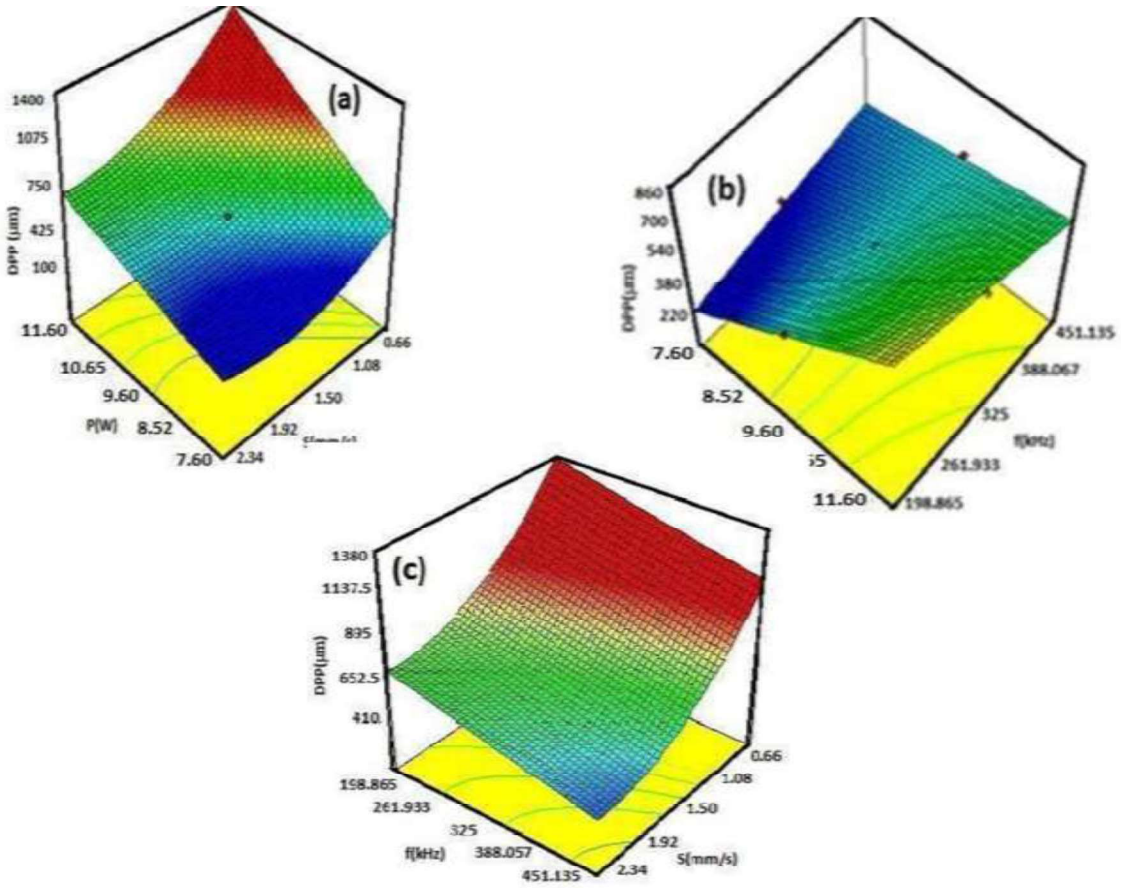

Figure 3.33 The interaction effects a) S and P, b) P and f and c) f and S; on DPP; appeared accordingly surface plots situating the third parameter at its individual Centre value.

3.2.6. Numerical Optimization

An optimization feature in the Statistical software Design-Expert identifies particular set of factor levels that meets the specified criteria for each response and factor. The design space is explored by this method, thus leveraging the mathematical model created to determine the factor settings which result in the best optimization by any combination of one or many objectives. Different goals are merged into an overall desirability function (D).

Table 3.17. Criteria chosen for numerical optimization of acrylic & polycarbonate

Response parameters	Limits		Goals	Importance
	Lower	Upper	Criterion	
P (W)	7.6	11.6	Within range	3
SS (mm/s)	0.66	2.34	Within range	3
f (kHz)	198.86	451.13	Within range	3
UL (N)	1065.52	1515.32	Maximize	3
WW (μm)	671.378	1528.22	Minimize	3
DPA(μm)	278.409	854.651	Maximize	3
DPP(μm)	348.837	919.05	Maximize	3

Table.3.18. Optimal welding parameters corresponding to the selected criteria for acrylic and polycarbonate

Sl. No.	P (W)	S (mm/s)	f (kHz)	UL (N)	WW (μm)	DPA (μm)	DPP (μm)	D
1	**7.600**	**0.719**	**451.130**	**1409.184**	**1215.113**	**774.074**	**767.864**	**0.648 Selected**
2	7.600	0.726	451.129	1409.619	1209.056	769.717	762.910	0.648
3	7.600	0.711	451.130	1408.613	1222.552	779.436	773.971	0.648
4	7.600	0.702	451.130	1408.012	1229.855	784.714	779.990	0.648
5	7.600	0.740	451.129	1410.394	1197.068	761.129	753.161	0.648

This optimization determines a point which maximizes the desirability function (D). In the present work, a common optimization criterion has been implemented and the goals were set to maximize the Ultimate Load and Depth of penetration as well as to minimize the weld width simultaneously. The process parameters were kept within the range of design space studied. Table 3.17 illustrates the criteria, indicating the goals i.e., upper and lower limits, as well as the importance of each goal for each response and factor. The best five sets of Pareto optimal parameter combinations for acrylic and polycarbonate for selected criteria are shown in Table 3.18. The optimal setting for maximum ultimate load and depth of penetration with minimum weld width can be obtained at the parameter setting of laser

power 7.6 W, scanning speed in the range of 0.702 mm/s to 0.740 mm/s and frequency of 451.130 kHz.

3.2.7. Validation/Confirmatory Test

The results of optimization obtained by desirability function analysis, have been validated by conducting confirmatory tests. Choice of welding parameters have been selected randomly from Table 3.16. Results of the experiments performed at optimum conditions were given in Table 3.17. As per the inference from Table 3.19. the error percentage between the optimum and the experimental values is significantly minimal thus validating the applied optimization technique.

Table 3.19. Confirmatory Test

Optimal Condition			Responses	UL (N)	WW (µm)	DPA (µm)	DPP (µm)
P (W)	S (mm/s)	f (kHz)					
7.600	0.719	451.130	Actual	1409.184	1215.113	774.074	767.864
			Predicted	1415.263	1227.364	782.087	771.453
			|Error %|	0.431	1.008	1.035	0.467

Chapter-4

4. CONCLUSIONS AND FUTURE SCOPE OF WORK

4.1. Conclusions

As per the results, data analysis of experiments and comprehensive discussion, conclusions are summarised below.

- Results indicated that increasing laser power initially increased weld width, but then it decreased, whereas the HAZ consistently expanded with increased power.
- The results of ANOVA show that scanning speed exhibited the maximum impact on weld width and HAZ, with a percentage contribution of 89.34% and 80.87%, respectively, while the other parameters had a nominal influence.
- FEM simulations aligned closely with experimental data, showing an average error of 8.09%.
- Weld quality analysis of 0.5 mm thick plates shows that maximum weld strength achieved is 372.60 N at 7.89 W power, 350 kHz frequency and 2.34 mm/s welding speed. Whereas, the minimum ultimate load of 121.15 N was obtained using a laser power with 7.42 W and a frequency of 300 kHz, whereas the welding speed is kept at 1 mm/s.
- Structural modelling (LS-Dyna) of laser weld predicts similar load-displacement characteristics compared to that resulting from a physical test.
- Ultimate load decreased with an increase in power and scanning speed but increased with frequency up to a point before it started to decline.
- Weld width decreased with an increase in scanning speed up to a threshold limit resulting in a low HAZ as well as a stronger weld. A further increment in scanning speed results in a weaker weld due to the inefficient melting which causes less efficient bonding.
- Frequency shows a contradictory trend in the case of depth of penetration. Lower power with higher frequency and higher power with lower frequency gives higher depth of penetration, thus stronger weld.
- When all of the responses are optimized in one setting, the parameter settings are: the power of 64.2014% of 12 W, frequency of 451.1340 kHz and a scanning speed of 0.6591 mm/s.

4.2 Limitations

- Transmission Laser Welding (TLW) requires differential optical properties between the two joining components where one must be laser transparent while the other should be laser-absorptive.
- For two transparent polymers, addition of absorbing agents (such as carbon black or specialized dyes) is required. However, these additives can degrade optical transparency, biocompatibility, and mechanical performance
- TLW processes are highly sensitive to part fit-up, thermal gradients, and material thickness variations.
- Sustainability Challenges - The use of non-recyclable additives and the need for high laser power to compensate for poor natural absorption contribute to an increased environmental footprint.
- The recyclability and life cycle impacts of laser-welded transparent plastic products was poorly studied. Many polymer combinations used in TLW are not easily separable at end-of-life, which poses additional challenges for circular economy approaches.

4.3 Future Scope of Work

- Clamping pressure can be included as a process parameter.
- Modelling can be done by varying spot diameters.
- CFD modelling can be incorporated to counter the porosity into the weld pool.
- Mechanical and thermal properties like TGA, DAC, DTA can be studied
- Microstructure & Surface analysis like SEM, TEM can be done.
- Meta-heuristic tools like PSO, GWO, ABC can be done
- Machine learning algorithms may be considered for optimization purposes

Future Directions-Looking forward, research should prioritize the development of additive-free TLW techniques for example, through the use of lasers at alternative wavelengths (Visible, UV and Tailored IR) that can induce selective interfacial heating without the need for absorbers. Advancements in laser beam shaping, adaptive control systems, and in-situ process monitoring (such as pyrometry or thermography) are also critical to improve process stability and reduce defect rates. More emphasis should be placed on integrating sustainability considerations into TLW research, including comprehensive life cycle assessment (LCA) studies of welded products, exploration of

biodegradable transparent polymers suitable for TLW, and methods for facilitating disassembly or material recovery at end-of-life. Addressing these aspects will be essential to ensure that TLW can evolve into a truly sustainable manufacturing solution for next-generation transparent plastic assemblies.

Bibliography

[1] N. Kumar, N. Kumar, A. Bandyopadhyay, Optimization of Pulsed Nd:YVO4 Through Transmission Laser Welding of Transparent Acrylic and Polycarbonate, Mater. Today Proc. 5 (2018) 5235–5243. https://doi.org/10.1016/j.matpr.2017.12.106.

[2] T. Klotzbuecher, M. Letschert, T. Braune, K.-S. Drese, T. Doll, Diode laser welding for packaging of transparent micro-structured polymer chips, Laser-Based Micropackaging 6107 (2006) 610704. https://doi.org/10.1117/12.649248.

[3] M. Aden, V. Mamuschkin, A. Olowinsky, Influence of carbon black and indium tin oxide absorber particles on laser transmission welding, Opt. Laser Technol. 69 (2015) 87–91. https://doi.org/10.1016/j.optlastec.2014.12.015.

[4] S.M. Sapuan, W.H. Haniffah, F.M. AL-Oqla, Y. Nukman, M. Enamul Hoque, M.L. Sanyang, Effects of reinforcing elements on the performance of laser transmission welding process in polymer composites: A systematic review, Int. J. Performability Eng. 12 (2016) 535–550.

[5] N. Kumar, M. Mukherjee, A. Bandyopadhyay, Comparative study of pulsed Nd:YAG laser welding of AISI 304 and AISI 316 stainless steels, Opt. Laser Technol. 88 (2017) 24–39. https://doi.org/10.1016/j.optlastec.2016.08.018.

[6] D. Grewell, A. Benatar, Welding of plastics: Fundamentals and new developments, Int. Polym. Process. 22 (2007) 43–60. https://doi.org/10.3139/217.0051.

[7] J.P. Coelho, M.A. Abreu, M.C. Pires, High-speed laser welding of plastic films, Opt. Lasers Eng. 34 (2000) 385–395. https://doi.org/10.1016/S0143-8166(00)00071-3.

[8] F. Sari, W.M. Hoffmann, E. Haberstroh, R. Poprawe, Applications of laser transmission processes for the joining of plastics, silicon and glass micro parts, Microsyst. Technol. 14 (2008) 1879–1886. https://doi.org/10.1007/s00542-008-0675-3.

[9] S. Reinl, Diode lasers used in plastic welding and selective laser soldering - Applications and products, Phys. Procedia 41 (2013) 234–240. https://doi.org/10.1016/j.phpro.2013.03.074.

[10] P. Hilton, Laser Welding of Fabrics Using Infrared Absorbing Dyes, … Spec. Mater. III, St Luois MO … (2000) 1–6. http://www.clearweld.cn/edufiles/CW of fabrics-materials solution conference 2000.pdf.

[11] A. Visco, C. Scolaro, A. Quattrocchi, R. Montanini, Response to fatigue stress of

biomedical grade polyethylene joints welded by a diode laser, J. Mech. Behav. Biomed. Mater. 86 (2018) 390–396. https://doi.org/10.1016/j.jmbbm.2018.07.006.

[12] Y. Kurosaki, K. Satoh, A fiber laser welding of plastics assisted by transparent solid heat sink to prevent the surface thermal damages, Phys. Procedia 5 (2010) 173–181. https://doi.org/10.1016/j.phpro.2010.08.042.

[13] E. Ghorbel, G. Casalino, S. Abed, Laser diode transmission welding of polypropylene: Geometrical and microstructure characterisation of weld, Mater. Des. 30 (2009) 2745–2751. https://doi.org/10.1016/j.matdes.2008.10.027.

[14] P.A. Atanasov, Laser welding of plastics: theory and experiments, Opt. Eng. 34 (1995) 2976. https://doi.org/10.1117/12.210747.

[15] T.B. Juhl, J.D.C. Christiansen, E.A. Jensen, Mechanical testing of polystyrene/polystyrene laser welds, Polym. Test. 32 (2013) 475–481. https://doi.org/10.1016/j.polymertesting.2013.01.009.

[16] H. Nakamura, M. Terada, Plastics welding with diode laser, Yosetsu Gakkai Shi/Journal Japan Weld. Soc. 72 (2003) 29–32. https://doi.org/10.2207/qjjws1943.72.189.

[17] B.G. Bryden, Welding of plastics with high power diode lasers, Ind. Rob. 31 (2004) 30–33. https://doi.org/10.1108/01439910410511975.

[18] N. Kumar, R. Rudrapati, P.K. Pal, Multi-objective Optimization in through Laser Transmission Welding of Thermoplastics Using Grey-based Taguchi Method, Procedia Mater. Sci. 5 (2014) 2178–2187. https://doi.org/10.1016/j.mspro.2014.07.423.

[19] B. Acherjee, A.S. Kuar, S. Mitra, D. Misra, Selection of process parameters for optimizing the weld strength in laser transmission welding of acrylics, Proc. Inst. Mech. Eng. Part B J. Eng. Manuf. 224 (2010) 1529–1536. https://doi.org/10.1243/09544054JEM1854.

[20] H.M. Shin, H.W. Choi, Design of energy optimization for laser polymer joining process, Int. J. Adv. Manuf. Technol. 75 (2014) 1569–1576. https://doi.org/10.1007/s00170-014-6241-5.

[21] M. Chen, G. Zak, P.J. Bates, Description of transmitted energy during laser transmission welding of polymers, Weld. World 57 (2013) 171–178. https://doi.org/10.1007/s40194-012-0003-5.

[22] M. Chen, G. Zak, P.J. Bates, 3D finite element modelling of contour laser transmission welding of polycarbonate, Weld. World 53 (2009).

https://doi.org/10.1007/BF03266731.

[23] M. Aden, Influence of the Laser-Beam Distribution on the Seam Dimensions for Laser-Transmission Welding: A Simulative Approach, Lasers Manuf. Mater. Process. 3 (2016) 100–110. https://doi.org/10.1007/s40516-016-0023-x.

[24] M. Geiger, T. Frick, M. Schmidt, Optical properties of plastics and their role for the modelling of the laser transmission welding process, Prod. Eng. 3 (2009) 49–55. https://doi.org/10.1007/s11740-008-0141-1.

[25] Y. Mubarak, P.J. Martin, M. Ahmad, Modeling of non-isothermal crystallization kinetics of isotactic polypropylene, Polymer (Guildf). 114 (2009) 3171–3182.

[26] C. Albano, J. Papa, E. González, O. Navarro, R. González, Temperature and crystallinity profiles in polyolefines isothermal and non-isothermal solidification processes, Eur. Polym. J. 39 (2003) 1215–1222. https://doi.org/10.1016/S0014-3057(02)00368-3.

[27] Y. Masubuchi, K. Watanabe, W. Nagatake, J.I. Takimoto, K. Koyama, Thermal analysis of shear induced crystallization by the shear flow thermal rheometer: Isothermal crystallization of polypropylene, Polymer (Guildf). 42 (2001) 5023–5027. https://doi.org/10.1016/S0032-3861(00)00886-7.

[28] J. KNEIP, Heat transfer in semi-transparent materials during laser interaction, J. Mater. Process. Technol. (2004). https://doi.org/10.1016/j.matprotec.2004.04.380.

[29] B. Acherjee, D. Misra, D. Bose, K. Venkadeshwaran, Prediction of weld strength and seam width for laser transmission welding of thermoplastic using response surface methodology, Opt. Laser Technol. 41 (2009) 956–967. https://doi.org/10.1016/j.optlastec.2009.04.007.

[30] C.Y. Wang, P.J. Bates, M. Aghamirian, G. Zak, R. Nicholls, M. Chen, Quantitative morphological analysis of carbon black in polymers used in laser transmission welding, Weld. World 51 (2007) 85–90. https://doi.org/10.1007/BF03266564.

[31] D. Grewell, P. Rooney, V.A. Kagan, Relationship between optical properties and optimized processing parameters for through-transmission laser welding of thermoplastics, J. Reinf. Plast. Compos. 23 (2004) 239–247. https://doi.org/10.1177/0731684404030732.

[32] E. Haberstroh, W.-M. Hoffmann, R. Poprawe, F. Sari, Laser transmission joining in microtechnology, Microsyst. Technol. 12 (2006) 1173–1173. https://doi.org/10.1007/s00542-006-0237-5.

[33] L. Li, S. Hong, R. Huang, Effect of pressure on the crystallization behaviour of

polyethylene terephthalate, J. Phys. Condens. Matter 14 (2002) 11195–11198. https://doi.org/10.1088/0953-8984/14/44/452.

[34] J. De Pelsmaeker, G.J. Graulus, S. Van Vlierberghe, H. Thienpont, D. Van Hemelrijck, P. Dubruel, H. Ottevaere, Clear to clear laser welding for joining thermoplastic polymers: A comparative study based on physicochemical characterization, J. Mater. Process. Technol. 255 (2018) 808–815. https://doi.org/10.1016/j.jmatprotec.2017.12.011.

[35] P. Jaeschke, V. Wippo, O. Suttmann, L. Overmeyer, Advanced laser welding of high-performance thermoplastic composites, J. Laser Appl. 27 (2015). https://doi.org/10.2351/1.4906379.

[36] H. Ghasemi, Y. Zhang, P.J. Bates, G. Zak, D.L. DuQuesnay, Effect of processing parameters on meltdown in quasi-simultaneous laser transmission welding, Opt. Laser Technol. 107 (2018) 244–252. https://doi.org/10.1016/j.optlastec.2018.05.047.

[37] B. Acherjee, Hybrid laser arc welding: State-of-art review, Opt. Laser Technol. 99 (2018) 60–71. https://doi.org/10.1016/j.optlastec.2017.09.038.

[38] X. Wang, H. Chen, H. Liu, P. Li, Z. Yan, C. Huang, Z. Zhao, Y. Gu, Simulation and optimization of continuous laser transmission welding between PET and titanium through FEM, RSM, GA and experiments, Opt. Lasers Eng. 51 (2013) 1245–1254. https://doi.org/10.1016/j.optlaseng.2013.04.021.

[39] X. Wang, H. Chen, H. Liu, Investigation of the relationships of process parameters, molten pool geometry and shear strength in laser transmission welding of polyethylene terephthalate and polypropylene, Mater. Des. 55 (2014) 343–352. https://doi.org/10.1016/j.matdes.2013.09.052.

[40] V. Mamuschkin, M. Aden, S. Glaser, C. Engelmann, A. Olowinsky, A. Gillner, Laser transmission welding of white thermoplastics with adapted wavelengths, ICALEO 2013 - 32nd Int. Congr. Appl. Lasers Electro-Optics (2013) 160–165. https://doi.org/10.2351/1.5062865.

[41] Z. Chen, Z. Gong, Y. Jiao, Y. Wang, K. Shi, J. Wu, Moisture stability improvement of asphalt mixture considering the surface characteristics of steel slag coarse aggregate, Constr. Build. Mater. 251 (2020) 118987. https://doi.org/10.1016/j.conbuildmat.2020.118987.

[42] W. Tao, X. Su, Y. Chen, Z. Tian, Joint formation and fracture characteristics of laser welded CFRP/TC4 joints, J. Manuf. Process. 45 (2019) 1–8.

https://doi.org/10.1016/j.jmapro.2019.05.028.

[43] J. Jiao, Z. Xu, Q. Wang, L. Sheng, W. Zhang, CFRTP and stainless steel laser joining: Thermal defects analysis and joining parameters optimization, Opt. Laser Technol. 103 (2018) 170–176. https://doi.org/10.1016/j.optlastec.2018.01.023.

[44] G. Casalino, E. Ghorbel, Numerical model of CO2 laser welding of thermoplastic polymers, J. Mater. Process. Technol. 207 (2008) 63–71. https://doi.org/10.1016/j.jmatprotec.2007.12.092.

[45] Z. Chen, Y. Huang, F. Han, D. Tang, Numerical and experimental investigation on laser transmission welding of fiberglass-doped PP and ABS, J. Manuf. Process. 31 (2018) 1–8. https://doi.org/10.1016/j.jmapro.2017.10.013.

[46] J.M.P. Coelho, M.A. Abreu, F. Carvalho Rodrigues, Modelling the spot shape influence on high-speed transmission lap welding of thermoplastics films, Opt. Lasers Eng. 46 (2008) 55–61. https://doi.org/10.1016/j.optlaseng.2007.07.001.

[47] S.P. Dwivedi, S. Sharma, Optimization of Laser Transmission Joining Process Parameters on Joint Strength of PET and 316 L Stainless Steel Joint Using Response Surface Methodology, J. Eng. (United Kingdom) 2014 (2014). https://doi.org/10.1155/2014/197060.

[48] M. Ilie, E. Cicala, D. Grevey, S. Mattei, V. Stoica, Diode laser welding of ABS: Experiments and process modeling, Opt. Laser Technol. 41 (2009) 608–614. https://doi.org/10.1016/j.optlastec.2008.10.005.

[49] C. Huang, Y. Gao, H. Liu, H. Chen, P. Li, X. Wang, Multi-factors interaction effects of process parameters on the joint strength of laser transmission joining between PC and PA66, Key Eng. Mater. 579–580 (2014) 91–96. https://doi.org/10.4028/www.scientific.net/KEM.579-580.91.

[50] M. Liu, D. Ouyang, J. Zhao, C. Li, H. Sun, S. Ruan, Clear plastic transmission laser welding using a metal absorber, Opt. Laser Technol. 105 (2018) 242–248. https://doi.org/10.1016/j.optlastec.2018.02.047.

[51] R. Prabhakaran, M. Kontopoulou, G. Zak, P.J. Bates, B.K. Baylis, Contour laser - Laser-transmission welding of glass reinforced nylon 6, J. Thermoplast. Compos. Mater. 19 (2006) 427–439. https://doi.org/10.1177/0892705706062200.

[52] M. Devrient, T. Frick, M. Schmidt, Laser transmission welding of optical transparent thermoplastics, Phys. Procedia 12 (2011) 157–165. https://doi.org/10.1016/j.phpro.2011.03.020.

[53] C. V. Katsiropoulos, G.A. Moraitis, G.N. Labeas, S.G. Pantelakis, Optimisation of

laser welding process for thermoplastic composite Materials with regard to component quality and cost, Plast. Rubber Compos. 38 (2009) 153–161. https://doi.org/10.1179/174328909X387847.

[54] I. Hadriche, E. Ghorbel, N. Masmoudi, G. Casalino, Investigation on the effects of laser power and scanning speed on polypropylene diode transmission welds, Int. J. Adv. Manuf. Technol. 50 (2010) 217–226. https://doi.org/10.1007/s00170-009-2511-z.

[55] Y.Y. Wang, A.H. Wang, Z.K. Weng, H.B. Xia, Laser transmission welding of Clearweld-coated polyethylene glycol terephthalate by incremental scanning technique, Opt. Laser Technol. 80 (2016) 153–161. https://doi.org/10.1016/j.optlastec.2016.01.008.

[56] A. Boglea, A. Olowinsky, A. Gillner, Fibre laser welding for packaging of disposable polymeric microfluidic-biochips, Appl. Surf. Sci. 254 (2007) 1174–1178. https://doi.org/10.1016/j.apsusc.2007.08.013.

[57] M. Devrient, B. Knoll, R. Geiger, Laser transmission welding of thermoplastics with Dual Clamping Devices, Phys. Procedia 41 (2013) 70–80. https://doi.org/10.1016/j.phpro.2013.03.053.

[58] A.S. Bideskan, P. Ebrahimzadeh, R. Teimouri, Fabrication of bi-layer PMMA and aluminum 6061-T6 laminates by laser transmission welding: Performance prediction and optimization, Int. J. Light. Mater. Manuf. 3 (2020) 150–159. https://doi.org/10.1016/j.ijlmm.2019.09.008.

[59] Z. Wang, L.I. Zhu, J.H. Wu, Grey relational analysis of correlation of errors in measurement, J. Grey Syst. 8 (1996) 73–78.

[60] E. Rodríguez-Vidal, I. Quintana, J. Etxarri, U. Azkorbebeitia, D. Otaduy, F. González, F. Moreno, Optical design and development of a fiber coupled high-power diode laser system for laser transmission welding of plastics, Opt. Eng. 51 (2012) 124301. https://doi.org/10.1117/1.oe.51.12.124301.

[61] S.K. Mazumdar, S. V. Hoa, Application of Taguchi method for process enhancement of on-line consolidation technique, Composites 26 (1995) 669–673. https://doi.org/10.1016/0010-4361(95)98916-9.

[62] N. Amanat, C. Chaminade, J. Grace, N.L. James, D.R. McKenzie, Optimal process parameters for thermoplastic polyetheretherketone joints fabricated using transmission laser welding and Lumogen® IR absorptive pigment, J. Laser Appl. 23 (2011). https://doi.org/10.2351/1.3552972.

[63] G.N. Labeas, G.A. Moraitis, C. V. Katsiropoulos, Optimization of laser transmission welding process for thermoplastic composite parts using thermo-mechanical simulation, J. Compos. Mater. 44 (2010) 113–130. https://doi.org/10.1177/0021998309345325.

[64] M. Demirel, B. Kayan, Application of response surface methodology and central composite design for the optimization of textile dye degradation by wet air oxidation, Int. J. Ind. Chem. 3 (2012) 1–10. https://doi.org/10.1186/2228-5547-3-24.

[65] X. Wang, C. Zhang, P. Li, K. Wang, Y. Hu, P. Zhang, H. Liu, Modeling and optimization of joint quality for laser transmission joint of thermoplastic using an artificial neural network and a genetic algorithm, Opt. Lasers Eng. 50 (2012) 1522–1532. https://doi.org/10.1016/j.optlaseng.2012.06.008.

[66] B. Acherjee, S. Mondal, B. Tudu, D. Misra, Application of artificial neural network for predicting weld quality in laser transmission welding of thermoplastics, Appl. Soft Comput. J. 11 (2011) 2548–2555. https://doi.org/10.1016/j.asoc.2010.10.005.

[67] W. Tillmann, A. Elrefaey, L. Wojarski, Toward process optimization in laser welding of metal to polymer, Materwiss. Werksttech. 41 (2010) 879–883. https://doi.org/10.1002/mawe.201000674.

[68] V.A. Kagan, Innovations in laser welding of thermoplastics: This advanced technology is ready to be commercialized, SAE Tech. Pap. (2002). https://doi.org/10.4271/2002-01-2011.

[69] M.R. Nakhaei, N.B. Mostafa Arab, G. Naderi, M. Hoseinpour Gollo, Experimental study on optimization of CO2 laser welding parameters for polypropylene-clay nanocomposite welds, J. Mech. Sci. Technol. 27 (2013) 843–848. https://doi.org/10.1007/s12206-013-0109-8.

[70] M.R. Nakhaei, N.B. Mostafa Arab, G. Naderi, Application of response surface methodology for weld strength prediction in laser welding of polypropylene/clay nanocomposite, Iran. Polym. J. (English Ed. 22 (2013) 351–360. https://doi.org/10.1007/s13726-013-0134-6.

[71] K.A. Hubeatir, Laser transmission welding of PMMA using IR semiconductor laser complemented by the Taguchi method and grey relational analysis, Mater. Today Proc. 20 (2020) 466–473. https://doi.org/10.1016/j.matpr.2019.09.167.

[72] R. Bhattacharya, N. Kumar, N. Kumar, A. Bandyopadhyay, A Study on the Effect of Process Parameters on Weld Width and Heat Affected Zone of Pulsed Laser

Welding of Dissimilar Transparent Thermoplastics Without Filler Materials in Lap Joint Configuration, Mater. Today Proc. 5 (2018) 3674–3681. https://doi.org/10.1016/j.matpr.2017.11.618.

[73] F. Lambiase, S. Genna, R. Kant, Optimization of laser-assisted joining through an integrated experimental-simulation approach, Int. J. Adv. Manuf. Technol. 97 (2018) 2655–2666. https://doi.org/10.1007/s00170-018-2113-8.

[74] T. Zoubeir, G. Elhem, Numerical study of laser diode transmission welding of a polypropylene mini-tank: Temperature field and residual stresses distribution, Polym. Test. 30 (2011) 23–34. https://doi.org/10.1016/j.polymertesting.2010.10.008.

[75] M. Aden, F. Liviany, A. Olowinsky, Joint strength for laser transmission welding of thermoplastics: A simulation approach, Int. Polym. Process. 28 (2013) 79–83. https://doi.org/10.3139/217.2674.

[76] L.S. Mayboudi, A.M. Birk, G. Zak, P.J. Bates, Laser transmission welding of a lap-joint: Thermal imaging observations and three-dimensional finite element modeling, J. Heat Transfer 129 (2007) 1177–1186. https://doi.org/10.1115/1.2740307.

[77] F. Becker, H. Potente, A step towards understanding the heating phase of laser transmission welding in polymers, Polym. Eng. Sci. 42 (2002) 365–374. https://doi.org/10.1002/pen.10954.

[78] H. Liu, W. Liu, X. Zhong, B. Liu, D. Guo, X. Wang, Modeling of laser heat source considering light scattering during laser transmission welding, Mater. Des. 99 (2016) 83–92. https://doi.org/10.1016/j.matdes.2016.03.052.

[79] M. Ilie, J.C. Kneip, S. Matteï, A. Nichici, C. Roze, T. Girasole, Through-transmission laser welding of polymers - temperature field modeling and infrared investigation, Infrared Phys. Technol. 51 (2007) 73–79. https://doi.org/10.1016/j.infrared.2007.02.003.

[80] D. Flock, M. Sickert, E. Haberstroh, Temperature measurement in laser transmission welding of plastics, Int. Polym. Sci. Technol. 40 (2013) 704–708. https://doi.org/10.1177/0307174x1304000401.

[81] C. Hopmann, S. Kreimeier, Modelling the Heating Process in Simultaneous Laser Transmission Welding of Semicrystalline Polymers, J. Polym. 2016 (2016) 1–10. https://doi.org/10.1155/2016/3824065.

[82] S.K. Sooriyapiragasam, C. Hopmann, Modeling of the heating process during the laser transmission welding of thermoplastics and calculation of the resulting stress

distribution, Weld. World 60 (2016) 777–791. https://doi.org/10.1007/s40194-016-0330-z.

[83] M. Speka, S. Matteï, M. Pilloz, M. Ilie, The infrared thermography control of the laser welding of amorphous polymers, NDT E Int. 41 (2008) 178–183. https://doi.org/10.1016/j.ndteint.2007.10.005.

[84] L.S. Mayboudi, A.M. Birk, G. Zak, P.J. Bates, Infrared observations and finite element modeling of a laser transmission welding process, J. Laser Appl. 21 (2009) 111–118. https://doi.org/10.2351/1.3184433.

[85] J.D. Van De Ven, A.G. Erdman, Laser transmission welding of thermoplastics - Part I: Temperature and pressure modeling, J. Manuf. Sci. Eng. 129 (2007) 849–858. https://doi.org/10.1115/1.2752527.

[86] J.J. Fuller, E.E. Marotta, Thermal Contact Conductance of Metal/Polymer Joints: An Analytical and Experimental Investigation, J. Thermophys. Heat Transf. 15 (2001) 228–238. https://doi.org/10.2514/2.6598.

[87] S. V. Bronnikov, V.I. Vettegren, S.Y. Frenkel, New approach to the description of young's modulus for highly oriented polymers. ii. relationship between young's modulus and thermal expansion of polymers over a wide temperature range, J. Macromol. Sci. Part B 32 (1993) 33–50. https://doi.org/10.1080/00222349308215470.

[88] P. Majumdar, H. Xia, A Green's function model for the analysis of laser heating of materials, Appl. Math. Model. 31 (2007) 1186–1200. https://doi.org/10.1016/j.apm.2006.04.007.

[89] N. Coluccelli, Nonsequential modeling of laser diode stacks using Zemax: Simulation, optimization, and experimental validation, Appl. Opt. 49 (2010) 4237–4245. https://doi.org/10.1364/AO.49.004237.

[90] A. Naqwi, F. Durst, Focusing of diode laser beams: a simple mathematical model, Appl. Opt. 29 (1990) 1780. https://doi.org/10.1364/ao.29.001780.

[91] Y. Ai, K. Zheng, Y.C. Shin, B. Wu, Analysis of weld geometry and liquid flow in laser transmission welding between polyethylene terephthalate (PET) and Ti6Al4V based on numerical simulation, Opt. Laser Technol. 103 (2018) 99–108. https://doi.org/10.1016/j.optlastec.2018.01.022.

[92] H. Potente, G. Fiegler, H. Haferkamp, M. Fargas, A. Von Busse, J. Bunte, An approach to model the melt displacement and temperature profiles during the laser through-transmission welding of thermoplastics, Polym. Eng. Sci. 46 (2006) 1565–

1575. https://doi.org/10.1002/pen.20638.

[93] L. Wilke, H. Potente, J. Schnieders, Simulation of quasi-simultaneous and simultaneous laser welding, Weld. World 52 (2008) 56–66. https://doi.org/10.1007/BF03266617.

[94] J. Grififths, C. Dowding, Optimization of process parameters in laser transmission welding for food packaging applications, Procedia CIRP 74 (2018) 528–532. https://doi.org/10.1016/j.procir.2018.08.130.

[95] B. Acherjee, 3-D FE heat transfer simulation of quasi-simultaneous laser transmission welding of thermoplastics, J. Brazilian Soc. Mech. Sci. Eng. 41 (2019). https://doi.org/10.1007/s40430-019-1969-3.

[96] S.M. Pawar, A. V. Moholkar, I.K. Kim, S.W. Shin, J.H. Moon, J.I. Rhee, J.H. Kim, Effect of laser incident energy on the structural, morphological and optical properties of Cu2ZnSnS4 (CZTS) thin films, Curr. Appl. Phys. 10 (2010) 565–569. https://doi.org/10.1016/j.cap.2009.07.023.

[97] A. Jonas, R. Legras, Thermal stability and crystallization of poly(aryl ether ether ketone), Polymer (Guildf). 32 (1991) 2691–2706. https://doi.org/10.1016/0032-3861(91)90095-Z.

[98] D. Bagheriasl, P.J. Carreau, C. Dubois, B. Riedl, Effect of cellulose nanocrystals (CNCs) on crystallinity, mechanical and rheological properties of polypropylene/CNCs nanocomposites, AIP Conf. Proc. 1664 (2015). https://doi.org/10.1063/1.4918445.

[99] X. Zhu, Y. Li, D. Yan, Y. Fang, Crystallization behavior of partially melting isotactic polypropylene, Polymer (Guildf). 42 (2001) 9217–9222. https://doi.org/10.1016/S0032-3861(01)00468-2.

[100] V.A. Kagan, R.G. Bray, W.P. Kuhn, Laser transmission welding of semi-crystalline thermoplastics-Part I: Optical characterization of nylon based plastics, J. Reinf. Plast. Compos. 21 (2002) 1101–1122. https://doi.org/10.1177/073168402128987699.

[101] V.A. Kagan, G.P. Pinho, Laser Transmission Welding of Semicrystalline Thermoplastics - Part II: Analysis of Mechanical Performance of Welded Nylon, J. Reinf. Plast. Compos. 23 (2004) 95–107. https://doi.org/10.1177/0731684404029360.

[102] B. Acherjee, A.S. Kuar, S. Mitra, D. Misra, Effect of carbon black on temperature field and weld profile during laser transmission welding of polymers: A FEM study,

Opt. Laser Technol. 44 (2012) 514–521. https://doi.org/10.1016/j.optlastec.2011.08.008.

[103] S. Katayama, Y. Kawahito, Laser direct joining of metal and plastic, Scr. Mater. 59 (2008) 1247–1250. https://doi.org/10.1016/j.scriptamat.2008.08.026.

[104] S. Abed, P. Laurens, C. Carrétéro, J.R. Deschamps, C. Duval, Diode laser welding of polymers: Microstructures of the welded zones for polypropylene, (2018) 1499–1507. https://doi.org/10.2351/1.5059820.

[105] H. Meyer, M. Zabic, S. Kaierle, T. Ripken, Optical coherence tomography for laser transmission joining processes in polymers and semiconductors, Procedia CIRP 74 (2018) 618–622. https://doi.org/10.1016/j.procir.2018.08.074.

[106] T. Frick, A. Schkutow, Laser transmission welding of polymers - Irradiation strategies for strongly scattering materials, Procedia CIRP 74 (2018) 538–543. https://doi.org/10.1016/j.procir.2018.08.118.

[107] B. Cosson, A.C. Akué Asséko, M. Dauphin, A non-destructive optical experimental method to predict extinction coefficient of glass fibre-reinforced thermoplastic composites, Opt. Laser Technol. 106 (2018) 215–221. https://doi.org/10.1016/j.optlastec.2018.04.009.

[108] L. Ma, L. Song, H. Wang, L. Fan, B. Liu, Synthesis and characterization of poly(propylene carbonate) glycol-based waterborne polyurethane with a high solid content, Prog. Org. Coatings 122 (2018) 38–44. https://doi.org/10.1016/j.porgcoat.2018.05.003.

[109] D. Hänsch, D. Haaf, H. Pütz, H.G. Treusch, A. Gillner, R. Poprawe, Welding of plastics with diode laser, (2018) G131–G140. https://doi.org/10.2351/1.5059191.

[110] S.T. Hsu, H. Tan, Y.L. Yao, Effect of excimer laser irradiation on crystallinity and chemical bonding of biodegradable polymer, Polym. Degrad. Stab. 97 (2012) 88–97. https://doi.org/10.1016/j.polymdegradstab.2011.10.006.

[111] X.F. Xu, P.J. Bates, G. Zak, Effect of glass fiber and crystallinity on light transmission during laser transmission welding of thermoplastics, Opt. Laser Technol. 69 (2015) 133–139. https://doi.org/10.1016/j.optlastec.2014.12.025.

[112] M. Wehner, P. Jacobs, R. Poprawe, Rapid prototyping of micro-fluidic components by laser beam processing, Laser-Based Micro- Nanopackaging Assem. 6459 (2007) 645908. https://doi.org/10.1117/12.697391.

[113] V. Kagan, R. Bray, A. Chambers, Forward to better understanding of optical characterization and development of colored polyamides for the infra-red/laser

welding: Part I - Efficiency of polyamides for infra-red welding, J. Reinf. Plast. Compos. 22 (2003) 533–547. https://doi.org/10.1106/073168403023283.

[114] A. Schmailzl, B. Quandt, M. Schmidt, S. Hierl, In-Situ process monitoring during laser transmission welding of PA6-GF30, Procedia CIRP 74 (2018) 524–527. https://doi.org/10.1016/j.procir.2018.08.131.

[115] E. Azhikannickal, P.J. Bates, G. Zak, Laser light transmission through thermoplastics as a function of thickness and laser incidence angle: Experimental and modeling, J. Manuf. Sci. Eng. 134 (2012). https://doi.org/10.1115/1.4007619.

[116] M. Villar, F. Chabert, C. Garnier, V. Nassiet, J.C. Diez, A. Sotelo, M.A. Madre, C. Duchesne, P. Cussac, Laser transmission welding as an assembling process for high temperature electronic packaging, 2016 Int. Conf. Electr. Syst. Aircraft, Railw. Sh. Propuls. Road Veh. Int. Transp. Electrif. Conf. ESARS-ITEC 2016 (2016). https://doi.org/10.1109/ESARS-ITEC.2016.7841379.

[117] A. Schmailzl, J. Käsbauer, J. Martan, P. Honnerová, F. Schäfer, M. Fichtl, T. Lehrer, J. Tesař, M. Honner, S. Hierl, Measurement of core temperature through semi-transparent polyamide 6 using scanner-integrated pyrometer in laser welding, Int. J. Heat Mass Transf. 146 (2020). https://doi.org/10.1016/j.ijheatmasstransfer.2019.118814.

[118] J. Brodhun, D. Blass, K. Dilger, Laser transmission welding of thermoplastic fasteners: Influence of temperature distribution in a scanning based process, Procedia CIRP 74 (2018) 533–537. https://doi.org/10.1016/j.procir.2018.08.123.

[119] A.B. Pereira, F.A.O. Fernandes, A.B. de Morais, J. Quintão, Mechanical strength of thermoplastic polyamide welded by Nd:YAG laser, Polymers (Basel). 11 (2019). https://doi.org/10.3390/polym11091381.

[120] T. Azimzadegan, S.A.A. Akbari Mousavi, Investigation of the occurrence of hot cracking in pulsed Nd-YAG laser welding of Hastelloy-X by numerical and microstructure studies, J. Manuf. Process. 44 (2019) 226–240. https://doi.org/10.1016/j.jmapro.2019.06.005.

[121] T. Rodts, S.R. Schmid, M.A. Selles, T. Pasang, S. Sanchez-Caballero, Selective laser fiber welding on woven polymer fabrics for biomedical applications, Mater. Sci. Eng. C 94 (2019) 628–634. https://doi.org/10.1016/j.msec.2018.10.018.

[122] A. Visco, C. Scolaro, White/light white polyethylene joints obtained by diode laser welding process, Int. J. Polym. Anal. Charact. 23 (2018) 354–361. https://doi.org/10.1080/1023666X.2018.1455025.

[123] M. Villar, C. Garnier, F. Chabert, V. Nassiet, D. Samélor, J.C. Dicz, A. Sotelo, M.A. Madre, In-situ infrared thermography measurements to master transmission laser welding process parameters of PEKK, Opt. Lasers Eng. 106 (2018) 94–104. https://doi.org/10.1016/j.optlaseng.2018.02.016.

[124] N. Kumar, A. Bandyopadhyay, Simulation of the effects of input parameters on weld quality in laser transmission welding (LTW) using a combined response surface methodology (RSM)-finite element method (FEM) approach, Lasers Eng. 36 (2017) 225–243.

[125] T. Kik, Heat source models in numerical simulations of laser welding, Materials (Basel). 13 (2020). https://doi.org/10.3390/ma13112653.

[126] J. Ahn, Experimental characterisation and numerical simulation of fibre laser welding of AA 2024-T3 and Ti-6Al-4V, (2016) 188–250.

[127] B. Acherjee, Laser transmission welding of polymers – A review on welding parameters, quality attributes, process monitoring, and applications, J. Manuf. Process. 64 (2021) 421–443. https://doi.org/10.1016/j.jmapro.2021.01.022.

[128] I. Burkhardt, V. Ventzke, S. Riekehr, N. Kashaev, J. Enz, Laser welding and microstructural characterization of dissimilar γ-TiAl-Ti6242 joints, Intermetallics 104 (2019) 74–83. https://doi.org/10.1016/j.intermet.2018.09.012.

[129] A. Das, R. Beaumont, I. Masters, P. Haney, Macro-modelling of laser micro-joints for understanding joint strength in electric vehicle battery interconnects, Materials (Basel). 14 (2021). https://doi.org/10.3390/ma14133552.

[130] K. Kumagai, M. Kuwahara, T. Yasuki, N. Koreishi, Development of Fracture Model for Laser Screw Welding, SAE Int. J. Passeng. Cars - Mech. Syst. 9 (2016) 280–288. https://doi.org/10.4271/2016-01-1344.

[131] S.A. Patil, F. Baratzadeh, H. Lankarani, Modeling of the Weld Strength in Spot Weld Using Regression Analysis of the Stress Parameters based on the Simulation Study, J. Mater. Sci. Res. 6 (2016) 51. https://doi.org/10.5539/jmsr.v6n1p51.

[132] F. Dave, M.M. Ali, R. Sherlock, A. Kandasami, D. Tormey, Laser transmission welding of semi-crystalline polymers and their composites: A critical review, Polymers (Basel). 13 (2021) 1–52. https://doi.org/10.3390/polym13050675.

[133] A. Kumar Sahu, S. Sankar Mahapatra, S. Chatterjee, Optimization of Electro-Discharge Coating Process using Harmony Search, Mater. Today Proc. 5 (2018) 12673–12680. https://doi.org/10.1016/j.matpr.2018.02.251.

Nitesh Kumar
09/07/25